

**CATALYTIC HYDROGENATION OF NITRILES TO  
AMINES**

**Thesis submitted in accordance with the requirements of the  
University of Cardiff for the degree of Doctor in Philosophy  
by**

**Sarah Glennie**

September 2006

UMI Number: U585015

All rights reserved

INFORMATION TO ALL USERS

The quality of this reproduction is dependent upon the quality of the copy submitted.

In the unlikely event that the author did not send a complete manuscript and there are missing pages, these will be noted. Also, if material had to be removed, a note will indicate the deletion.



UMI U585015

Published by ProQuest LLC 2013. Copyright in the Dissertation held by the Author.  
Microform Edition © ProQuest LLC.

All rights reserved. This work is protected against  
unauthorized copying under Title 17, United States Code.



ProQuest LLC  
789 East Eisenhower Parkway  
P.O. Box 1346  
Ann Arbor, MI 48106-1346

---

## ACKNOWLEDGEMENTS

---

I would like to thank my academic supervisors Graham Hutchings and Stuart Taylor at Cardiff University. I would also like to thank Johnson Matthey for their financial support and Peter Johnson and Ken Griffin from Johnson Matthey for their intellectual contributions and advice and for making me so welcome and helping me on site.

I would like to thank all the technical staff at Cardiff University, especially Alun Davies for his patience and help with all my mechanical repairs, Ricky Fearn for glass repairs and Rob Jenkins for his help with the GC-MS. I would also like to thank Nick Dummer for all his help with the autoclave and trickle-bed reactors.

I would also like to thank my lab mates over the years from lab 1.88 and friends around the department especially Chris Jones, Tom Davies, Darragh Ryan, Graham Laing and Sarah Waters for all their help and support both in and outside the lab.

Outside of university I wish to thank my housemates in Cardiff, Ellie and Adam for their support over the year since leaving university during the write up. I would especially like to thank Simon; I would truly never have managed to finish the thesis without him and cannot thank him enough for his tireless support and encouragement. Lastly and most importantly I need to thank my family for their unending support both financial and emotional throughout.

---

## ABSTRACT

---

The adiponitrile hydrogenation reaction, relevant for the production of aminocapronitrile and hexamethyldiamine; precursors for Nylon 6 and Nylon 6, 6 respectively, has been investigated.

Three different reactor systems were used; trickle-bed reactor, fixed-bed gas-phase reactor and the stirred-tank autoclave reactor. This meant comparisons between flow system and batch process could be made.

Supported metal catalysts were investigated as alternatives for the currently industrially used Raney catalyst. Precious metals, specifically rhodium, were compared with the base metals nickel and cobalt on the basis of activity and selectivity. Mixed metal alloy catalysts were also prepared and comparisons drawn. Finally a range of supports were also tested.

Both flow systems were found to be of limited use with problems attributed to the practical applications of the reactor systems. Using Autoclave activity data as a standard it was possible to define differences in activity between each of the catalysts prepared.

---

# CONTENTS

---

Declaration	ii
Acknowledgements	iii
Abstract	iv
Contents	v
Abbreviations	viii
List of Figures	xi
List of Tables	xv
<b>1. Introduction</b>	<b>1</b>
1.1. Aims of the project – Catalytic Hydrogenation of Nitriles to Amines	2
1.1.1. Adiponitrile hydrogenation for Nylon Production	3
1.2. Introduction to catalysis	4
1.2.1. Homogeneous catalysts	6
1.2.2. Heterogeneous catalysts	6
1.3. Supported Metal Catalysts	7
1.3.1. Raney Nickel	7
1.4. Previous literature	8
1.4.1. Rhodium catalyst for hydrogenation of nitriles	8
1.4.2. Rhodium catalysts for hydrogenation of adiponitrile	9
1.4.3. Iron based catalysts for hydrogenation of adiponitrile	10
1.4.4. Nickel based catalysts for adiponitrile hydrogenation	11
1.4.5. Lamellar Double Hydroxides (LDH)	27
1.4.6. Ruthenium Cobalt catalysts	30
1.5. References	33
<b>2. Experimental Techniques</b>	<b>37</b>
2.1. Catalyst preparation	38
2.1.1. Nickel on silica	39
2.1.2. Rhodium catalysts – 5% Rh/SiO <sub>2</sub> , 5% Rh/Al <sub>2</sub> O <sub>3</sub> and 5% Rh/Graphite	40
2.1.3. Nickel and cobalt catalysts – 5% Ni/Al <sub>2</sub> O <sub>3</sub> and 5% Co/Al <sub>2</sub> O <sub>3</sub>	40
2.1.4. Mixed metal catalysts – 2.5%-2.5% Rh-Co/Al <sub>2</sub> O <sub>3</sub> and 2.5%-2.5% Rh-Ni/Al <sub>2</sub> O <sub>3</sub>	41
2.2. Characterisation	42
2.2.1. TPR analysis	42
2.2.2. BET surface area analysis	43

2.2.3.	XRD analysis	45
2.2.4.	Atomic Absorption Spectroscopy	47
2.3.	Catalyst Testing	49
2.3.1.	Autoclave Stirred-Tank Reactor	49
2.3.1.1.	Sample Preparation for Analysis	50
2.4.	Product Analysis	50
2.4.1.	Gas Chromatography	50
2.4.2.	Infrared Spectroscopy	56
2.4.3.	Nuclear Magnetic Resonance Spectroscopy (NMR)	58
2.5.	References	60
<b>3.</b>	<b>Reactor Construction</b>	<b>61</b>
3.1.	Flow Systems	62
3.2.	Fixed-Bed Gas-Phase Reactor	64
3.3.	Product Analysis	72
3.4.	Trickle-Bed reactor	73
3.5.	Conclusion	77
3.6.	References	79
<b>4.</b>	<b>Characterisation</b>	<b>80</b>
4.1.	Powder X-Ray Diffraction	81
4.1.1.	Pricat Catalysts	82
4.1.2.	Nickel on Magnesia Catalysts	84
4.1.3.	Silica Supported Catalysts	87
4.2.	Temperature Programmed Reduction	91
4.2.1.	20% Ni/SiO <sub>2</sub>	91
4.2.2.	5% Ni/Al <sub>2</sub> O <sub>3</sub>	93
4.2.3.	2.5% Rh/SiO <sub>2</sub>	95
4.2.4.	2.5%-2.5% Ni-Rh/Al <sub>2</sub> O <sub>3</sub>	96
4.2.5.	2.5%-2.5% Co-Rh/Al <sub>2</sub> O <sub>3</sub>	97
4.3.	BET Surface Area Determination	99
4.4.	Scanning Electron Microscopy	103
4.5.	Conclusions	113
4.6.	References	116
<b>5.</b>	<b>Activity Testing</b>	<b>117</b>
5.1.	Introduction	118
5.2.	Autoclave Reactor	118
5.2.1.	Pricat catalysts	118
5.2.2.	Pricat discussion	118
5.2.3.	Nickel on silica catalyst	125

5.2.3.1.	Catalyst S12 - Ni/SiO <sub>2</sub>	125
5.2.4.	5% Ni/SiO <sub>2</sub> (MO4446)	128
5.2.4.1.	Discussion – Ni catalysts	129
5.2.5.	Supported Rhodium catalysts	129
5.2.5.1.	2.5% Rh/SiO <sub>2</sub> (JM catalysts)	130
5.2.5.2.	5% Rh/SiO <sub>2</sub> (MO4433)	131
5.2.5.3.	5% Rh/SiO <sub>2</sub> (MO4434)	133
5.2.5.4.	5% Rh/Al <sub>2</sub> O <sub>3</sub> trilobes (MO4435)	134
5.2.5.5.	Discussion – Rh <i>vs</i> Ni	136
5.2.5.6.	Discussion – Rhodium catalysts compared	137
5.2.6.	Mixed Metal Catalysts	139
5.2.6.1.	2.5%-2.5% Ni-Rh/Al <sub>2</sub> O <sub>3</sub> and 2.5%-2.5% Co-Rh/Al <sub>2</sub> O <sub>3</sub>	139
5.2.6.2.	Discussion - Mixed Metals	142
5.2.7.	Discussion – Autoclave	143
5.3.	Fixed-Bed Gas Phase	144
5.3.1.	Pricat Catalysts	144
5.3.2.	Nickel Catalysts	144
5.3.3.	Rhodium Catalysts	145
5.3.3.1.	Infrared Spectroscopy	146
5.3.3.2.	Nuclear Magnetic Resonance (NMR) Spectroscopy	149
5.3.4.	Discussion - Fixed-Bed Gas-Phase Reactor	155
5.4.	Trickle-Bed Reactor	155
5.4.1.	Trickle-Bed Reactor <i>vs</i> Autoclave 20% Ni/SiO <sub>2</sub>	155
5.4.2.	Trickle-Bed Reactor - Rhodium Catalysts	156
5.4.2.1.	5% Rh/SiO <sub>2</sub> (MO4433)	157
5.4.2.2.	5% Rh/Al <sub>2</sub> O <sub>3</sub> (MO4435)	162
5.4.2.3.	2.5%-2.5% Ni-Rh/Al <sub>2</sub> O <sub>3</sub> (MO4450)	163
5.4.3.	Discussion – Trickle-Bed-Reactor	165
6.	<b>Conclusion</b>	<b>166</b>

---

## ABBREVIATIONS

---

$\delta_H$	Chemical shift of proton NMR
°C	Degrees centigrade
Å	Anstrom
AAS	Atomic Absorption Spectroscopy
ACH	Azocycloheptane
ACN	Aminocapronitrile
ADN	Adiponitrile
Atm	Atmosphere
bar	Unit of pressure
BET	Brunauer Emmett Teller
BPC	Buchii Pressflow Gas Controller
cm	Centimetre
CSTR	Continuous Stirred Tank Reactor
DSC	Differential Scanning Calorimetry
EXAFS	Extended X-Ray Fluorescence Absorption Fine Structure
FID	Flame Ionisation Detector
Fig.	Figure
FT-NMR	Fourier Transform Nuclear Magnetic Resonance
g	Grams
GC	Gas Chromatography
GC-MS	Gas Chromatography Mass-Spectrometer
HMD	Hexamethyldiamine
HME	Hexamethyleneimine

HPLC	High Performance Liquid Chromatography
IR	Infrared
JCPDS	Joint Committee on Powdered Diffraction Standards
kPa	Kilopascal
LDH	Lamellar Double Hydroxides
MFC	Mass Flow Controller
MgO	Magnesium oxide
min	Minute
mL	Millilitres
MO4433	5%Rh/SiO <sub>2</sub> on SP189725
MO4434	5%Rh/SiO <sub>2</sub> on SP874905
MO4435	5%Rh/Al <sub>2</sub> O <sub>3</sub>
MO4443	5%Ni/Al <sub>2</sub> O <sub>3</sub>
MO4445	5%Co/Al <sub>2</sub> O <sub>3</sub>
MO4446	5%Ni/SiO <sub>2</sub>
MO4449	2.5%Co-2.5%Rh/Al <sub>2</sub> O <sub>3</sub>
MO4450	2.5%Ni-2.5%Rh/Al <sub>2</sub> O <sub>3</sub>
NiO	Nickel Oxide
NMR	Nuclear Magnetic Resonance
P	Actual pressure
P <sub>0</sub>	Initial pressure
Pa	Pascal
ppm	Parts per million
PR	Pressure Regulator
PVP	polyvinylpyrrolidone

$S_{act}$	Active surface area
SEM	Scanning Electron Microscopy
$SiO_2$	Silica
TBR	Trickle-Bed Reactor
TCD	Thermal Conductivity Detector
TEM	Transmission Electron Microscopy
TPR	Temperature Programmed Reduction
V	Volts
XPS	X-Ray Photoelectron Spectroscopy
XRD	X-Ray Diffraction

---

## LIST OF FIGURES

---

Figure 1.1	Adiponitrile Hydrogenation Reaction	3
Figure 1.2	Nylon 6 and Nylon 6,6 formations	4
Figure 1.3	Activation energy profile for a catalysed and un-catalysed reaction	5
Figure 1.4	ADN hydrogenation	21
Figure 1.5	Azacycloheptane formation	23
Figure 2. 1	Absorption isotherms indicating point of monolayer coverage	43
Figure 2.2	Powder X-Ray Diffractometer	45
Figure 2.3	Scattering of monochromatic X-ray beam by a crystal lattice	46
Figure 2.4	Atomic Absorption Spectrometer	47
Figure 2.5	Schematic of the Gas Chromatograph	52
Figure 2.6	Flame Ionisation Detector	53
Figure 1.7	GC Adiponitrile Calibration	53
Figure 2.8	GC Hexamethyldiamine Calibration	54
Figure 2.9	Adiponitrile GC calibration graph	55
Figure 2.10	Hexamethyldiamine GC calibration graph	55
Figure 2.11	Common Absorption bands in organic molecules	57
Figure 2.12	Chemical shifts in $^1\text{H}$ NMR	59
Figure 3.1	Continuous stirred-tank reactor	62
Figure 3.2	Trickle-bed reactor	63
Figure 3.3	Fixed Bed Gas Phase Micro Reactor	64
Figure 3.4	Hydrogen Mass Flow Controller Calibration Graph	65
Figure 3.5	Helium Mass Flow Controller Calibration	66
Figure 3.6	Adiponitrile Saturator	67

Figure 3.7	Adiponitrile Vapour Pressure	68
Figure 3.8	Vapour Pressures Vs Temperatures	69
Figure 3.9	Gas-phase reactor	70
Figure 3.10	Gas-phase reactor modified	71
Figure 3.11	TBR Body showing distributor head and frit glass plate	73
Figure 3.12	Blockage in the TPR reactor showing liquid build up on catalyst bed	74
Figure 3.13	TBR Cycling System	75
Figure 4.1	XRD pattern for Pricat Catalysts	82
Figure 4.2	XRD Pattern for M1r5	85
Figure 4.3	XRD pattern M1c	86
Figure 4.4	XRD pattern for 20% Loading Ni/SiO <sub>2</sub>	87
Figure 4.5	XRD pattern for Ni/SiO <sub>2</sub> at different reduction temperatures	89
Figure 4.6	20% Ni/SiO <sub>2</sub> XRD showing different reduction conditions	90
Figure 4.7	TPR 20%Ni/SiO <sub>2</sub>	92
Figure 4.8	TPR of MO4443 – 5%Ni/Al <sub>2</sub> O <sub>3</sub>	94
Figure 4.9	TPR of 2.5% Rh/SiO <sub>2</sub>	95
Figure 4.10	TPR of MO4450 2.5% Rh-2.5% Ni/Al <sub>2</sub> O <sub>3</sub>	96
Figure 4.11	MO4449 - 2.5%-2.5%Co-Rh/Al <sub>2</sub> O <sub>3</sub>	98
Figure 4.12	BET Surface Areas	99
Figure 4.13	MgO catalyst BET surface areas	101
Figure 4.14	Effect of Chloride Ion on Surface Area	102
Figure 4.15	SEM image of Alumina Trilobes	104
Figure 4.16	SEM image of silica support SP189725	106
Figure 4.17	SEM image of silica support SP874905	107
Figure 4.18	SEM image of MO4433	108

Figure 4.19	SEM image of MO4434 before washing	110
Figure 4.20	SEM image of MO4434 after washing in NH <sub>3</sub>	111
Figure 4.21	SEM image of MO4445	112
Figure 5.1	Graph of Selectivity against Pressure for Pricat Ni62/15P	119
Figure 5.2	Pricat Ni 62/15P Adiponitrile hydrogenation at 150°C, 10 bar	120
Figure 5.3	Pricat Ni 62/15P Adiponitrile hydrogenation at 150°C, 20 bar	121
Figure 5.4	Pricat Ni62/15P Adiponitrile hydrogenation at 150°C, 30 bar	122
Figure 5.5	Hydrogen uptake data for Pricat Ni 62/15P	123
Figure 5.6	Activity data for 20% Ni/SiO <sub>2</sub> at 150°C, 20 bar	126
Figure 5.7	Activity data for 20% Ni/SiO <sub>2</sub> at 150°C, 30 bar.	127
Figure 5.8	Activity data for 5% Ni/SiO <sub>2</sub> at 200°C, 30 bar	128
Figure 5.9	Activity data for 2.5% Rh/SiO <sub>2</sub> at 150°C, 30 bar	130
Figure 5.10	Activity data for 2.5% Rh/SiO <sub>2</sub> at 200°C, 30 bar	131
Figure 5.11	Activity data for 5% Rh/SiO <sub>2</sub> at 150°C, 30 bar (MO4433)	132
Figure 5.12	Activity data for 5% Rh/SiO <sub>2</sub> at 150°C, 30 bar (MO4434)	134
Figure 5.13	Activity data for 5% Rh/Al <sub>2</sub> O <sub>3</sub> at 150°C, 30 bar	135
Figure 5.14	Hexamethyleneimine formation	136
Figure 5.15	Product composition of ADN hydrogenation in autoclave at 150°C, 30 bars, and 18 hours by different catalysts	138
Figure 5.16	Hydrogen uptake during ADN hydrogenation at 150°C, 30 bar for different catalysts	139
Figure 5.17	Hydrogen up take data for mixed metal catalysts compared with single metal catalysts	140
Figure 5.18	Mixed metal and single metal catalyst, selectivity comparisons	141
Figure 5.19	IR spectrum of Adiponitrile	147
Figure 5.20	IR spectrum of product P105	148

Figure 5.21	IR spectrum of product P108	148
Figure 5.22	$^1\text{H}$ NMR spectrum of adiponitrile	149
Figure 5.23	$^1\text{H}$ NMR spectrum of hexamethyldiamine	150
Figure 5.24	$^1\text{H}$ NMR spectrum of P105	151
Figure 5.25	$^1\text{H}$ NMR spectrum of P105 (enlarged)	152
Figure 5.26	Comparison of P105 NMR spectra	153
Figure 5.27	$^1\text{H}$ NMR Spectrum of P108	154
Figure 5.28	Blockage in the TPR tube	157
Figure 5.29	IR spectrum of TB203	158
Figure 5.30	$^1\text{H}$ NMR spectrum of TB203	159
Figure 5.31	Comparison of TB203 $^1\text{H}$ NMR spectra	160
Figure 5.32	TB203 Rate Profile	161
Figure 5.33	IR Spectrum of TB204	162
Figure 5.34	$^1\text{H}$ NMR Spectrum of TB204	163
Figure 5.35	$^1\text{H}$ NMR Spectrum of TB205	164
Figure 5.36	IR Spectrum of TB205	164

---

## LIST OF TABLES

---

Table 3.1	Adiponitrile vapour pressures	68
Table 4.1	Peak Assignment Table – Pricat Ni 62/15 P and Pri Ni 55/5P	83
Table 4.3	Peak assignment table for XRD of M1r5	85
Table 4.4	Peak assignment table for XRD of M1c	86
Table 4.5	Peak Assignment Table for 20% Ni/SiO <sub>2</sub>	88
Table 4.6	BET surface area chart key	99
Table 4.7	Effect of washing on surface area	103
Table 5.1	Gas Phase Activity Data	144
Table 5.2	Gas-phase reaction conditions	145
Table 5.3	Trickle-Bed vs. Autoclave 20%Ni/SiO <sub>2</sub>	155

*Chapter 1*

INTRODUCTION

---

## 1. INTRODUCTION

---

### 1.1. Aims of the Project – Catalytic Hydrogenation of Nitriles to Amines

The selective hydrogenation of nitriles to primary amines is one of the key stages in the production of many amines used in the manufacturing industry. This project focuses specifically on the process of hydrogenation of adiponitrile (ADN) to aminocapronitrile (ACN) and hexamethyldiamine (HMD). These hydrogenation products are the precursors for production of Nylon 6 and Nylon 6,6 respectively [1]. Previously this has been done over Raney Nickel, but these catalysts produce many by products of cyclic amines and imines which require costly separation processes and result in waste.

The purpose of this project is to find an alternative heterogeneous catalyst for this process with both aminocapronitrile and hexamethyldiamine as the desired products and to investigate different reactor types.

Ideally it might be possible to tailor the reaction towards one or other of these products in a controlled manor by altering reaction conditions. Supported noble metal catalysts will be investigated e.g. Rh, Pd, Pt, Ru and Au on supports such as alumina, carbon or silica. Reactions will be undertaken in an autoclave and products analysed by gas chromatography (GC). Catalysts will be characterised by a range of methods including metal dispersion, surface area, metal particle size distribution and transmission electron

microscopy (TEM). The aim being to link method of preparation with structure and reactivity and gain an insight in to the mechanism by which the reaction takes place.

Three types of reactor are compared; the liquid phase flow system of the Trickle-Bed, the liquid phase batch process in the Autoclave and the gas-phase reaction in a gas phase reactor. The development of a gas-phase fixed-bed reactor from scratch is a key part of this project.

### 1.1.1. Adiponitrile Hydrogenation for Nylon Production

The adiponitrile hydrogenation reaction is important industrially for the production of Nylon 6 and Nylon 6,6. Figure 1.1 shows the adiponitrile hydrogenation reaction.

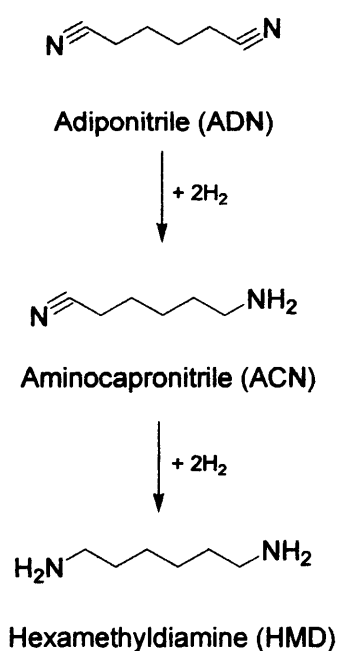


Figure 1.1 - Adiponitrile hydrogenation reaction

Figure 1.2a shows the reaction from caprolactam to Nylon 6, caprolactam is formed from cyclisation of aminocapronitrile. Nylon 6 is thus named as it has 6 carbons between each repeating unit.

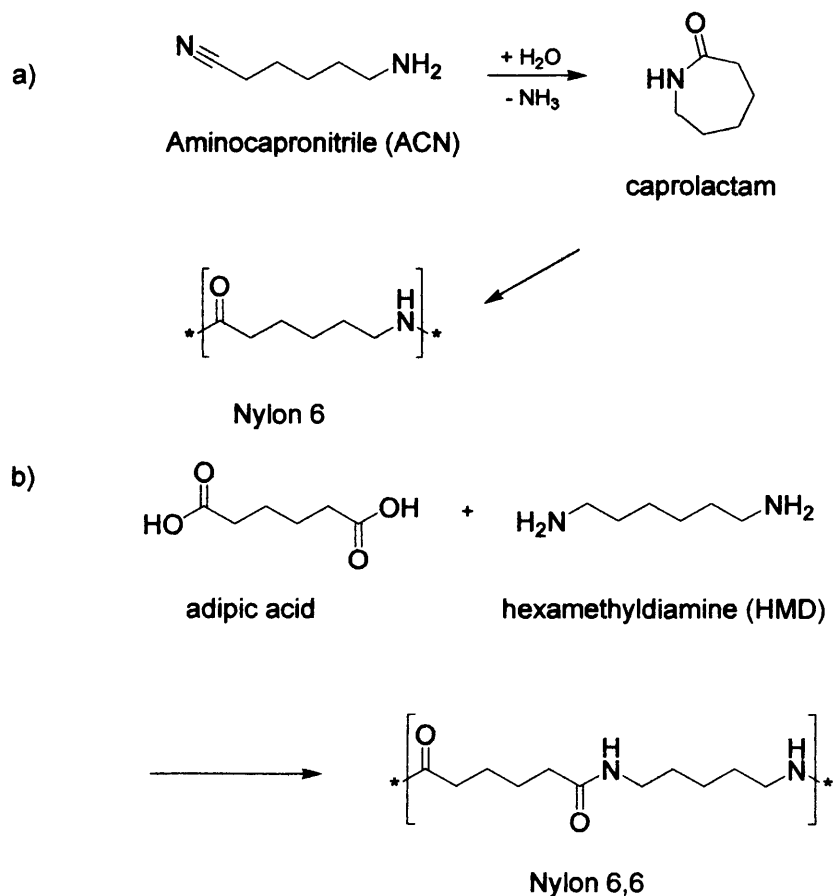


Figure 1.2 – a) Nylon 6 and b) Nylon 6,6 formations

Nylon 6,6 on the other hand is made from the reaction between adipic acid and hexamethylene diamine. This results in a polymer with two different groups of 6 carbons repeating thus calling it Nylon 6,6. This reaction scheme can be seen in figure 1.1b

## 1.2. Introduction to Catalysis

Catalysts have been used since ancient times in processes such as making wine, bread and cheese. The term catalysis was coined by Jöns Jakob Berzelius in 1835 who wrote “I shall therefore call it the catalytic power of substances, and the decomposition by means of this power catalysis, just as we use the word analysis to denote the separation of the component parts of bodies by means of ordinary chemical forces. Catalytic power actually means that substances are able to awake affinities which are asleep at this temperature by their mere presence and not by their own affinity”.

According to collision theory for a reaction to occur between two or more molecules, these molecules need to collide with sufficient energy to react. This required energy is termed activation energy. A catalyst speeds up the reaction by reducing the activation energy required for the reaction to occur, figure 1.3 shows the energy profile of an exothermic reaction with or without a catalyst present.

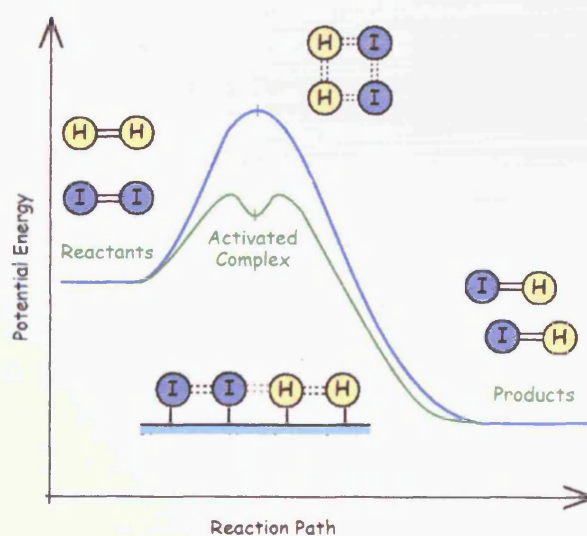


Figure 1.3 – Activation energy profile for a catalysed (green) and un-catalysed (blue) reaction

The second requirement for a successful reaction is that the molecules must collide in a correct orientation such that the correct bonds can be broken and formed in order to form the desired products. A catalyst does this by influencing the orientation of the activated complex formed, the intermediate, such that it is correct for reaction. The catalyst then dissociates from the reactant molecules and remains unchanged and can go on to catalyse further reactions.

There are two main types of catalysts [2]:

- Heterogeneous catalysts
- Homogeneous catalysts

These will be discussed in the following sections.

### *1.2.1. Homogeneous Catalysts*

A homogeneous catalyst is one that is present in the same state as the reactants. Usually homogeneous catalysts come in the form of liquids and are used in liquid phase reactions. The problem with a homogeneous catalyst system is separation of product and catalyst. The action of a homogeneous catalyst is usually to coordinate with the reactant molecules and bring them together for reaction to occur. Contemporary examples of homogeneous catalysis utilizing metal complexes include hydroformylation, Ziegler-Natta polymerization, hydrogen transfer catalysis, hydrogenation, and C-H activation.

### 1.2.2. Heterogeneous Catalysts

Heterogeneous catalysis occurs when the catalyst and the reactant are in different phases. The most common example is a solid catalyst and liquid or gaseous reactants [2]. The heterogeneous catalyst works by adsorbing the reactants to active sites on the catalyst's surface. Once on the surface, the molecule can form a stable activated complex, weakening bonds within the molecule allowing it to react with other molecules on the surface or to break up or rearrange itself.

### 1.3. Supported Metal Catalysts

Heterogeneous catalysis is commonly achieved with the catalyst in question being a metal and the reactants in liquid or gas form. The metal catalysts can be either bulk metal or supported metals. A variety of relatively inert supports can be used such as silica, alumina, graphite or titania [3]. The metal is dispersed on the catalyst surface and thus more metal active sites are available for reaction than in a bulk metal catalyst where much of the metal is within the bulk of the catalyst and not as easily accessed [4].

#### 1.3.1. Raney Nickel

Raney Ni is a skeletal catalyst invented in 1927 by Murray Raney [5]. It is formed by the melting of the active metal and aluminium in a crucible to form an alloy. The skeletal

structure is then created by leaching of aluminium out of the alloy by dissolving in sodium hydroxide [6].

This skeletal structure has large surface area and can store hydrogen gas. For this reason, the catalyst is pyrophoric [7]. When supplied, it is stored as a slurry in water. Care should be taken never to expose Raney nickel to air. Even after reaction, Raney nickel contains significant amounts of hydrogen gas, and will ignite when exposed to air.

Adiponitrile hydrogenation over Raney nickel, in the literature, is mostly done over the catalyst in a slurry bubble, three phase reactor. [6, 8, 9, 10, 11, 12]

## 1.4. Previous Literature

### 1.4.1. Rhodium Catalyst for hydrogenation of nitriles

Rhodium has been proved to be an effective catalyst for oxidation [13] but also for various hydrogenations e.g. [14, 15, and 16] as well as for amine hydrogenation e.g. [17]. It was found that the same selectivity pattern was favoured for gas and liquid phase hydrogenation with ruthenium being best followed by rhodium then nickel [18]. Mixed Ni-Rh catalysts have proved an effective catalysts [19, 20], for hydrogenation of butyronitrile a mixture of Rh and Ni on NaY showing the Rh is able to promote Ni reduction and increase hydrogenation rates [21].

1.4.2. Rhodium Catalyst for hydrogenation of adiponitrile

Mares et al [22] report the use of highly dispersed Rhodium on a magnesia support for the conversion of adiponitrile to hexamethyldiamine. It was found that commercial magnesia had a very low surface area and was prone to surface agglomeration thus lost its activity rapidly. High surface area magnesia was produced by hydrating commercial magnesia to  $\text{Mg}(\text{OH})_2$  then calcining. The temperature and duration of these processes were found to be the major experimental variables. The optimum values found were 22 hours hydration,  $\text{MgO}/\text{Mg}(\text{OH})_2$  ratio 0.15 and 24 hours calcination. This gave a surface area of  $270\text{m}^2/\text{g}$  measured by the standard BET method for nitrogen desorption at  $-196^\circ\text{C}$ . Selectivities to aminonitriles remain high even at 90% conversion. They conclude that the enhanced selectivities were due to the basic nature of the  $\text{MgO}$  support facilitating desorption of basic compounds e.g. amines, and the high dispersion of Rh. Increasing concentration of adiponitrile had no effect on the formation of hexamethyldiamine but increased the production of cyclic by products, best selectivities for diamine formation were found in lowest concentration of adiponitrile. Ammonia was used to suppress the formation of cyclic imines and bis( $\omega$ -cyanoalkyl)amines thus increasing the formation of 6-aminocapronitrile. Neat ammonia would therefore be the best medium for reaction and they found that this was possible by using their highly dispersed catalyst. Increased hydrogen pressure was found to increase the intermediate imine hydrogenation and therefore reduces its reaction with the amino group of 6-aminocapronitrile. Therefore increased imine hydrogenation increases the formation of hexamethyldiamine. This concluded that 6-aminonitrile is favoured at low adiponitrile concentrations in neat ammonia and high hydrogen pressure. A selectivity of 94% at a conversion of 70% was reported [23].

Pellegata et al.[24] investigated the use of rhodium nanoparticles on polyvinylpyrrolidone (PVP) as a hydrogenation catalyst. They looked at the hydrogenation of five different substrates one of which was adiponitrile. They were interested in finding catalysts suitable for reaction in aqueous conditions. The water soluble polymer polyvinylpyrrolidone was chosen. Hydrogenation of adiponitrile at 80°C under 5 and 40 bar H<sub>2</sub> pressure with a catalyst to substrate ratio of 1/1500 for 9 hours resulted in conversions of adiponitrile to 6-aminocapronitrile of 33% and 85% respectively. The kinetics of the reaction was found to be zero order with respect to hydrogen and substrate.

Alini et al. [25, 19] also investigated Rh in adiponitrile hydrogenation and found that, in a slurry reactor, Rh/Al<sub>2</sub>O<sub>3</sub> could partially hydrogenate adiponitrile to aminocapronitrile with a conversion of 60% and selectivity of 99%. This catalyst was prepared using an ion exchange method.

#### *1.4.3. Iron Based Catalysts for hydrogenation of adiponitrile*

The effect of alkali dopants on catalytic activity of iron catalysts was investigated by Fierro et al. [26]. Addition of a dopant affects the surface characteristics of the catalyst; this was investigated using XRD and XPS. Surface area measurements by BET found the surface area decreases with the addition of an alkali dopant and this increase is related to the increase of atomic volume of the dopant. Alkali metals with smaller atomic radii were found to migrate to the surface faster than those with larger electronic radii. The

surface atomic ratio of dopant to iron was found to be higher than the bulk in all cases. Due to their larger size, caesium ions could remain at the surface of the micropores from the beginning of the impregnation.

Surface acidity was measured using gaseous base adsorption under oxygen free conditions. Weak and strong acid centres were found and differentiated by using different adsorbed bases; quinoline that titrates strongly acidic centres and pyridine and cyclohexylamine that titrate strong and weak acid centres. Surface acidity was found to increase as ionic radii of dopant increased non-doped <math>Na^+ < K^+ < Cs^+</math>. The greatest increase in acid centres was found for  $Cs^+$  doped iron. This was put down to the structural differences between the  $Cs_2O$  (anti-Cd- $Cl_2$ ) and the other alkali oxides (anti-fluorite).

Catalytic activity was investigated for the conversion of adiponitrile to 6-aminocapronitrile (ACN). Conversion was found to increase with temperature and with the number of surface acid sites. Selectivity to ACN was found to be higher at lower temperatures. Cs doped catalysts showed 0% conversion possibly due to irreversible adsorption of reaction products.

#### 1.4.4. Nickel Based Catalysts for adiponitrile hydrogenation

Nickel catalysts are most common in the hydrogenation of adiponitrile. Research has investigated nickel on a variety of supports and with a number of different dopants.

### *Unsupported NiO catalysts*

Unsupported NiO catalysts have been investigated by Medina et al [27]. The activation energies of reduction, catalytic activities and selectivities for the hydrogenation of adiponitrile were investigated for pure NiO and potassium doped NiO catalysts.

Using TPR non-stoichiometric NiO was found to have lower initial activation energy of reduction than stoichiometric NiO. Thus non-stoichiometric NiO starts autocatalytic nucleation at a lower temperature. As the temperature of reduction increases, the surface area of NiO decreases possibly due to sintering. Potassium is shown to be a reducibility inhibitor for NiO.

Stoichiometric NiO is highly sintered and has low BET surface area, and thus lower conversions. The conversions increase with increased degree of reduction. Degree of reduction increases with increased temperature but after reduction to temperatures over 623K, the conversions decrease. Larger crystallite size is accompanied by an increased degree of sintering at higher temperatures which results in lower surface area and so lower conversions. High selectivities for hydrogenation of adiponitrile to 6-aminohaxanenitrile are only reached at low conversions for stoichiometric NiO.

Conversions for non-stoichiometric NiO increases with the increased degree of reduction but decreases for catalysts reduced at temperatures above 573K. These catalysts exhibit lower surface areas and lower conversions due to sintering as before. Non-stoichiometric NiO precursors become completely reduced at 500K but at this temperature it is found that the Ni phase present is not well suited for selective production of aminocapronitrile.

The precursors are required to be reduced at temperatures of 623-673K in order for this selectivity to improve. Doping with potassium inhibits NiO reduction and the temperature required for full reduction reaches 573-623K. At this temperature selectivity to aminocapronitrile improves.

Potassium appears to decrease the number of surface active sites for the production of hexamethyldiamine and azacycloheptane caprolactam formation. Active sites for production of aminocapronitrile are still available after sintering and potassium doping. This indicates that the process is structure dependent.

This catalytic process can be biased towards certain products by altering the reduction temperature and the conditions of the reaction. In order to produce aminocapronitrile, a sintered doped or un-doped NiO catalyst is favoured. 1,6-hexanedinitrile and azacycloheptane are favoured by very active un-sintered un-doped catalysts under low space velocity and high reaction temperature.

#### *Fe<sub>2</sub>O<sub>3</sub> supported nickel catalysts*

A study of Fe<sub>2</sub>O<sub>3</sub> supported nickel catalysts with varying contents of potassium dopants were compared with bulk nickel catalysts [28]. These catalysts were tested for the hydrogenation of adiponitrile in the vapour phase at 180°C and 1 atm pressure. Fe<sub>2</sub>O<sub>3</sub> supported nickel catalysts exhibit XRD pattern for metallic iron after reduction at 225°C. Potassium promoted nickel catalysts do not show any metallic nickel even after reduction at temperatures above 420°C. The NiO phase is always present and the magnetite phase

is obtained over the reduction temperature range 225-325°C and  $\alpha$ -Fe is found over 290°C. They conclude that magnetite and  $\alpha$ -Fe inhibit reduction of NiO and the formation of Ni microcrystalites.

Of all the phases present in the catalysts  $\text{Fe}_2\text{O}_3$ ,  $\text{Fe}_3\text{O}_4$ , Fe and NiO, only reduced nickel proved to be catalytically active for adiponitrile hydrogenation. Bulk nickel showed higher conversions when reduced at temperatures of 200-300°C. Those reduced at higher temperatures e.g. 390°C had larger crystallite sizes and lower conversions. As the potassium content was increased, Ni particle size and degree of reduction decreased.

Selectivities of 100% for bulk nickel catalyst reduced at 390°C, 90% for reduced catalysts at 390°C prepared with  $3.5 \times 10^{-3} \text{gKg}^{-1} \text{Fe}_2\text{O}_3$  and 100% for catalysts also reduced at 390°C supported on  $\alpha$ Fe prepared with no potassium. It was found that when selectivity to aminocapronitrile increased, the selectivity to hexamethyldiamine decreased and vice-versa. This indicates that these two products are formed at different active sites. Also it is noted that azacycloheptane formation tends to be obtained with hexamethyldiamine thus implying that these two products form at the same active sites.

#### *Potassium Doped Graphite Supported Nickel Catalysts*

The effects of potassium dopants on a graphite supported nickel catalysts were investigated by Medina et al [29]. These catalysts were assessed for catalytic activity for the hydrogenation of adiponitrile at 433K at 1 atm pressure in the absence of ammonia.

Activation energies for reduction of NiO in graphite supported catalysts were higher than that of the unsupported catalyst. Graphite can be lost at temperatures above 723K due to glassification this was shown by XRD. Graphite and potassium were shown by XPS to be inhibiting the reduction of NiO.

Conversion was found to increase with increased degree of NiO reduction but potassium was found to improve the selectivity towards aminocapronitrile. The addition of potassium increases the basicity of the catalyst favouring desorption of amines and alters the distribution of surface active sites responsible for certain reaction products. No higher amines or imine intermediates were found in this study. Increase in reaction temperature causes an increase in the production of azacycloheptane; aminocapronitrile is favoured at lower temperatures. Increase in space velocity seems to favour the formation of aminocapronitrile due to more efficient amine desorption.

This reaction could be tailored towards any of the three reaction products by altering conditions. If aminocapronitrile is required then a graphite supported nickel catalyst doped with  $1-3 \times 10^{-3}$  g K<sub>2</sub>O/g catalyst is required. For hexamethylenimine, potassium free graphite supported nickel catalyst may be used with low space velocities and high reaction temperatures. The fully hydrogenated product hexamethyldiamine may be produced by reaction on a graphite supported potassium-free catalyst with high space velocities and low reaction temperatures. Although high temperatures can cause graphite glassification in the presence of reduced nickel. Graphite was found to reduce sintering of metallic nickel.

Potassium encourages the selectivity to hexamethyldiamine, 100% selectivity to hexamethyldiamine was obtained at 50% conversion for catalyst with K content  $1.4 \times 10^3$  g/g catalyst and 0.21g Ni/graphite.

### *Nickel supported on $\alpha$ -alumina*

Studies of nickel on  $\alpha$ -alumina show the effect that the support has on the activation energies of NiO reduction and selectivities in the hydrogenation of adiponitrile [30, 31]. The effect of the support on the activation energy of reduction is investigated [30]. The catalytic hydrogenation of adiponitrile at 443K and 1 atm is carried out in the absence of ammonia.

Activation energies of reduction were found to increase with the  $\alpha$ -alumina supported nickel catalysts, proving the inhibiting effect of  $\alpha$ -alumina on NiO reduction.  $\alpha$ -Alumina is thought to inhibit the reduction of NiO because it increases dispersion inhibiting autocatalytic nucleation of reduced nickel. The activation energies of reduction converge for supported and unsupported nickel catalysts at high degrees of reduction. Complete reduction of NiO on  $\alpha$ -alumina was found above 623 K the alumina support was found to increase the reduction temperature thus backing up the idea that it inhibits reduction.

XPS confirms the NiO reduction inhibiting effect of  $\alpha$ -alumina. Complete reduction is also favoured by higher surface dispersion, increased Ni content and decreased reduction temperatures. Crystallite size increases with increase in reduction temperature as shown by XRD. This may be due to the sintering effect mentioned earlier.

Conversion increases at higher degrees of NiO reduction and with increased nickel content and it decreases with nickel sintering at high temperatures. Selectivity to aminocapronitrile increases at lower nickel contents, high space velocities and higher metallic sintering.  $\alpha$ -alumina prevents sintering and allows conversions to remain high for catalysts reduced at high temperatures. Sintering probably produces metal sites favourable for the production of aminocapronitrile.

#### *Potassium Doped $\alpha$ -alumina supported nickel catalysts*

The effect of potassium doping on these  $\alpha$ -alumina supported nickel catalysts were investigated [31]. Hydrogenation of adiponitrile was carried out under the same condition as above. As before  $\alpha$ -alumina was found to increase the activation energy of reduction and thus the temperature of reduction for NiO on the supported metal catalysts. Potassium was also found to inhibit the reduction of NiO. Ni metal was found to be present in large quantities at higher reduction temperatures and lower potassium contents.

Conversions decrease with decrease in nickel surface area. The nickel area decreases with increasing reduction temperature and increased potassium dopant levels. Nickel dispersion is fairly constant for all catalysts. Selectivity to aminocapronitrile increases with potassium content.

Potassium or  $\alpha$ -alumina seems to have a structural effect on the catalyst, creating more sites active for the production of aminocapronitrile causing the highly selective pathway. There is thought to be low surface area coverage by reactants shown in the low quantity of oligomerization products.

### *$\gamma$ -Alumina-supported NiO catalysts*

Nickel supported on  $\gamma$ -alumina was tested for the hydrogenation of adiponitrile at 443K, 1 atm pressure and in the absence of ammonia [32]. The reaction conditions are the same as for the  $\alpha$ -alumina supported nickel catalysts previously described and the potassium doped  $\alpha$ -alumina.

The shape of TPR curves was sigmoid in agreement with the nucleation model of nickel reduction.  $\gamma$ -Alumina was found to inhibit reduction of NiO phase much more than  $\alpha$ -alumina and unsupported NiO. This implies a greater degree of interaction between  $\gamma$ -alumina and NiO. Differentiated curves for reduction show two weight losses in the NiO unsupported and  $\alpha$ -alumina supported catalysts. Weight losses in these two samples could be from two dominant ranges of particle sizes present in the oxide. This is less evident in the  $\alpha$ -alumina supported NiO catalyst because of the texture-regulating action that alumina has upon NiO. The  $\gamma$ -alumina supported catalyst has four different weight losses. Two of these losses are due to loss of surface hydroxyl groups as water. The other two are due to NiO phase reduction.

A new phase was identified by TPR measurements, a nickel aluminate at the NiO/  $\gamma$ -alumina interface. It is formed at calcination temperatures above 623K and affects the

final degree of reduction of the catalyst. This phase is not detected by XRD and is therefore not crystalline. XRD only detects the NiO and reduced-nickel phases. The nickel aluminate phase caused low levels of reduction as some of the NiO was trapped inside shells of nickel aluminate and some is in the form of nickel aluminate spinel both are not freely available for reduction. This leaves more than 25% of the NiO unreduced.

The only products of the hydrogenation reaction were 6-aminohexanenitrile, hexane-1,6-diamine and hexamethyleneimine. Pure  $\gamma$ -alumina was not found to be catalytically active. Unreduced catalysts produced no conversion. The degree of reduction of the reduced catalysts was very low, 40-75% but they managed to achieve full conversion. These  $\gamma$ -alumina catalysts have high thermal stability and no significant metal sintering is shown at high temperatures. This is due to the high stabilising and dispersing effect of  $\gamma$ -alumina.

Catalyst conversions increase significantly with increase in nickel content and degree of reduction of catalyst. Selectivity's of 100% can be found towards hexamethyleneimine especially in the catalysts with high nickel loading and higher reduction temperatures. No linear secondary or tertiary amines are found perhaps due to low surface coverage of reactants.

Detailed characterisation of several  $\gamma$ -alumina supported nickel catalysts was undertaken [35]. The catalysts were found to have mesopores with diameters between 20 and 100 Å. The NiO crystallites were found to be octahedral and larger than the pore mouths of the support. The surface characteristics of the support remain constant under these

conditions. XPS shows surface  $\text{Ni}^{2+}$  and surface reduced nickel. SEM micrographs show the presence of nickel aluminate shells are more prevalent in lower nickel loading and the octahedral NiO crystallites are more apparent for higher nickel loading. At calcination temperatures above 623K nickel aluminate is present in layers between zero and several atoms thick covering the whole surface of the support. At calcination temperatures above 623K with reduction temperatures higher than 673K the catalytically active reduced nickel is present on top of the nickel aluminate layer either as octahedral crystallites or encapsulated in voided nickel aluminate shells.

### *Silica supported Ni-B catalysts*

Ni-B/SiO<sub>2</sub> has been used for many hydrogenation reactions such as cyclopentadiene [34, 35, 36] and heptadecyl cyanide [36]. High selectivity to primary amines was found in the hydrogenation of nitriles over Ni-B/SiO<sub>2</sub> catalysts [38, 34] specifically adiponitrile over Ni-B/SiO<sub>2</sub> amorphous catalyst at 1 atm [38].

XRD showed the Ni-B/SiO<sub>2</sub> catalyst to be amorphous. EXAFS shows a lack of long range order for the fresh Ni-B/SiO<sub>2</sub> alloy only short range order of first near neighbour atom layer. This structure can be transformed in to a well ordered structure on heating to 873K for 2 hours in flowing N<sub>2</sub>. The crystallized Ni-B/SiO<sub>2</sub> shows diffraction peaks for metallic Ni and crystalline Ni<sub>2</sub>B alloy. DSC analysis shows that for the supported Ni-B catalyst crystallization begins around 694K. This is 80K higher than for the unsupported Ni-B catalyst. The SiO<sub>2</sub> support appears to be thermally stabilizing. MgO dopant showed no significant effect on structural properties of Ni-B amorphous alloy. The active surface areas ( $S_{\text{act}}$ ) remained the same for Ni-B/SiO<sub>2</sub> and Ni-B/SiO<sub>2</sub>-MgO. On

crystallization the Ni loading and Ni to B atomic ratio remained the same but there is a big decrease in the  $S_{act}$  due to gathering of Ni active sites at high temperature. XPS shows Ni and B are each present in two states in the amorphous catalyst. Ni present as metallic nickel and NiO and the boron present as NiB alloy and  $B_2O_3$ . Ni and B have strong interactions, the bonding electrons of boron occupy vacant d-orbitals of nickel, making the B electron deficient and the Ni electron rich.

The three main products of hydrogenation were found, hexamethyldiamine, aminocapronitrile (the hemi hydrogenated product) and hexamethyleneimine (a by product). This led them to adopt the Volf and Pasek mechanism shown in figure 1.4

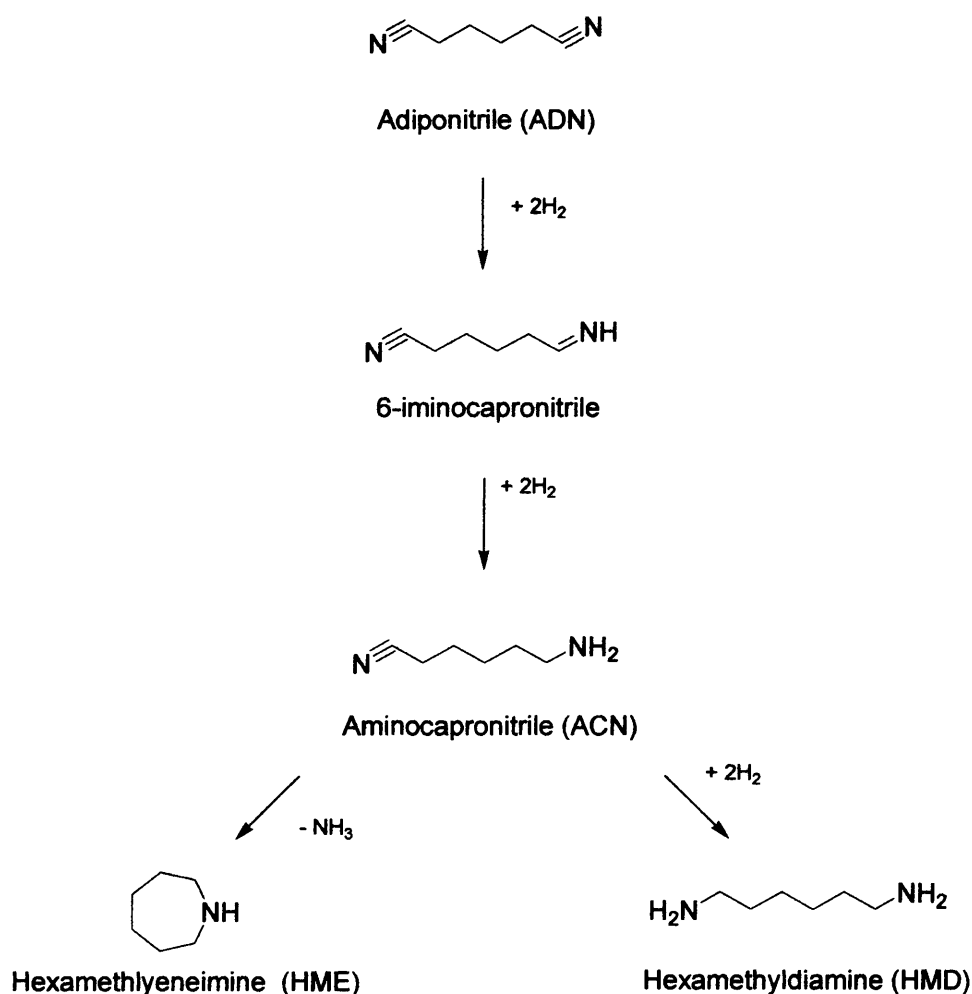


Figure 1-4 - ADN hydrogenation [38]

At 100% adiponitrile conversion on supported Ni-B amorphous catalysts the only by product formed was hexamethyleneimine (HME). With MgO modifier, the selectivity to HMD increased. Conversion was found to decrease significantly when the Ni loading was decreased but this had no effect on the product distribution or selectivity. With a reduction in the reaction temperature the conversion rate falls and selectivity to HMD also falls due to an increase in the production of hexamethyleneimine.

The crystallized Ni-B/SiO<sub>2</sub> catalyst has lower conversions and HMD selectivities, large amounts of hexamethyleneimine are formed and 6-aminohexanenitrile which cause the low levels of HMD. Ni/SiO<sub>2</sub> catalysts have higher conversions but lower selectivity to HMD than this crystallized catalyst and unlike the NiB/SiO<sub>2</sub> catalyst, a rise in reaction temperature is coupled to a rise in hexamethyleneimine formation.

The Ni-B/SiO<sub>2</sub> amorphous catalyst shows no significant change in selectivity and conversion after 72 hours, unsupported Ni-B catalysts shows an abrupt decrease in both factors after only 7 hours. This is due to the high temperature reached because adiponitrile hydrogenation is an exothermic process. The supported catalyst is thermally stabilized and lasts longer.

The formation of aminocapronitrile was found to be strongly dependent on the activity of the catalyst. The Ni-B/SiO<sub>2</sub> and Ni-B/ SiO<sub>2</sub>-MgO amorphous catalysts proved to have high activity due electronic interactions of Ni and alloying B in the amorphous state. Loading of Ni had no significant effect. Activity of Ni sites was found to decrease with decrease in reaction temperature causing increased formation of aminocapronitrile.

It was proposed that the by-product is formed by the reaction shown in fig 1.5 [38]

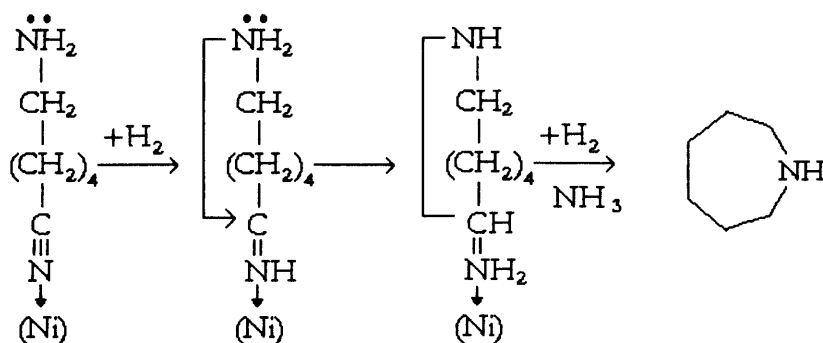


**Figure 1.5 – Formation of hexamethylenimine (side product) over Ni catalyst [38]**

Electron deficient Ni sites could polarize the cyano group making the carbon more electropositive and susceptible to attack. The B atoms in the mixed catalysts donate electrons to the Ni causing less hexamethylenimine formation. Decomposition of the Ni-B alloy in the crystalline form accounts for increased formation of the cyclic by-product and decrease in formation of HMD. MgO acts as an electron donor and could be responsible for inhibiting hexamethylenimine formation in the catalyst with mixed support.

### *Ni-MgO catalysts*

Ni, Co and ruthenium are the most widely used catalysts for primary amine formation [39]. Serra et al. [39] investigated Ni-MgO catalysts for the hydrogenation of adiponitrile. Nickel-magnesia catalysts had previously been shown to have high activity for the hydrogenation of the dinitrile 1,4-butanedinitrile [40]. In comparison with a bulk NiO catalyst they showed higher selectivities and conversions to primary amine. The basicity of the MgO support encouraged desorption of amine products and discourages

condensation reactions, thus preventing catalyst deactivation. Ammonia was not required to suppress by-product formation as the basic support was sufficient. Highest selectivity to 4-aminobutanenitrile 85% was reached at full conversion at reaction temperature of 343K and  $13,000\text{h}^{-1}$  space velocity.

Two Ni-MgO catalysts were produced and compared with Raney Nickel for the hydrogenation of adiponitrile. The different preparation methods of the two catalysts resulted in one containing a solid solution phase of Ni with Mg, detected by XRD. Raney nickel had higher surface area than either of the NiO-MgO catalysts. Catalyst A was prepared by thermal decomposition of  $\text{Ni}(\text{NO}_3)_2 \cdot 6\text{H}_2\text{O}$  and MgO then calcined in static air. The NiO and MgO phases are able to interact stronger than catalyst B. Catalyst B was prepared by controlled thermolysis of  $\text{Ni}(\text{NO}_3)_2 \cdot 6\text{H}_2\text{O}$  at 373K for 14 days producing  $\text{Ni}_3(\text{NO}_3)_2(\text{OH})_4$ , which is then mixed with MgO and calcined under flowing argon at 523K. An XRD study of calcination temperature and its effect on Ni/MgO catalysts was undertaken by Arena et al. [41]. This makes diffusion between NiO and MgO phases difficult.

XRD patterns show that precursors for catalyst A exhibit solid solution phase due to the closer interaction between NiO and MgO phases. This catalyst has a larger surface area than catalyst B which was accredited to a higher sintering effect in the sample not having formed solid solution.

After reduction Raney nickel and catalyst B show metallic nickel phase only and the degree of reduction,  $\alpha=1$ . Catalyst A shows an XRD diffraction pattern for Ni metal and NiO-MgO solid solution, at a degree of reduction,  $\alpha=0.71$ . It has smaller Ni crystallite size than catalyst B and a higher surface area, both due to lower sintering. The partial

agglomeration of particles in catalyst B can be seen in SEM images compared before and after reduction of catalytic precursors.

By-products such as dimers are formed, by intermolecular amine-imine condensation reactions. The basic nature of the MgO support favours elimination of amines and so could prevent secondary reactions. Raney Nickel has high catalytic activity so favours hydrogenation of intermediates rather than condensations. The higher metallic area of Raney-Ni and catalyst A cause higher amounts of cracking products. The scheme for formation of all products proposed in this paper illustrates a dependence on hydrogen concentration for certain products to form.

1,6-hexanediamine requires similar amounts of hydrogen to the cyclisation products and therefore these reactions compete. All three catalysts showed high selectivity to the diamine. Formation is favoured at high H<sub>2</sub>/adiponitrile ratios and at lower reaction temperatures. Higher reaction temperatures can cause cyclisation and cracking products.

Lowest hydrogen consumption is required for the production of 6-aminohexane. At low reaction temperatures less hydrogen is available so hemi hydrogenated products are favoured. The presence of octahedral crystals in the catalysts A and B may be the reason for higher selectivities to aminocapronitrile.

Selectivity to 1,6-hexanediamine is high for all catalysts. Catalyst A at 363K and full conversion produced 96% selectivity for 1,6-hexanediamine. This may be due to the solid solution phase. The Ni-MgO catalysts showed higher selectivity to aminocapronitrile than the Raney-Ni catalyst. For catalysts A and B a drop in the reaction temperature and H<sub>2</sub>/ADN ratio favours hemi-hydrogenation. This high

selectivity could also be due to the presence of octahedral crystallites which may be the active sites for monoamine production. Highest selectivities (38% and 77%) and conversions (87% and 85%) were found for catalysts A and B at 383K, H<sub>2</sub>/ADN ratio of 100/2 and a space velocity of 10242h<sup>-1</sup>. Arena et al. [42] also investigated Ni/MgO and considered the promoting effect of alkali metal inclusion.

### *Ziegler-Sloan-Lapport catalysts*

Nickel, Cobalt and Ruthenium are investigated along with bimetallic Ziegler-Sloan-Lapport catalysts for the hydrogenation of adiponitrile to hexamethyldiamine in a paper by V. Balladur et al [43]. The bimetallic catalysts were NiCr, NiTi and CoFe. The paper also discusses the effect of water and dopants on the hydrogenation reaction selectivity and activity.

Mild reaction conditions were used, 20 bar pressure H<sub>2</sub>, 120°C-180°C. No ammonia was required in this reaction as would have been used in a Raney nickel catalyst reaction to minimise side reaction products and secondary amines. Activity measurements were made in terms of hydrogen consumption and quoted as mmole of H<sub>2</sub>/g of catalyst/s. Selectivity measurements were made using internal standard of undecane in isopropanol and analysed by GC with an FID detector.

Water was found to significantly reduce selectivity to the primary amine. Water content of the precursor salts and solvent water concentration significantly increased the production of secondary amine side products and therefore reduced the hexamethyldiamine production. Doped catalysts showed far less vulnerability to water.

Another effect noted was that water reacts with alkylaluminium residues from the catalyst precursor materials to eventually form alumina, which is a known promoter for secondary and tertiary amine formation.

Monometallic catalysts showed a trend in activities decreasing from Ni, Co to Ru and a reverse effect on selectivities so for example Ruthenium was highly selective but poorly active. Results for the Ni and Co based catalysts doped with Fe, Cr and Ti showed that the selectivity was improved but at cost of a lowered activity. Dopant/Ni ratio does not have a big effect on activity and selectivity, levels even out at a low dopant concentration.

Activity increases with increased temperature for all the catalysts studied, implying durability of the catalyst. Selectivity to HMD increased for Ni based catalysts with increased temperature but the opposite occurred for Co based catalysts.

#### 1.4.5. Lamellar Double Hydroxides (LDH)

Lamellar double hydroxides were shown to be of use in gas-phase hydrogenation of acetonitrile. Increasing the Mg content of the LDH was found to decrease the reducibility of Ni and the amount of residual acid sites [44, 45, and 46]. Acid sites were said to be responsible for coupling reactions resulting in by-product formation and the target product was formed on the metal sites in a dual-functional mechanism as proposed by Verhaak et al [47]. Due to these two antagonistic effects they found an optimum Mg content for the catalyst where  $(\text{Mg}/(\text{Mg}+\text{Ni}))=0.23$  for which the selectivity to the primary amine mono-ethylamine was 92.6% at 99% acetonitrile conversion [44].

Thermal treatment of catalysts prepared from LDH precursors was investigated as reduction and calcination temperature was found to affect the acid-base characteristics of the support and the electron density of the Ni active sites [48]. A low ratio of weak Brønsted sites to basic sites was found to be optimal for selectivity to mono-ethylamine. This was found for catalysts prepared by calcination at 623K and reduction at 723K for which 94.6% selectivity was achieved at a conversion of 47%. The selectivity fell at higher conversions reaching 92% selectivity at 99% conversion [48]. They concluded that the increased selectivity was due to increased basicity of support and not to change in electron density of Ni active sites.

Lamellar double hydroxides containing  $\text{Ni}^{2+}/\text{Mg}^{2+}/\text{Al}^{3+}$  were studied for catalytic activity in the half-hydrogenation of adiponitrile [49]. Various compositions of a catalyst prepared by co-precipitation of an aqueous solution containing  $\text{Ni}(\text{NO}_3)_2 \cdot 6\text{H}_2\text{O}$ ,  $\text{Mg}(\text{NO}_3)_2 \cdot 6\text{H}_2\text{O}$  and  $\text{Al}(\text{NO}_3)_3 \cdot 9\text{H}_2\text{O}$  with a solution of NaOH which was added drop wise at 293K under stirring were used. This results in  $\text{Ni}^{2+}/\text{Mg}^{2+}(\text{Al}^{3+})\text{O}$  phase.

XRD showed the samples to be well-crystallised LDH structures with no excess phase present.  $\text{Ni}^{2+}$  cations were isomorphously substituted for  $\text{Mg}^{2+}$  in the layers of the LDH structure. Before calcination the surface area is low, this increases on thermal treatment at high temperatures. The highest surface area was found in the catalyst named AR5 in which  $(\text{Mg}/\text{Mg}+\text{Ni})=0.20$ . Mixed oxide phases and spinel-like phases are present and their relative amounts vary with varying chemical composition. The AR5 catalyst has the best compromise between these phases resulting in its high surface area.

Temperature programmed reduction showed that as the Mg content increased, the reduction of  $\text{Ni}^{2+}$  to  $\text{Ni}^0$  occurred at higher temperatures. Degree of Ni reduction varies from 62% in a sample of high Mg content to 93% in the Mg free sample. Chemisorption of  $\text{H}_2$  was used to show the accessibility of  $\text{Ni}^0$  phases at 823K, which was the temperature that the reaction occurs at. This was found to be a maximum for the sample AR5 with 10% accessibility.

The target molecule for the catalytic experiments was ACN; HMD, ACH and longer chain amines were the main by-products. This agreed with previous reaction schemes suggested as can be seen in figure 1.4. An inorganic base KOH was present in the reaction medium to improve selectivity to aminonitrile. KOH is thought to neutralise some acid sites responsible for condensation reactions. In the absence of KOH, a transimination reaction occurs, forming cyclic ACH. The optimum concentration of KOH required in this reaction was the same as has been reported for the Raney nickel catalyst.

The catalyst is reactivated in  $\text{H}_2$  pressure with HMD, water and KOH. This step was investigated and selectivity to ACN was found to increase with increased reactivation pressure but found an optimum temperature for reactivation of 423K. After reactivation, two phases are present, Ni metal and  $\text{Mg}(\text{Al})\text{O}$  periclase-type phase with varying amounts of Ni substituted for Mg depending on the sample composition. The degree of LDH structure reconstruction was considered. LDH structure can be reconstructed by rehydroxylation of the mixed oxide phase in an aqueous solution; this is more difficult for the Ni-containing mixed oxides than for the Mg-containing mixed oxides. The impact on ACN hydrogenation has been investigated for the AR5 catalyst. It was found that selectivity to ACN improved with in-situ reactivation. XRD patterns showed that LDH

reconstruction had taken place during the reactivation stage. The optimum reactivation temperature was found to be 423K resulting in highest selectivities to ACN. An optimum quantity of water was found to be 9.6 vol%. H<sub>2</sub>O was found to promote selectivity by reconstruction of LDH phase and formation of a hydrophilic interface at the metal surface, making desorption of ACN easier, thus reducing the number of molecules further hydrogenated to hexamethyldiamine.

Transamination reactions take place both on the acid sites in the support and on the metal sites in a bi-functional mechanism [47]. These reactions result in by-products and less aminocapronitrile. Mg present in the catalyst increases the number of acid sites but decreases their strength [44]. High electron density of Ni in the AR5 sample is thought to be the reason for its high selectivity to ACN, as it allows for faster desorption of ACN. This is found by IR spectroscopy of adsorbed CO.

#### *1.4.6. Ruthenium-Cobalt Catalysts*

The synergistic effect of ruthenium and cobalt together has been studied by Iglesia et al. [51]. They investigated Ru-Co/TiO<sub>2</sub> and on SiO<sub>2</sub>. Ru was seen to reduce the temperature of reduction for Co in Ru-Co catalysts precursors. This implies that the two metals are in intimate contact. In this paper the catalyst was being investigated for action in Fischer-Tropsch synthesis. It was found that the presence of Ru also inhibited the formation of carbon deposits from CO/H<sub>2</sub> mixtures.

There are two identifiable steps in the reduction of  $\text{Co}_3\text{O}_4/\text{TiO}_2$  precursors that can be identified by differential thermal gravimetric analysis (DTG). The step converting  $\text{Co}_3\text{O}_4$  to  $\text{CoO}$  was strongly affected by Ru, the second step of  $\text{CoO}$  conversion to  $\text{Co}$  was effected but to a lesser extent.  $\text{Co-Ru}/\text{TiO}_2$  requires high temperature calcinations treatments to allow close contact between the two metal components. After calcinations at 673K, the precursor reduction temperature was the same as the mono-metallic catalyst. After high temperature calcinations at 773-823K the reduction temperature was much lower. Oxidation is suggested to enhance the interactions between Co and Ru. Oxidation produces highly mobile Ru oxides and Ru-Co oxides. A  $\text{Co}_2\text{RuO}_4$  spinel isostructural with  $\text{Co}_3\text{O}_4$  is produced. Solid solutions of  $\text{Co}_{3-x}\text{Ru}_x\text{O}_4$  can form on the surface of  $\text{Co}_3\text{O}_4$  crystallites during calcination.

SEM micrographs show that after calcination, Ru is found present only along with Co within large metal particulates. Ru present in other areas is undetectable. In samples not calcined before reduction, there is no Ru found in the Co crystallites. EXAFS shows the Co fraction in the first Ru coordination shell increases from about 0.3 to 0.48 as calcination temperature increases from room temperature to 773K. This proves there is improved mixing. Dispersion of large Co particles is apparently unaffected by calcination. Along with the mixing process, creating oxidised species at high temperatures also causes sintering.

Chemisorption of  $\text{O}_2$  at room temperature after reduction shows that the Ru species have migrated inwards away from the surface of the catalyst. Less  $\text{O}_2$  is chemisorbed than before and this is because Ru atoms have gone in to the large Co crystallites.

Bimetallic synergy is also observed on Co-Ru/SiO<sub>2</sub>. Addition of Ru to a Co/SiO<sub>2</sub> catalyst increases the cobalt activity by a factor of almost two without increasing cobalt dispersion. Selectivity to C<sub>5+</sub> in the Fischer-Tropsch synthesis increases from 82% to 86.1% with Ru addition. Calcination is also required to induce the observed bimetallic synergy.

These ruthenium-cobalt supported catalysts have been found to be highly active for adiponitrile hydrogenation. Kusaka et al [52] investigated the nitrile group hydrogenation by supported and unsupported ruthenium-cobalt catalysts. The support used was SiO<sub>2</sub>, which is known to be a structural promoter in iron-based catalysts used in the production of ammonia. It increases the number of surface sites in the fresh catalyst [51]. A synergistic effect is thought to exist between the two metals which are both active for hydrogenation [51].

Supported RuCo catalyst showed only a reduction stage for Ru(II) reduction, no Co(II) reduction was found. Co species supported by SiO<sub>2</sub> were found to be less reducible [52]. Co in the Co(OH)<sub>2</sub> and CoCO<sub>3</sub> species was found to be reducible under similar conditions.

Co(II) in the unsupported Ru(OH)<sub>x</sub>/Co(OH)<sub>y</sub> catalyst was easily reduced to Co<sup>0</sup> even at 473K. The ruthenium enhances the reducibility of the Co lowering its reduction temperature. As the Ru content increases the Ru reduction temperature increases and the Co reduction temperature decreases.

## 1.5. References

1. Augustine, Robert L., **Heterogeneous Catalysis for the Synthetic Chemist.** (Marcel Dekker, Inc, 1996)
2. G. C. Bond, **Heterogeneous Catalysis - Principles and Applications.** (Oxford Scientific Productions, 1987)
3. Solymosi, F.; Tombácz, I.; Koszta, J. **Journal of Catalysis** 1985, **95**, 578
4. Bond, G. C. **Accounts of Chemical Research** 1993, **26**, 490
5. Raney, M. **Method of Producing Finely-Divided Nickel.** US 1628190, 1927
6. Orchard, J. P.; Tomsett, A. D.; Wainwright, M. S.; Young, D. J. **Journal of Catalysis** 1983, **84**, 189
7. . Nickel aluminide MSDS. **Electronic Space Products International (1994)**, Last retrieved January 25, 2006
8. Gavroy, D.; Joly-Vuillemin, C.; Cordier, G.; Fouilloux, P.; Delmas, H. **Catalysis Today** 1995, **24**, 103
9. Joly-Vuillemin, C.; de Bellefon, C.; Delmas, H. **Chemical Engineering Science** 1996, **51**, 2149
10. Li, H.; Xu, Y.; Deng, J.-F. **New Journal of Chemistry** 1999, **23**, 1059
11. Matthieu, C.; Dietrich, E.; Delmas, H.; Jenck, J. **Chemical Engineering Science** 1992, **47**, 2289
12. Yu, X.; Li, H.; Deng, J.-F. **Applied Catalysis A: General** 2000, **199**, 191
13. Hwang, C.-P.; Yeha, C.-T.; Zhu, Q. **Catalysis Today** 1999, **51**, 93

14. Kusama, h.; Bando, K. K.; Okabe, K.; Arakawa, h. *Applied Catalysis A: General* 2001, **205**, 285
15. Weng, W.-Z.; Peia, X.-Q.; Lia, J.-M.; Luo, C.-R.; Liua, Y.; Lina, H.-Q.; Huang, C.-J.; Wan, H.-L. *Catalysis Today* 2006, **111**, 53
16. Wu, T.; Yanb, Q.; Maoa, F.; Niua, Z.; Zhanga, Q.; Lia, Z.; Wan, H. *Catalysis Today* 2004, **121**, 93
17. Huang, Y.; Sachtler, W. M. H. *Applied Catalysis A: General* 1999, **182**, 365
18. Huang, Y.; Sachtler, W. M. H. *Journal of Catalysis* 1999, **188**, 215
19. Alini, S.; Bottino, A.; Capannelli, G.; Carbone, R.; Comite, A.; Vitulli, G. *Journal of Molecular Catalysis A: Chemical* 2003, **206**, 363
20. Hou, Z.; Yashima, T. *Catalysis Letters* 2003, **89**, 193
21. Huang, Y.; Sachtler, W. M. H. *Journal of Catalysis* 1999, **184**, 247
22. Mares F, Galle, J E, Diamond S E, Regina F J, *Journal of Catalysis* 1988, **112**, 145-156
23. Allied Corporation, US Patent 489348 (1983)
24. Pellegatta, J.-L. et al. *Journal of Molecular Catalysis A: Chemical* 2002, **178**, 55-61
25. Alini, S.; Bottino, A.; Capannelli, G.; Comite, A.; Paganelli, S. *Applied Catalysis A: General* 2005, **292**, 105
26. Fierro, J. L. G., Medina, F., Salagre P. & Sueiras J. E. *Journal of Molecular Catalysis*, 1990, **61**, 197-205
27. Medina, F.; Salagre, P.; Fierro, J. L. G.; Sueiras, J. E. *Journal of Catalysis* 1993, **142**, 392-405

28. Medina, F.; Salagre, P.; Sueiras, J. E.; Fierro, J. L. G. *Journal of Molecular Catalysis* 1991, **68**, L17-L20.
29. Medina, F.; Salagre, P.; Sueiras, J. E.; Fierro, J. L. G. *Applied Catalysis A: General* 1993, **99**, 115-129
30. Medina, F.; Salagre, P.; Fierro, J. L. G.; Sueiras, J. E. *Journal of the Chemical Society Faraday Transactions* 1993, **89**, 3507-3512
31. Medina, F.; Salagre, P.; Sueiras, J. E.; Fierro, J. L. G. *Journal of the Chemical Society Faraday Transactions* 1993, **89**, 3981-3986
32. Medina, F.; Salagre, P.; Fierro, J. L. G.; Sueiras, J. E. *Journal of the Chemical Society Faraday Transactions* 1994, **90**, 1455-1459
33. Salagre P, Fierro J.L.G, Medina F & Sueiras J.E., *Journal of Molecular Catalysis A: Chemical*, 1996, **106**, 125-134
34. Wang, W.; Li, H.; Li, H.; Li, Y.; Deng, J. F. *Applied Catalysis A: General* 2000, **203**, 301
35. Wang, W.; Qiao, M.-H.; Yang, J.; Xie, S.; Deng, J. F. *Applied Catalysis A: General* 1997, **163**, 101
36. Wang, W.; Qiao, M.-H.; Li, H.; Dai, W.-L.; Deng, J. F. *Applied Catalysis A: General* 1998, **168**, 151
37. Xie, S.; Li, H.; Li, H.; Deng, J. F. *Applied Catalysis A: General* 1999, **189**, 45
38. Hexing Li, Yeping Xu, Hui Li, Jing Fa Deng, *Applied Catalysis A: General*, 2001, **216**, 51-58
39. Serra M, Salagre P, Cesteros Y, Medina F, Sueiras J.E, *Journal of Catalysis*, 2002, **209**, 202-209

40. Serra M, Salagre P, Cesteros Y, Medina F, Sueiras J.E, *Journal of Catalysis*, 2001, **197**, 210-219
41. Arena, F.; Frusteri, F.; Parmaliana, A.; Plyasova, L.; Shmakov, A. N. *Journal of the Chemical Society Faraday Transactions* 1996, **92**, 469
42. Arena, F.; Frusteri, F.; Parmaliana, A. *Applied Catalysis A: General* 1999, **187**, 127
43. Balladur, V., Fouilloux, P. Bellefon, C. d. *Applied Catalysis A: General*, 1995, **133** 367-376
44. Medina Cabello, F.; Tichit, D, Coq B, Vaccari A, Thy Dung N.. *Journal of Catalysis* 1997, **167**, 142-152.
45. Medina Cabello, F., Duartre R, Tichit D, Coq B, Dung N.T, Salagre, P & Sueiras J. E *Journal of Molecular Catalysis A: Chemical*, 1997, **119**, 201-212.
46. Cordier, G.; Popa, J.-M. Metallic compounds useful as catalysts. In US **6005145**, 1999
47. Verhaak M.J.F.M, van Dillen A.J, & Geus J.W, *Catalysis Letters* 1994, **26**, 37-53.
48. Dung N.T, Tichit D, Chiche B.H& Coq B, *Applied Catalysis A: General* 1998, **169**, 179-187
49. Tichit, D.; Durand, R.; Rolland, A.; Coq, B.; Lopez, J.; Marion, P. *Journal of Catalysis* 2002, **211**, 511-520.
50. Medina, F.; Salagre, P.; Sueiras, J. E.; Fierro, J. L. G. *Journal of Molecular Catalysis* 1991, **68**, L17-L20
51. Iglesia E, Soled S.L, Fiato R.A & Via G.H, *Journal of Catalysis*, 1993, **143**, 345-368
52. Kusaka, H.; Hara, Y.; Onuk, M.; Akai, T.; Okuda, M. *Journal of Catalysis*, 1996, **161**, 96-106.

*Chapter 2*

EXPERIMENTAL

---

## **2. EXPERIMENTAL TECHNIQUES**

---

This chapter describes the experimental procedures used in this project. The method of catalyst preparation is detailed for each catalyst used. Methods of characterising these catalysts and their precursors involve instrumentation which is schematically described along with a brief explanation of the background theory. Catalyst testing equipment is briefly described here although this is gone in to in more detail in Chapter 3. The product analysis equipment is also discussed here.

### **2.1. Catalyst Preparation**

Catalysts have been prepared on a variety of supports using a variety of methods. The main method of preparation used was incipient wetness. Incipient wetness describes the impregnation of the support when the active elements are contained in a volume of solution corresponding to the pore volume of the support. The procedure has also been referred to as pore volume impregnation or dry impregnation. [1] The catalyst prepared for use in the trickle-bed reactor must be made on large particles to allow flow through the trickle-bed reactor. For this purpose granulated supports and extrudates have been used. The supports used were two different silica, SP874905 and SP189725 and alumina extrudates in the form of trilobes provided by Johnson Matthey. For use in the autoclave it is possible to use powdered supports.

2.1.1. Nickel on silica

Ni/SiO<sub>2</sub> catalysts have been prepared by an incipient wetness technique [2] following a method by Li et al [3]. Low loading catalysts were prepared following this method. Fumed silica was impregnated with nickel so there is 0.010g of nickel to every gram of SiO<sub>2</sub>. Pore volume for the fumed silica was not known and so the amount of water required to form a paste was measured by adding water drop wise to the support until wetness was observed. This volume was found to be 10ml water per g SiO<sub>2</sub>. This volume of water when added to the powdered support forms a paste taken as the point of incipient wetness. This was then dried in an oven over night and then reduced at 600°C for 6 hours in a tube furnace under 5% H<sub>2</sub>/Ar. Using this same method 20% loading Ni catalysts were also prepared on fumed silica. In order to produce 20% loading Ni/SiO<sub>2</sub> with nickel nitrate hexahydrate it is necessary to do two impregnation and drying steps as the required amount of nickel nitrate hexahydrate would not dissolve in to the volume of water required to fill 90% of the pores of SiO<sub>2</sub>.

The NiSiO<sub>2</sub> reduction temperature has been ascertained using the TPR method. Reduction was complete by 600°C. The influence of the experimental set up for the of reduction has also been investigated. Initially reduction was done in a tube furnace with flowing 5% H<sub>2</sub>/Argon flowing over the catalyst precursors which were placed in a quartz boat in the furnace. Later on in the project it was considered that full reduction had not taken place so other methods of reduction were investigated. Passing gas through the sample instead of over the sample was looked at. This was initially done in the TPR tube as a model for reduction in-situ in the reactor tube.

2.1.2. Rhodium catalysts – 5%Rh/SiO<sub>2</sub>, 5%Rh/Al<sub>2</sub>O<sub>3</sub> and 5%Rh/Graphite

Rhodium catalysts have been prepared using rhodium chloride on two types of granulated silica and on alumina trilobes. The rhodium chloride was weighed out to provide 5% rhodium by weight of the total weight of the intended catalyst. For a 100g batch of catalyst 5g of rhodium was required thus 11.7426g rhodium (II) chloride was weighed out. To obtain 95g of silica support 100g had to be weighed out in order to take in to account the wetness of the given support. The alumina support was assumed to be dry. The rhodium salt was dissolved in to an appropriate amount of deionised water in order to fill 90% of the pores according to the relevant pore volume. For the granulated silica (SP874905) provided by Johnson Matthey pore volume was known to be 0.9cm<sup>3</sup>/g so in order to fill the pores 90g water per g of catalyst is required and to fill 90% of the pores 81g water per g of catalyst. For granulated silica (SP189725) pore volume was known to be 1.2cm<sup>3</sup>/g and 90ml solution was pored over the support in a mechanical tumbler and tumbled to ensure even absorption of the solution. These were then dried in a 60°C oven followed by reduction at 250°C in a vertical tube furnace under flowing 5%H<sub>2</sub> in N<sub>2</sub> for two hours.

2.1.3. Nickel and Cobalt catalysts – 5%Ni/Al<sub>2</sub>O<sub>3</sub>, and 5%Co/Al<sub>2</sub>O<sub>3</sub>

Nickel and Cobalt catalysts have been prepared by dry impregnation following a similar method to that described above. Catalysts were prepared using the nitrates and chlorides of both metals and have been prepared using two different methods. Firstly both metals

have been used in a straight forward incipient wetness preparation and another set of catalysts have been prepared using both sets of the metals in an incipient wetness technique incorporating a precipitation step.

Both preparations involve impregnating the support with a solution containing appropriate amounts of the metal salt while tumbling in the mechanical stirrer as before. The incipient wetness with precipitation method then involves adding 1M solution of NaOH to the drum and mixing for 10 min. This is followed by two washings with water and then the products from both preparation methods are dried at 100°C overnight. All the samples are then calcined at 350°C and reduced at 250°C under 5% H<sub>2</sub>/Ar.

#### 2.1.4. Mixed metal catalysts -- 2.5%-2.5%Rh-Co/Al<sub>2</sub>O<sub>3</sub> and 2.5%-2.5%Rh-Ni/Al<sub>2</sub>O<sub>3</sub>

The mixed metal catalysts were prepared using rhodium (II) chloride and either cobalt nitrate or nickel nitrate. The catalysts were made using the method above where the total metal loading was made to be 5%/wt consisting of a 2.5%/wt contribution from each metal. These catalysts were tumbled in solution as described above and then dried at 100°C, and reduced at 250°C in a tube furnace under flowing 5% H<sub>2</sub>/Ar.

## 2.2. Characterisation

The characterisation techniques described here include temperature programmed reduction (TPR), surface area determination by the Brunauer, Emmett and Teller (BET) method, powder X-ray diffraction (XRD), atomic absorption spectroscopy (AAS) and scanning electron microscopy (SEM).

### 2.2.1. *TPR analysis*

Temperature programmed reduction is a technique in which the number of reducible species can be determined and the temperature of reduction can be measured. For a sample to be suitable for TPR analysis it need only have reducible species present.

Temperature programmed reduction was done using an Autochem 2910 analyser. Powdered and granulated samples (0.1- 0.5g) are loaded in to a quartz glass U-tube resting on glass wool. A thermocouple sits in the sample and detects the temperature. This tube is held within a temperature-controlled oven and sealed allowing gases to pass over as it is heated. In the TPR reaction firstly the sample is oxidised in 2-5% O<sub>2</sub>/He then for the reduction stage 10% hydrogen in argon gas mixture is passed through the sample while the temperature is increased in a linear ramp the ramp rate used can effect clarity of data. A ramp rate of 10°C/min was used. Changes in thermal conductivity of the exiting gas are measured and indicate the change in the composition of the gas mixture which can be quantified. Changes in the composition of the gas with respect to hydrogen indicate reduction taking place.

### 2.2.2. BET surface area analysis

Many different procedures can be used to gain an understanding of the surface area of a catalyst [4]. In order to ascertain the surface area of the catalysts the Bruauer, Emmett and Teller Method [5] was employed. In this method the physisorption of  $N_2$  gas is measured over a range of temperatures. The Micrometrics Gemini was used and samples were degassed for 45 min at  $150^\circ\text{C}$  in nitrogen prior to analysis. The sample ( $\sim 0.1\text{g}$ ) is contained in a  $\frac{1}{4}$ " BET tube and inserted in to the machine where a similar tube is also held as an empty reference. Both tubes are filled with nitrogen and submerged in a Dewar containing liquid nitrogen. The pressure is then increased so that nitrogen liquefies and creates a monolayer on the surface of the catalyst. Monolayer formation can be shown in figure 2.1 as point B. Only in samples in which monolayer coverage can be attained is the BET method applicable. In the BET experiment pressure,  $P$ , is measured relative to the saturated vapour pressure of the probe gas,  $P_0$ . Type II isotherms (figure 2.1a) occur in nonporous structures or macroporous materials [6]. Type IV (figure 2.1b) are relevant to mesoporous substances in which further rapid increase in adsorption occurs at higher values of  $P/P_0$  where capillary condensation is occurring [7].

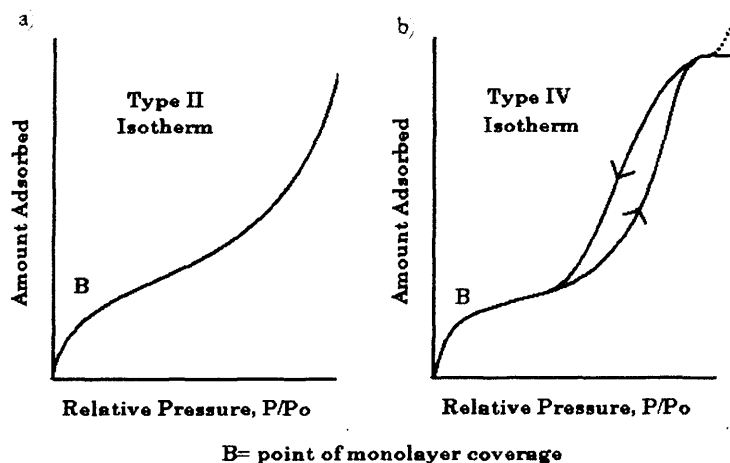


Figure 2-1 - Absorption isotherms indicating point of monolayer coverage

The volume of nitrogen required to create monolayer coverage is equal to the surface area and monolayer capacity can be calculated by use of the BET equation (Eq1, Eq2).

$$\frac{P}{V_a(P_0 - P)} = \left[ \frac{(C - 1)}{(V_m C)} \right] \frac{P}{P_0} + \frac{1}{V_m C} \quad (\text{Eq1})$$

$$\frac{P}{P_0} = \text{Relative Pressure} = \frac{\text{Pressure}}{\text{Saturated Vapour Pressure}} \quad (\text{Eq2})$$

$V_a$  = Volume adsorbed

$V_m$  = Monolayer Capacity

$C$  = BET constant

The adsorption isotherm is created and from this the surface area can be calculated using the following equation (Eq3).

$$\text{Surface Area} = \frac{V_m N_a}{M V_0} \quad (\text{Eq 3})$$

Surface Area =  $V_m \sigma N_a / M V_0$

$V_m$  = Monolayer Capacity

$N_a$  = Avogadro's Number

$M$  = Mass of Sample

$V_0$  = Molar Volume of Gas

The Micrometrics Gemini BET surface area machine was connected to a computer and the software carried out these calculations.

2.2.3. *XRD analysis*

Powder X-ray diffraction has been used for identification of phases and crystallinity for many of the catalyst and precursors used. In order for a substance to be identified by XRD it must be crystalline and the crystals must be of sufficient crystallite size for the X-ray radiation to be diffracted. A schematic diagram of the X-Ray diffractometer [8] is shown in figure 2.2.

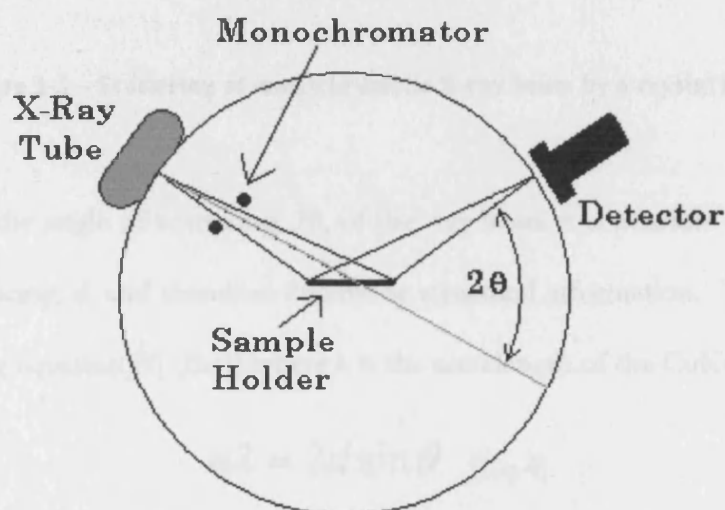


Figure 2-2 – Powder X-Ray Diffractometer

In the X-Ray tube Cu  $K\alpha$  radiation is produced by bombarding the copper metal source with high energy electrons which cause an electron hole to form in the k shell which is immediately filled with an electron from the L shell accompanied by emission of an X-ray quantum. This beam is then focused through a monochromator in order to emit a single wavelength of radiation in phase. This monochromatic beam is diffracted by the atoms arranged in a periodic lattice within the crystal as show in figure 2.3.

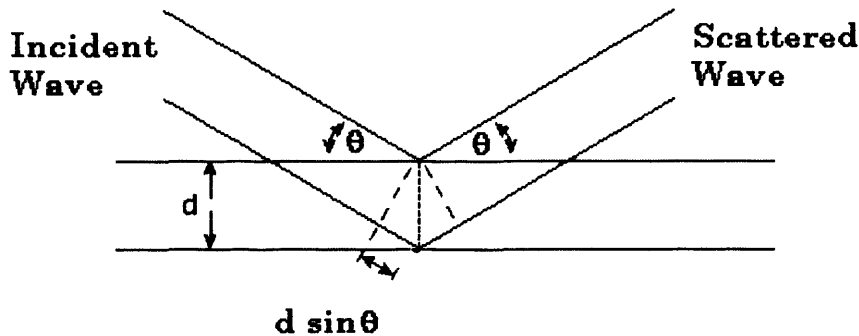


Figure 2-3 – Scattering of monochromatic X-ray beam by a crystal lattice.

By measuring the angle of scattering,  $2\theta$ , of the X-ray beam it is possible to determine the inter lattice spacing,  $d$ , and therefore determine structural information. This is calculated using the Bragg equation [9] (Eq4) where  $\lambda$  is the wavelength of the  $\text{CuK}\alpha$  radiation.

$$n\lambda = 2d \sin \theta \quad (\text{Eq 4})$$

XRD analysis is done using an Enraf Nonius FR590 X-ray generator emitting  $\text{Cu } k_{\alpha}$  radiation and the diffracted X-ray beam detected by a fixed arc detector in the range of  $4^{\circ}$  to  $124^{\circ}$ . Powdered samples are loaded in to an aluminium plate and spun through  $360^{\circ}$  during analysis.

Powder patterns are interpreted by comparing with data from the JCPDS database of known substances. Peaks can be attributed to crystal structure reflections, which can then be assigned to known phases.

### 2.2.4. Atomic Absorption Spectroscopy

Atomic absorption spectroscopy (AAS) is a method of determining the concentration of certain elements in a solution. Figure 2.4 shows the schematic diagram of the Atomic Absorption Spectrometer.

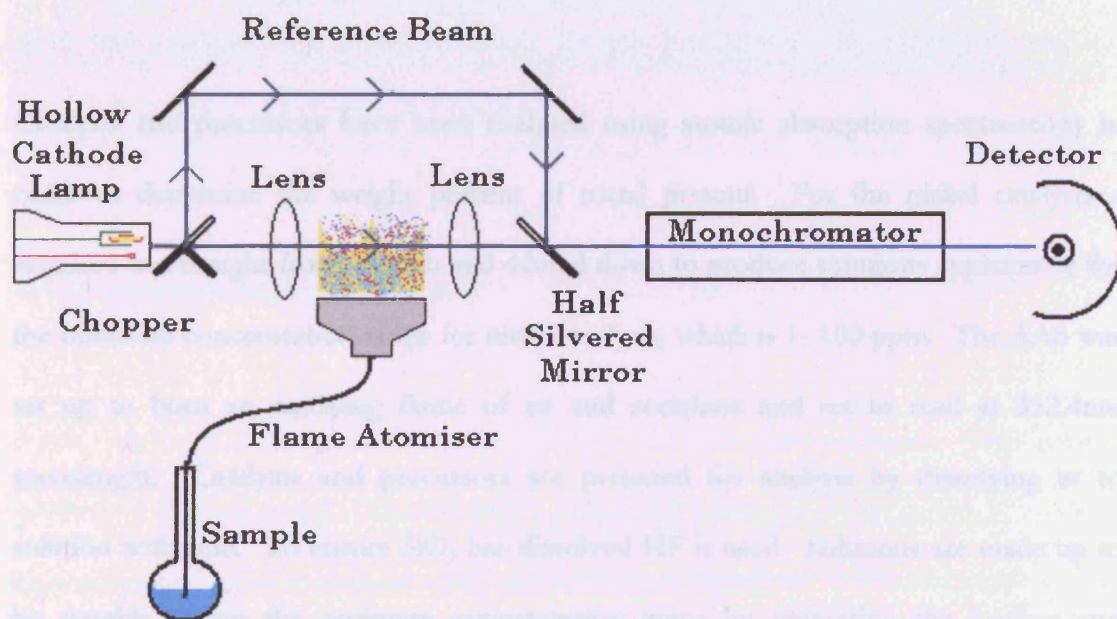


Figure 2-4 - Atomic Absorption Spectrometer

Every element absorbs radiation at certain characteristic wavelengths relating to the energy required to excite one outer electron from the ground state to one of the possible excited states. The solution must be atomised so that a mist of gaseous ions or elementary ions are created. These then absorb energy at their characteristic wavelength and this absorbance is measured. The hollow cathode lamp is used to produce the radiation required. These consist of a cylindrical cathode and a tungsten anode. The cathode is made of, or coated with, the analyte metal and these are contained within a

glass tube filled with neon or argon. A large potential of about 300V is created producing argon or neon cations and anions which strike the cathode in a process called sputtering. The sputtered atoms are excited and on returning to the ground state they emit radiation. The radiation emitted is equal to the energy required to raise an outer electron from the ground state to one of the excited states. This value is specific for each element and there can be a few transitions possible so a few wavelengths may be selected for each elements analysis.

Catalysts and precursors have been analysed using atomic absorption spectroscopy in order to determine the weight percent of metal present. For the nickel catalysts a standard was bought from Aldrich and diluted down to produce solutions appropriate for the optimum concentration range for nickel analysis, which is 1- 100 ppm. The AAS was set up to burn an oxidising flame of air and acetylene and set to read at 352.4nm wavelength. Catalysts and precursors are prepared for analysis by dissolving in to solution with acid. To ensure  $\text{SiO}_2$  has dissolved HF is used. Solutions are made up to be roughly within the optimum concentration range by estimating the loading and calculating appropriate amounts to dissolve.

## 2.3. Catalyst Testing

For catalyst testing three reactors were used. A fixed-bed flow reactor was used for gas-phase flow reactions, an autoclave for liquid phase stirred-tank studies and a trickle bed reactor (TBR) for liquid-phase flow reactions. Both flow systems operate under near ambient pressure and the autoclave is capable of operating at high temperature and pressure. In this section the autoclave will be described as it was used as provided. The other two reactors were built specifically for this project and the process of building those will be discussed further in Chapter 3.

### 2.3.1. *Autoclave Stirred-Tank Reactor*

Batch, liquid-phase reactions were undertaken in a Parr micro-reactor. This reactor consists of a sealed vessel equipped with a stirrer and heating mantle capable of reaching high temperatures and pressure. The gas inlet is connected to a Buchii Pressflow Gas Controller (BPC) which regulates the feed of hydrogen to the reactor. By setting the desired pressure for the vessel the BPC feeds additional hydrogen in as it is used up to maintain a constant pressure within the vessel. This hydrogen uptake is monitored by a computer connected to the BPC and a graph of hydrogen uptake can be produced.

Reactions were done at 10, 20 and 30 bar pressure. The reactor vessel was 25ml total capacity and filled with 15ml liquid reactants. For each run 0.25g of catalyst was used. The stirrer speed was 1000rpm, this was the maximum reliable stirring speed. The maximum speed was used to help minimise mass transfer effects on the reaction efficiency. Reactions were done at a range of temperatures between 100°C and 300°C.

depends of the relative mobility of each analyte. This separation can be facilitated by altering the various aspects of the GC. The most important are:

- Column packing – Stationary Liquid Phase
- Temperature Programme

Column packing is very important and different stationary phases are available for separation according to different physical properties of the desired analyte. Columns are available which separate according to boiling point or polarity. In the case of a polarity column, the more polar the molecule the stronger the interaction with the liquid phase causing slower progress along the column and relatively longer elution times. For the separation of amine products in this project a 30m Chrompack CP-Sil 8CB Amine capillary column was used. This column separates according to the relative boiling points of the products being analysed. Smaller molecules would elute faster than larger molecules. The temperature programme can be used to ensure efficient separation and shorter run times.

Samples are introduced to the GC column via a heated injector port. This port is heated to very high temperatures in order to vaporise the solution. A microlitre syringe was used to inject 0.1µl volumes in to the column.

Figure 2.5 shows the schematic diagram of the Gas Chromatograph as was used in this project.

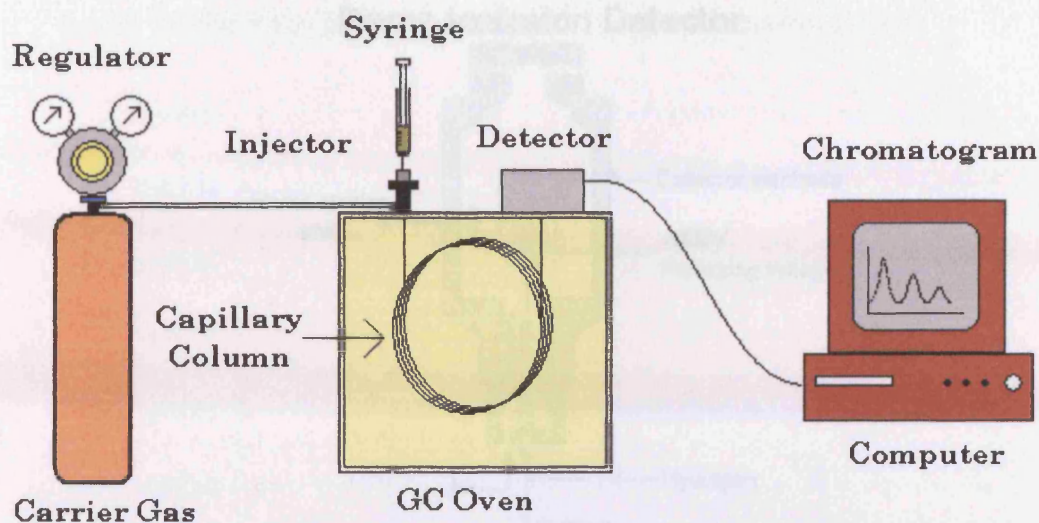


**Figure 2-5 – Schematic of the Gas Chromatograph**

Once product separation is achieved in the column, the products must then be detected. A variety of detectors are available the most common of which is the thermal conductivity detector (TCD) and the flame ionisation detector (FID). In this project the flame ionisation detector alone was used.

An FID consists of a hydrogen/air flame and a collector plate. The effluent from the GC column passes through the flame, which breaks down organic molecules and produces ions. The ions are collected on a biased electrode and produce an electrical signal. The FID is extremely sensitive with a large dynamic range; its only disadvantage is that it destroys the sample. Figure 2.6 shows a schematic diagram of an FID.

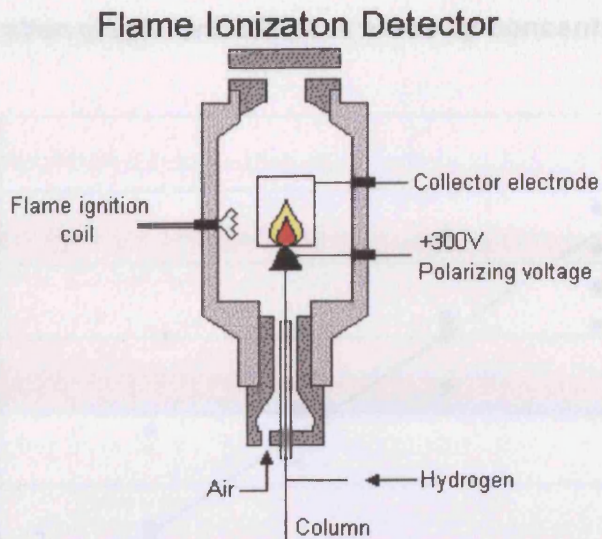


Figure 2-6 – Flame Ionisation Detector [11]

The GC was calibrated for hexamethyldiamine and adiponitrile by preparing standard solutions of known concentration of each and injecting them in the GC. The area under the curve of the GC trace was found to be proportional to the amount of each present. Several injections at each standard value were used and the un-modified data is shown in figures 2.7 and 2.8

Area of adiponitrile peak vs concentration of adiponitrile

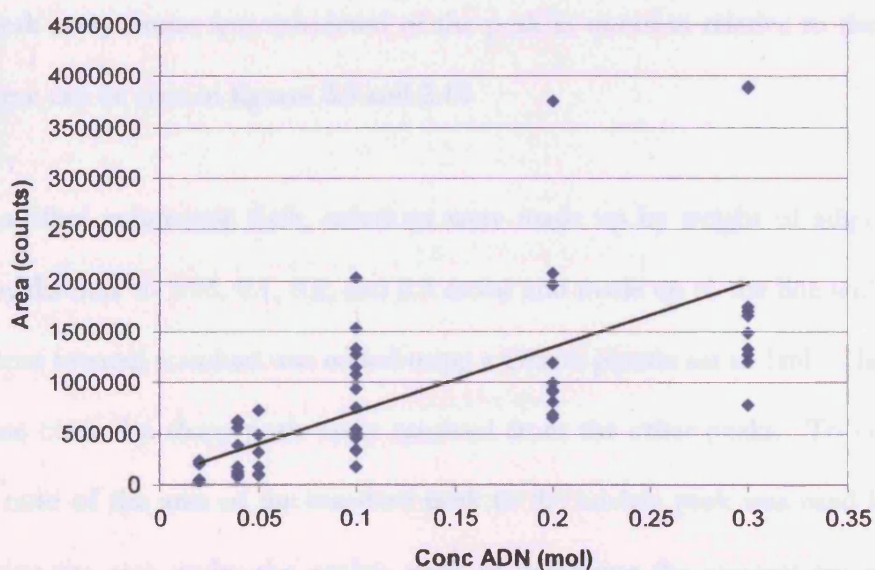


Figure 2-7 - GC Adiponitrile Calibration

### Calibration graph for HMD peak areas by concentration

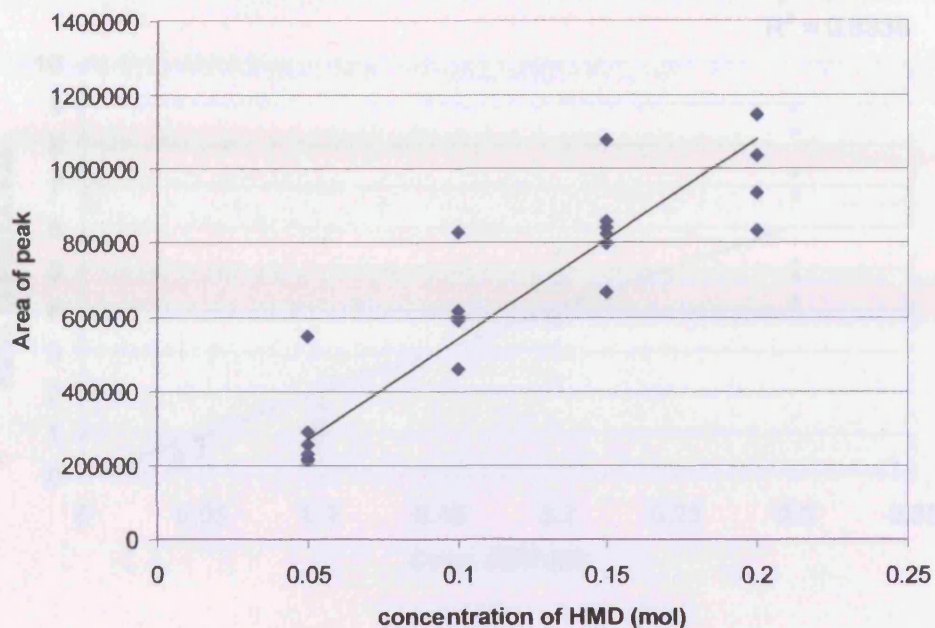


Figure 2-8 - GC Hexamethyldiamine Calibration

Injections by hand carry inherent human errors of reproducibility between each injection. This is evidently a problem here because of the large spread of data. In order to prevent this error affecting the results, an internal standard of non-reactive p-xylene was introduced to each standard sample for analysis so that instead of using an absolute value for the peak area, a ratio was calculated of the peak in question relative to the p-xylene peak. These can be seen in figures 2.9 and 2.10.

Thus, in a 50ml volumetric flask, solutions were made up by weight of adiponitrile or hexamethyldiamine to 0.05, 0.1, 0.2, and 0.3 molar and made up to the line with ethanol. 1ml p-xylene internal standard was added using a Gilson pipette set to 1ml. This volume of p-xylene created a sharp peak easily resolved from the other peaks. To correct the data, the ratio of the area of the standard peak to the analyte peak was used instead of simply using the area under the analyte peak to determine the amount present. This corrects for the variation created by the uncertainty in volumes injected.

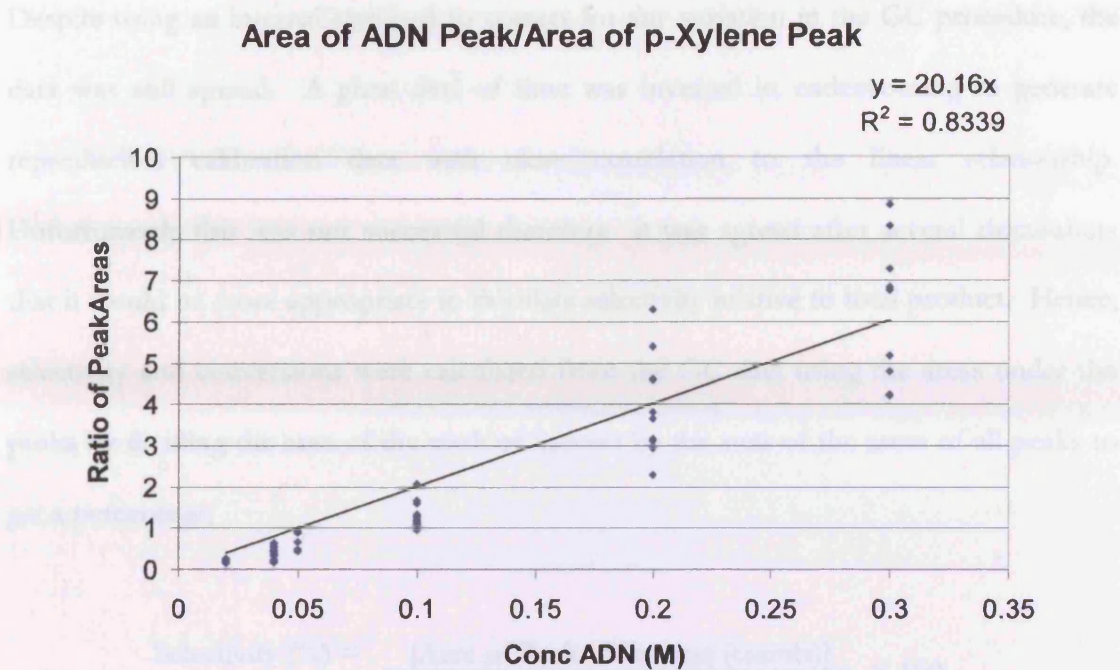


Figure 2-9 – Adiponitrile GC calibration graph (as a ratio of ADN to internal standard)

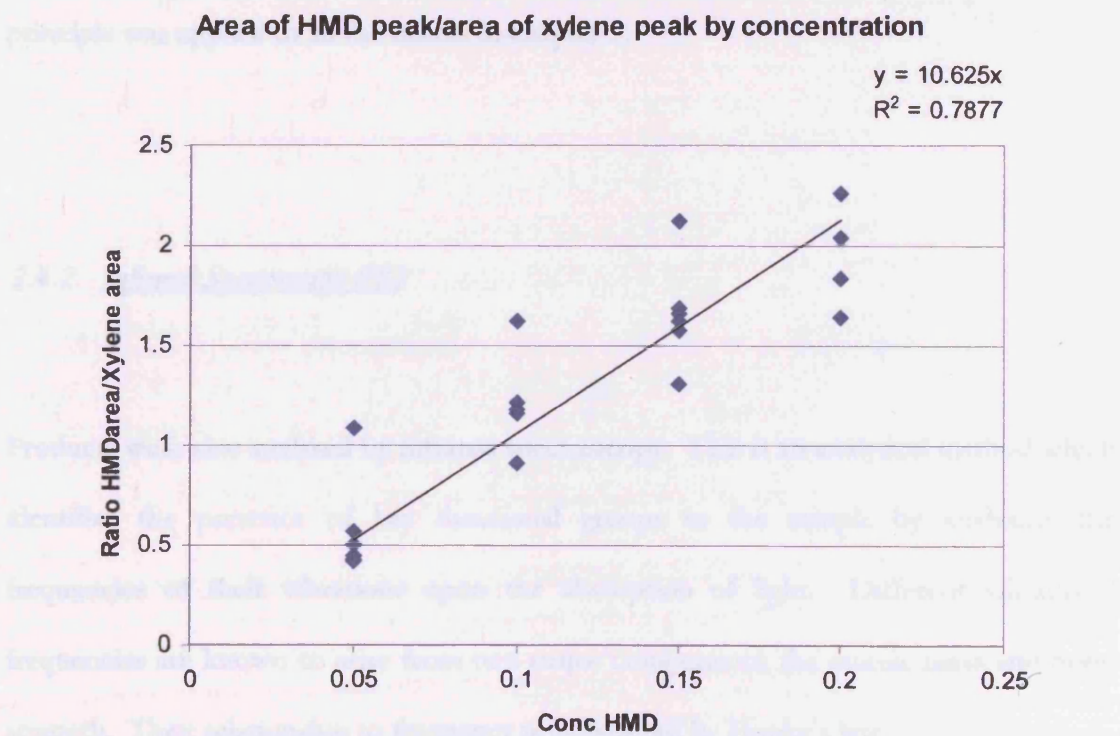


Figure 2-10 – Hexamethyldiamine GC calibration graph (as a ratio of HMD to internal standard)

Despite using an internal standard to correct for any variation in the GC procedure, the data was still spread. A great deal of time was invested in endeavouring to generate reproducible calibration data with close correlation to the linear relationship. Unfortunately this was not successful therefore it was agreed after several discussions that it would be more appropriate to calculate selectivity relative to total product. Hence, selectivity and conversions were calculated from the GC data using the areas under the peaks by dividing the area of the peak of interest by the sum of the areas of all peaks to get a percentage;

$$\text{Selectivity (\%)} = \frac{[\text{Area of Peak of Interest (counts)}]}{\Sigma[\text{Total peak areas (counts)}]} \times 100$$

Conversion was calculated with respect to the amount of residual starting material. This principle was applied to all the results in chapter 5.

#### 2.4.2. *Infrared Spectroscopy (IR)*

Products were also analysed by infrared spectroscopy. This is an analytical method which identifies the presence of key functional groups in the sample by analysing the frequencies of their vibrations upon the absorption of light. Different vibrational frequencies are known to arise from two major components; the atomic mass and bond strength. Their relationship to frequency is considered by Hooke's law;

$$\nu = \frac{\pi c \sqrt{(k/\mu)}}{2}$$

where  $\mu = \frac{m_1 m_2}{m_1 + m_2}$

$\nu$  = frequency

$c$  = speed of light

$k$  = bond tension constant

$\mu$  = reduced mass

$m_1$  = mass of atom 1

$m_2$  = mass of atom 2

Using Hooke's law, it can be seen that a bond between two light atoms will vibrate at a higher frequency than one between two heavier atoms. Furthermore, the stronger the bond, the higher the vibration frequency, *i.e.*  $C\equiv N > C=N > C-N$ , see figure 2.11.

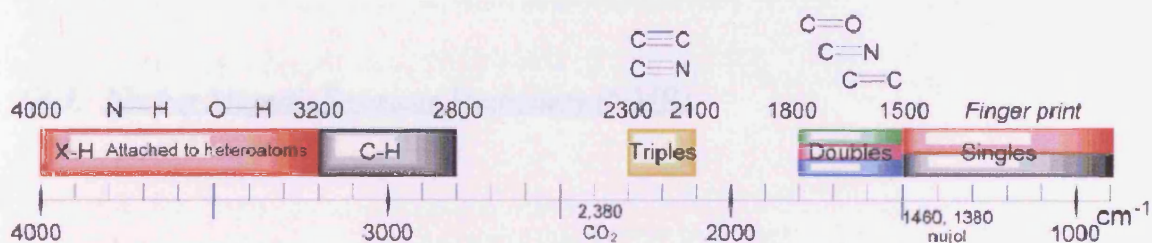


Figure 2-11 – Common absorption bands in organic molecules.

In order to make the bond vibrate a beam of light is passed through both a reference cell and a sample cell. The bonds in the molecules of the analyte absorb the IR light at wavelengths corresponding to the frequency of their vibrations with each bond resonating at a distinct frequency. The required frequency is expressed as a wave number ( $\text{cm}^{-1}$ ) and the strength of the absorptions are calculated as the difference between the sample beam and reference beam. The detector calculates then translates the

results to give a characteristic IR spectrum. Only changes to a bonds dipole moment cause an IR active vibration with symmetrical vibrations being said to be IR inactive. Figure 2.11 shows the characteristic wavelengths absorbed by the bonds in common functional groups.

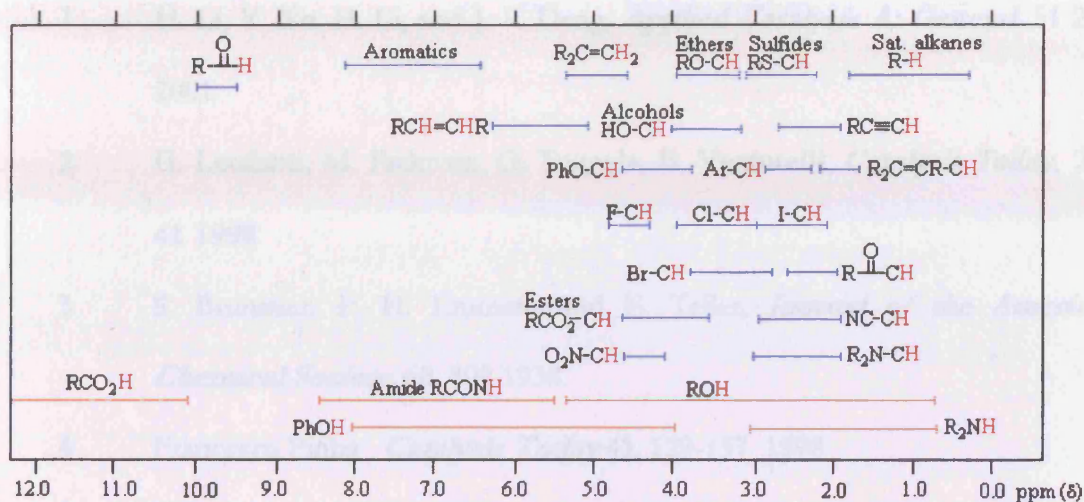
With the above in mind, IR has a distinct application to this project as it is able to distinguish between the key functional elements present in the various starting materials, intermediates and product. Of particular use is the  $C\equiv N$  stretching frequencies which are typically found at  $2200-2250\text{cm}^{-1}$ .

Samples were analysed using a Perkin Elmer 1600 series Fourier transform infrared spectrometer. Solvent was allowed to evaporate and the samples were used neat as liquid film dispersions between sodium chloride plates.

#### 2.4.3. Nuclear Magnetic Resonance Spectroscopy (NMR)

Nuclear magnetic resonance spectra were also used in product identification. Nuclear magnetic resonance, or NMR, is a phenomenon which occurs when the nuclei of certain atoms are immersed in a static magnetic field and exposed to a second oscillating magnetic field, which causes precession. Each nucleus therefore resonates at a certain frequency and as a result of spin relaxation, gives a peak on the NMR spectra. In  $^1\text{H}$  NMR this peak has an integral area proportional to the number of protons resonating. Each proton has a chemical shift (ppm) which is influenced by the atoms and groups neighbouring it. These groups are distinguished by their influence on the electron

shielding of the magnetic nuclei and force the chemical shift up field or down field. The approximate chemical shifts of hydrogen, according to their locality, are tabulated below.

2-12 – Chemical shifts in <sup>1</sup>H NMR

<sup>1</sup>H NMR spectra were recorded on a Bruker DPX 400 instrument at 400MHz. Samples were prepared as dilute solutions in deuteriochloroform. Chemical shifts are quoted relative to residual chloroform present within deuteriochloroform at 7.27ppm.

## 2.5. References

- 1 H. Li, Y. Xu, H. Li, and J. F. Deng, *Applied Catalysis A: General*, 51 216, 2001.
- 2 G. Leofanti, M. Padovan, G. Tozzola, B. Venturelli, *Catalysis Today*, 207 41 1998
- 3 S. Brunauer, P. H. Emmett, and E. Teller, *Journal of the American Chemical Society*, 60, 309 1938.
- 4 Francesco Pinna , *Catalysis Today* 41, 129-137 1998
- 5 Robert L. Augustine, *Heterogenous Catalysis for the Synthetic Chemist*, Marcel Dekker, Inc, ISBN 0-8247-9021-9
- 6 Douglas A. Skoog, Donald M. West and F. James Holler, *Fundamentals of Analytical Chemistry* 7<sup>th</sup> Edition, Saunders College Publishing, ISBN 0-03-005938-0
- 7 Anthony R. West, *Basic Solid State Chemistry*, Second Edition, John Wiley & Sons, ISBN 0-471-98755-5
- 8 Mark T. Weller, *Inorganic Materials Chemistry*, Oxford University Press, ISBN 0-19-8557981
- 9 Varian GC-FID, University of Nebraska, New England, U.S.A, viewed 10 July 2006, [www.chem.unl.edu/uic/gc-fid.html](http://www.chem.unl.edu/uic/gc-fid.html)
- 10 Charles N. Satterfield, *Heterogeneous Catalysis in Industrial Practice*, 2nd edition Krieger Pub Co;, ISBN 1-57-5240025
- 11 Brunauer, S., L. S. Deming, W. S. Deming, and E. Teller, *J. Am. Chem. Soc.*, 62, 1723, 1940

*Chapter 3*

*REACTOR*  
**CONSTRUCTION**

---

### 3. REACTOR CONSTRUCTION

---

#### 3.1. Flow Systems

The use of a continuous flow system for fine chemical production is highly sought after in industry. Batch methods such as the stirred tank reactor and autoclaves [1-4] have their draw backs. An operator is required to constantly refill the system and remove the product. The catalyst must be separated from the product before use and this catalyst can suffer breakdown due to the agitation of the stirrer at rapid speeds. These factors all add to the cost of an industrial process.

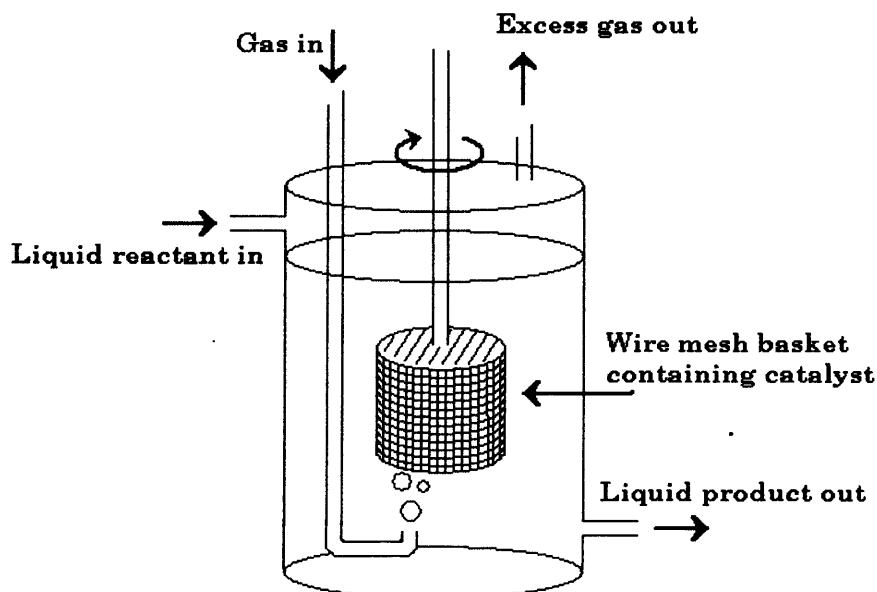


Figure 3-1 - Continuous stirred-tank reactor

A flow system eliminates these problems by fixing the catalyst in place and passing the reactants over it. Reactants get fed in one end and products emerge at the other end. Two types of reactor involving solid catalyst and both gaseous and liquid reactants,

termed three phase reactor [7, 8], are the trickle-bed reactor (TBR) and the continuous stirred-tank reactor (CSTR) [5, 6].

In figure 3.1 the continuous stirred-tank reactor is shown with the catalyst held within a wire basket in the centre of the reactor. Gases are bubbled in through a tube in to the base of the apparatus. Liquid reactants are fed through an inlet at the top and removed in continuous flow through an outlet at the bottom. This type of reactor can be set up in sequence such that typically three of these reactors can be used to achieve higher conversion.

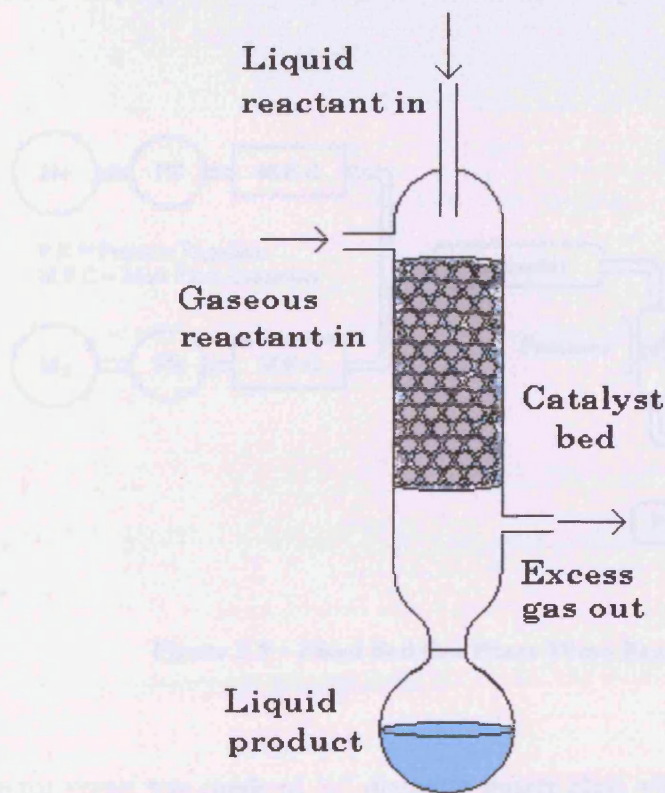


Figure 3-2 – Trickle-bed reactor [6]

The trickle-bed reactor can be seen in figure 3.2. Liquid and gases are fed in through separate inlets at the top of the reactor and passed over the long catalyst bed. The catalyst must be supported on large particles to allow steady flow. A lot of research has gone in to the engineering aspects of this reactor type [9-11].

### 3.2. Fixed-Bed Gas-Phase Reactor

Gas phase flow reactors have been used in many catalytic reactions [12-21]. The fixed bed reactor for the purpose of this project was initially set up with a saturator as shown in figure 3.3

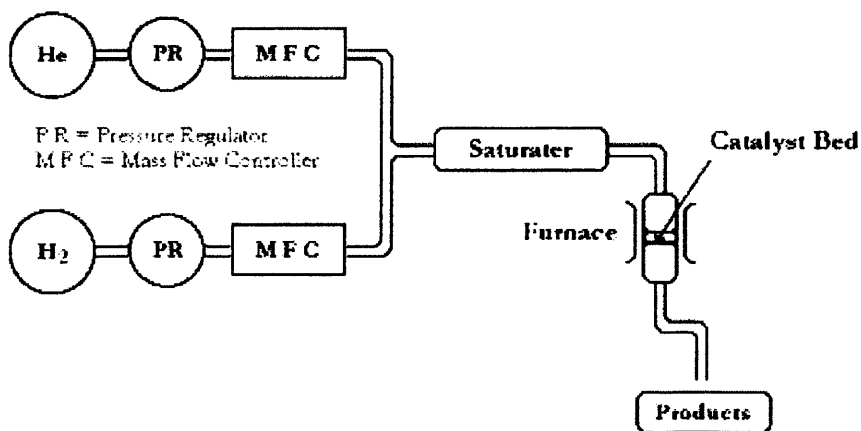
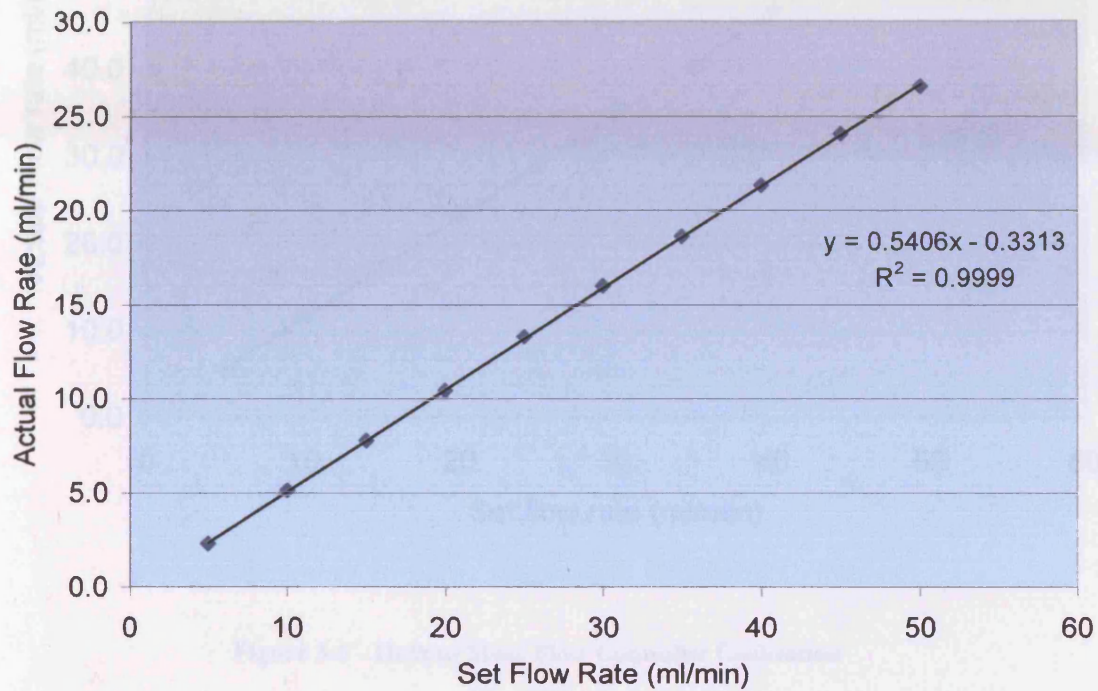


Figure 3-3 – Fixed Bed Gas Phase Micro Reactor

A glass reactor vessel was made of 1/2" diameter quartz glass with a medium porosity frit-glass plate in the middle to support the catalyst and allow reaction products to pass through. Cajon fittings (Swagelok) were used to create the glass-metal junction. Mass flow controllers were used to control accurately the delivery of gases in specific amounts to the reactor.

*Calibration of Mass Flow Controllers***Figure 3-4 - Hydrogen Mass Flow Controller Calibration Graph**

Calibration of mass flow controllers using a bubble meter produced straight line graphs relating the flow rate set on the mass flow controller control electronics with the actual resulting gas flow rate. For hydrogen the following equation was calculated from the graph showing this relationship (Figure 3.4):

$$\text{Actual Flow Rate} = 0.5406 (\text{Set Flow Rate}) - 0.3313$$

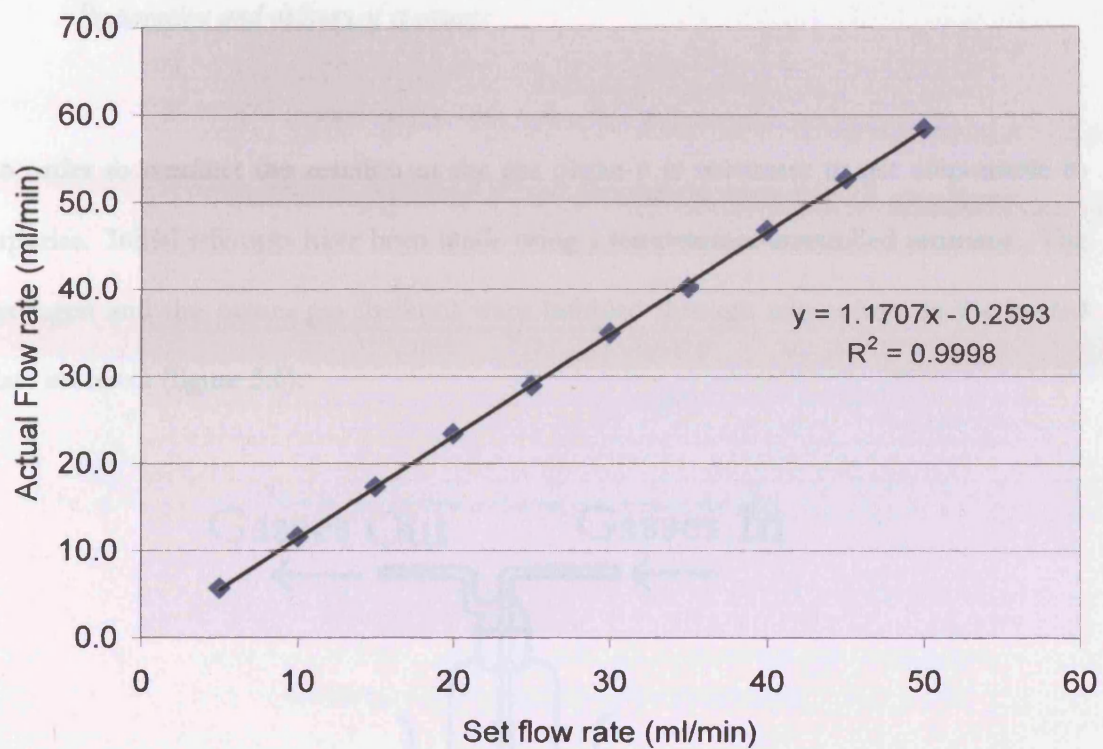


**Figure 3-5 - Helium Mass Flow Controller Calibration**

For helium the following equation was calculated from the graph (figure 3.5) showing this relationship.

$$\text{Actual Flow Rate} = 1.1707 (\text{Set Flow Rate}) - 0.2593$$

Preparation and delivery of reactants

In order to conduct the reaction in the gas phase it is necessary to get adiponitrile to vaporise. Initial attempts have been made using a temperature-controlled saturator. The hydrogen and the carrier gas (helium) were bubbled through adiponitrile in the heated glass saturator (figure 3.6).

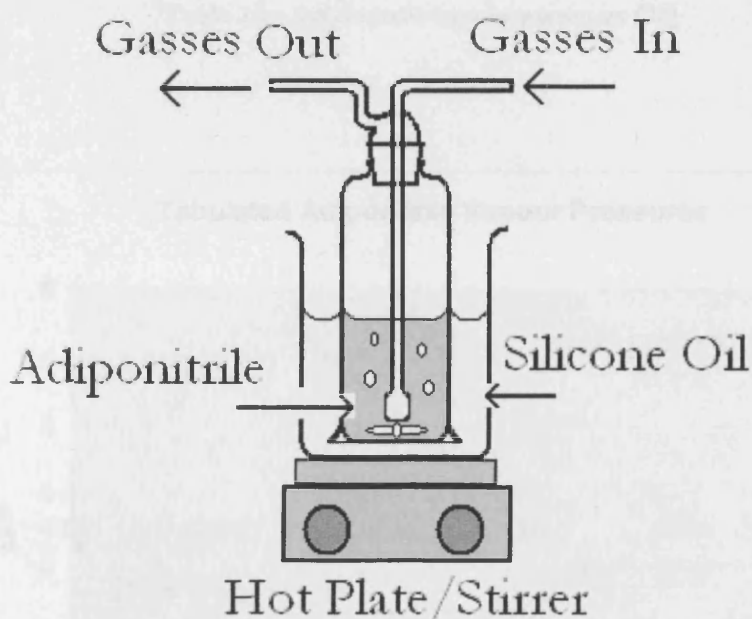


**Figure 3-6 – Adiponitrile Saturator**

The hot plate (figure 3.6) was capable of reaching 200°C at which temperature it is expected that the gas passing through should contain 10% adiponitrile vapour. A stirring rod was positioned inside the Dreschler bottle to allow good heat transfer throughout. The temperature inside the bottle was checked using a thermocouple and was found to be the same as the oil outside. Foil was wrapped round the vessel to reduce loss of heat to the atmosphere. The glass outlet and inlet were modified to ¼" in order to be fixed to the metal system by Cajon fittings.

Temperature	Vapour Pressure
30°C	1 Pa
61°C	10 Pa
100°C	100 Pa
148.6°C	1kPa
211.8°C	10kPa
297°C	100kPa

Table 3.1 - Adiponitrile vapour pressures [22]

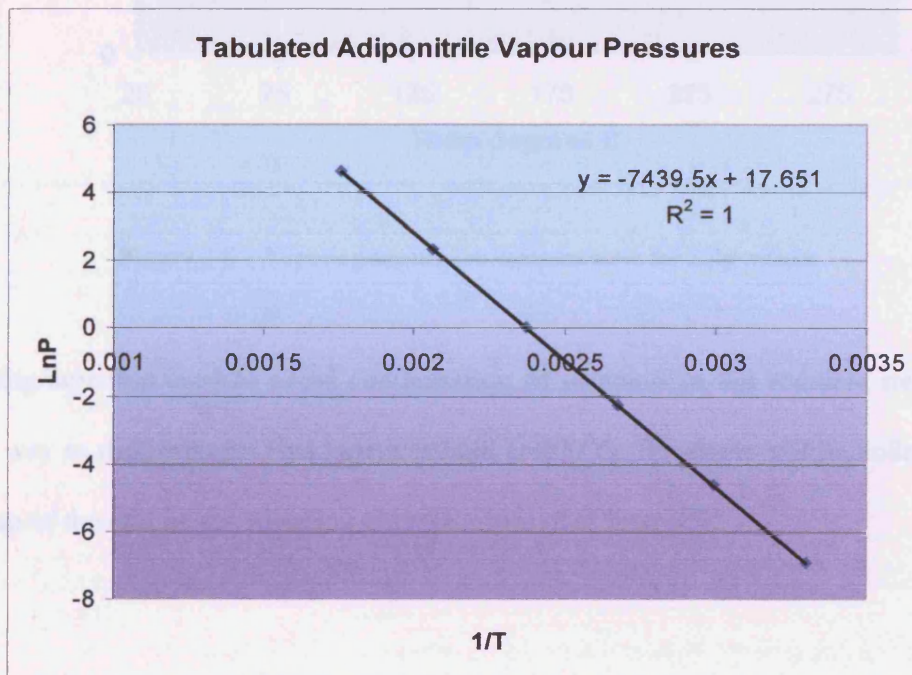


Figure 3-7 – Adiponitrile Vapour Pressure from reference data in figure 3.1.

Concentration of adiponitrile in the gas stream could be controlled using knowledge of adiponitrile vapour pressure. Vapour pressures from the literature are shown in table 3.1. It can also be seen in figure 3.7 graphically. By calculating the log relationship of vapour

pressure and temperature it is possible to predict percentage liquid in vapour phase at any temperature this can be seen in figure 3.8.

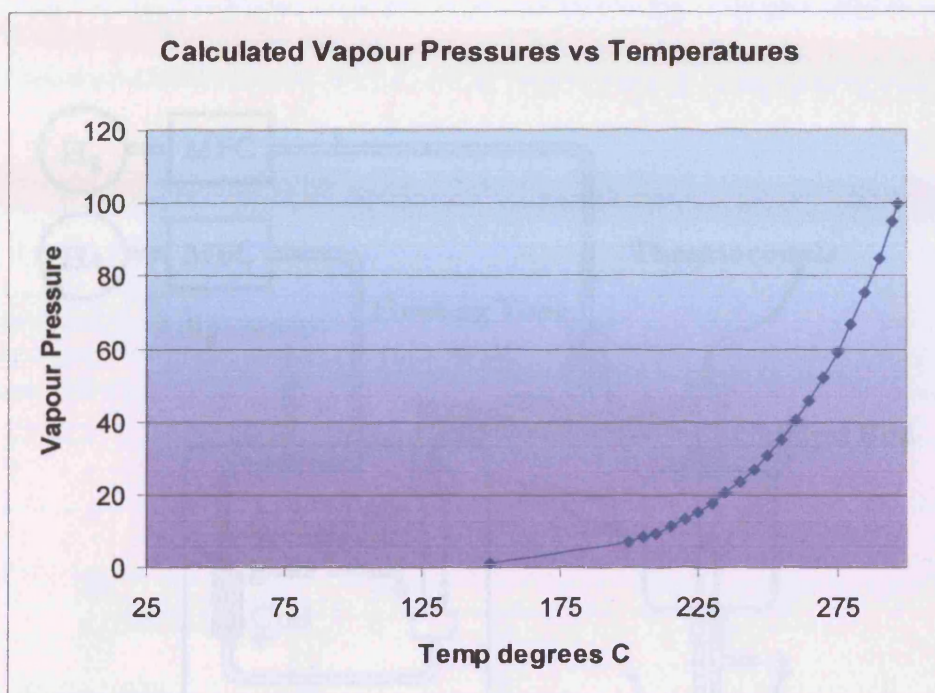


Figure 3-8 – Vapour pressures vs temperatures for adiponitrile

A heating tape was used to avoid condensation of reactants in the stainless steel tubing on the way to the reactor. This tape was held at 200°C. Products will be collected in a cold trap at the end of the stream at a temperature of at least 0°C.

This system has not been successful at getting adiponitrile in to the gas stream. Running 75ml/min of helium through the saturator for at least four hours has resulted in no product in the cold trap and no significant difference in the volume of adiponitrile in the saturator. In a paper by Li et al [5] adiponitrile was dissolved in EtOH and vaporised in a bubbling type evaporator at 250°C. Following this a 50:50 mix of adiponitrile and EtOH was investigated. It was found that the EtOH evaporated first while the saturator was

heating up. The EtOH collected was analysed in the gas chromatograph and no significant amounts of adiponitrile were detected.

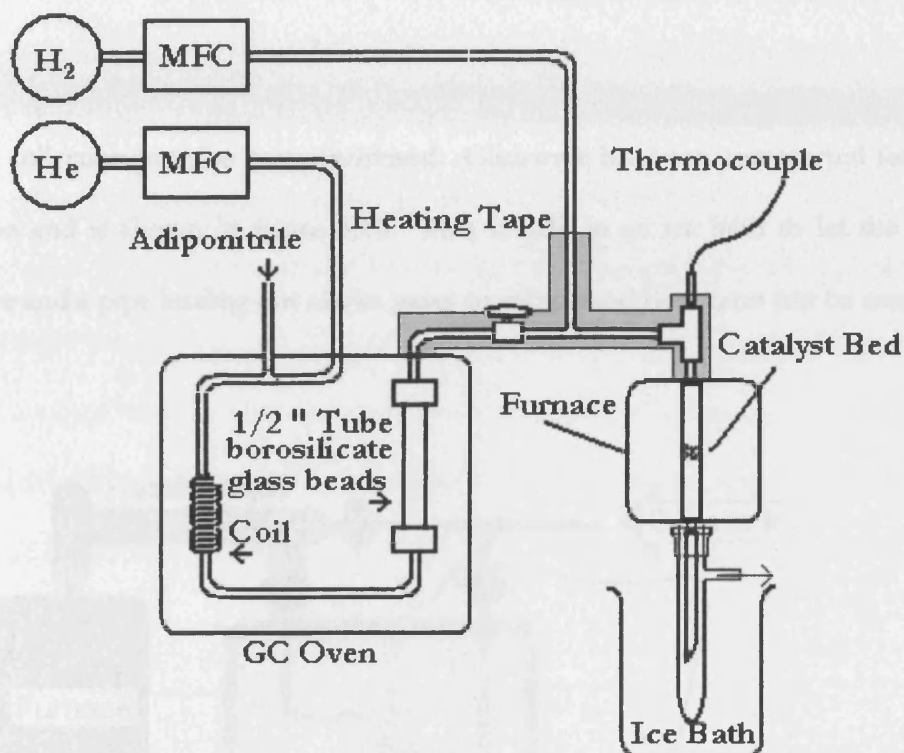


Figure 3-9 – Gas Phase Reactor

In order to obtain gas-phase adiponitrile alterations had to be made to the reactor. Figure 3.9 shows the changes. Adiponitrile is fed by a peristaltic pump in to a system of heating coils and tubing held within a GC oven. Helium is still used as a carrier gas and meets the adiponitrile in the GC oven to drive it through. The gas is driven up through a half-inch steel tube filled with borosilicate glass beads. These beads allow greater heat transfer and thus the gas comes in to equilibrium so that the adiponitrile vapour pressure correctly predicts its gas phase concentration. The GC oven is better for heating as it provides accurately controlled and maintained temperature. Hydrogen is added to the

stream after it leaves the GC oven and the pipes are covered with heating tape to maintain the temperature and stop the gas-phase adiponitrile condensing on the way to the reactor. A valve is placed after the oven and before the hydrogen inlet to enable *in situ* reduction of catalysts in the reactor bed, bypassing the adiponitrile vapourisation steps.

Product collection has also been optimised. Glassware has been constructed for product collection and is shown in figure 3.10. This is held in an ice bath to let the products condense and a pipe leading out allows gases to escape and flow rates can be measured.

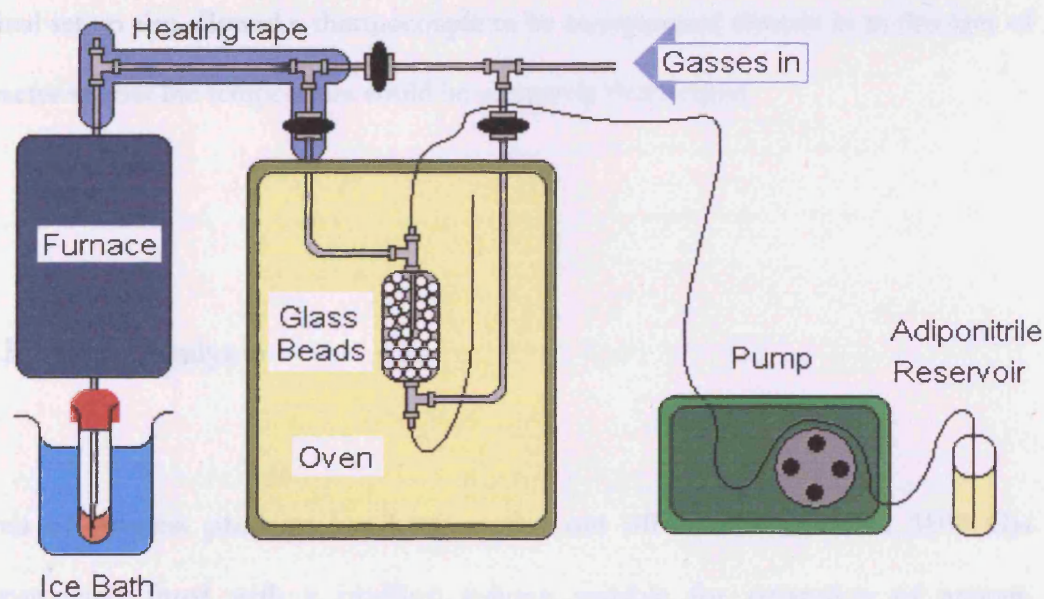


Figure 3-10 – Gas Phase Reactor modified

Further alterations to the reactor can be seen in figure 3.10. This figure shows how a system of valves was installed above the oven section of the reactor in order to allow gases to flow directly to the furnace bypassing the oven section. This allows for *in situ* reduction within the reaction tube and allows direct shut off of the reactant feed at the

end of the reaction while still being able to pass gases over the reactor bed during cooling.

Another modification which can be seen in figure 3.10 is the heat exchange system for getting adiponitrile in to the gas phase. The long 1/2" tube filled with beads was replaced by a long large diameter vessel capable of being filled with far more beads and fitted at the top with a T-piece to allow adiponitrile to enter through the top directly in to the heat exchange area. The previous design had the liquid meeting the gases in a T-piece which could become constricted and blocked. This method allows better mixing of gas and liquid and intends there to be a greater chance of getting adiponitrile in to the gas-phase. The final set up also allowed a thermocouple to be incorporated directly in to this area of the reactor so that the temperature could be accurately determined.

### **3.3. Product Analysis**

Analysis of reaction products has been carried out off-line on a Varian 3800 Gas Chromatograph fitted with a capillary column suitable for separation of amines. Identification of products has been elucidated using a GC-MS from Perkin Elmer. NMR and IR have also been used to identify products. This has been described in chapter 2.

The samples once collected from the reactor were diluted with solvent and injected in the GC. Samples were refrigerated at all times possible in order to reduce any product degradation.

### 3.4. Trickle-Bed Reactor

The third reactor type investigated was the Trickle-Bed Reactor.

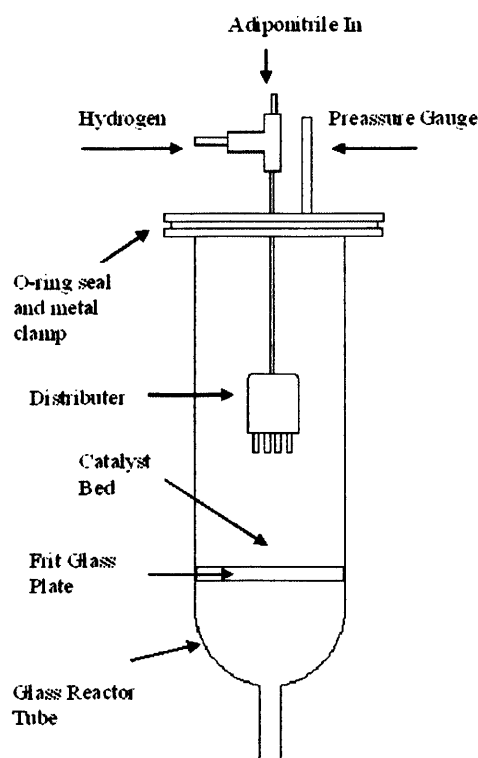


**Figure 3-11 – Trickle-bed Reactor Body showing distributor head and frit glass plate**

The reactor is a combination of custom built glass and Swagelok. The body of the reactor tube is constructed of Pyrex glass with a coarse frit situated in the lower portion before the glass tapers to a 1/8" pipe. A large pore frit had to be used as the adiponitrile is very viscose and so care must be taken to avoid blockage and maintain flow. This was a problem which arose with the use of the adiponitrile reaction in this system. This problem can be seen in figure 3.12.

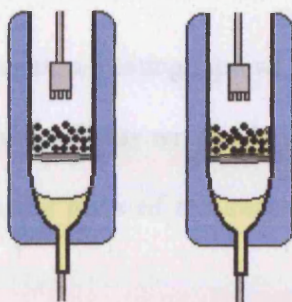


**Figure 3-12 – Blockage in the TPR tube showing liquid build up on catalyst bed.**

This pipe is fitted using 1/8" Cajon fittings to 1/8" stainless steel tubing. The catalyst sits on the frit glass plate. The catalyst bed consists of 0.5g granulated catalyst. The catalyst particles were interspersed with silicon carbide to fill the gaps between the granules to allow better even flow of liquids and gases over the catalyst bed.

Gases are fed in through a regulator and the flow is further cut down and controlled by a needle valve before entering the reactor through the T-piece situated at the top. Liquid is pumped using an HPLC pump and meets the gas flow at this T-piece as shown on Figure 3.11. The pump was set to flow at 1ml/min. This pipe follows down inside the reactor body to a distributor head created with six equally distanced 1/8" pipe ends which act to ensure even distribution of the liquid over the surface of the catalyst bed. A pressure gauge is in place so that the internal pressure of the reactor can be monitored. The pressure inside the reactor is to be maintained at around 0.5 bar gauge ideally.

The glass flange at the top of the reactor tube is fixed in place and sealed using rubber O-rings and a custom built metal clamp which fastens down on a Teflon ring between metal and glass. A hydrogen detector is used to ensure no leaks are occurring prior to use of the equipment.

The temperature was increased using a heating tape wrapped round the reactor body. To help maintain a steady temperature foil was wrapped in layers around the heating tape. A thermocouple inserted between the glass of the reactor tube and the heating tape was used to measure temperature.

Between runs, methanol MeOH was run through the reactor to clean it of organic residue and a solution of Aqua Regia was run through the frit glass plate to dissolve away any residual metals which may block the pores.

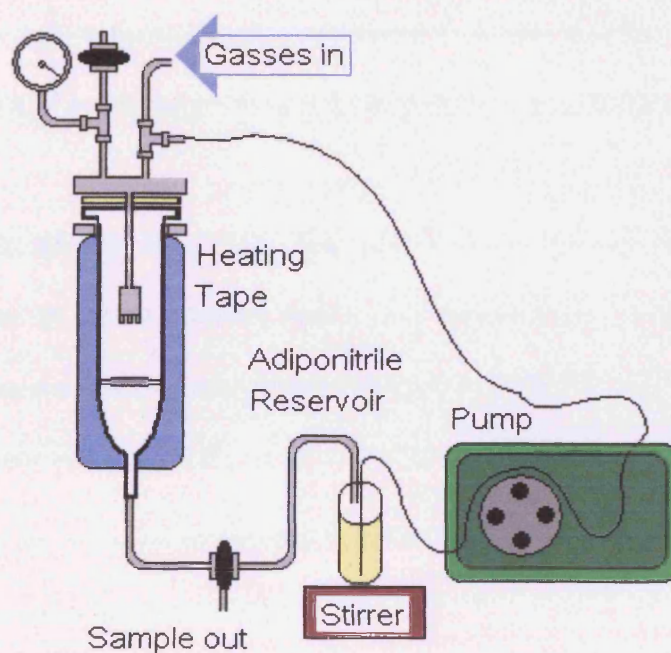


**Figure 3-13 – TBR Cycling System**

Reactions have also been undertaken in the trickle-bed reactor as shown in figure 3.13. The reaction here is liquid phase and is operating at 0.5 bar gauge. The distributor

ensures that the liquid flows evenly over the whole bed. 0.5g of granulated catalyst is used and the whole reactor is made of Pyrex and enclosed in heating tape to attain a temperature of 150°C for reaction. This is currently the temperature limit for safe operation of the trickle-bed in its current form. It is possible to either run the trickle bed as a single pass process or the effluent can be recycled to increase contact time.

### **3.5. Conclusion**

Three reactors were used in this project. The stirred tank reactor was used with little or no modification. The flow type reactors needed to be very specifically tailored to their purpose. The gas-phase reactor required building from scratch and the trickle-bed reactor was already in existence but required modification. This building process consisted of a lot of trial and error particularly to obtain vaporisation of adiponitrile for gas phase and good flow in the trickle bed and led to a greater understanding of the requirements of a small scale reactor for this process.

The most important factor involved in the use of the gas-phase reactor is temperature. Due to the high boiling point of adiponitrile and thus low volatility this was a difficult task. Activity data to be shown in chapter 5 will prove the success or otherwise of this.

The difficulty in running the trickle bed reactor arose due to the viscosity of the adiponitrile. Smooth running proved harder than expected due to the frit glass plate in place for holding the catalyst. In future for such a high viscosity liquid it would be advisable to use an even coarser frit or some sort of metal grating.

### 3.6. References

- 1 Li, H.; Xu, Y. *Materials Letters* 2001, **51**, 101.
- 2 *US Patent 489348* Allied Corporation, (1983)
- 3 Huang, Y.; Sachtler, W. M. H. *Applied Catalysis A: General* 1999, **182**, 365.
- 4 Huang, Y.; Sachtler, W. M. H. *Journal of Catalysis* 1999, **188**, 215.
- 5 Alini, S.; Bottino, A.; Capannelli, G.; Carbone, R.; Comite, A.; Vitulli, G. *Journal of Molecular Catalysis A: Chemical* 2003, **206**, 363.
- 6 Crezee, E.; hoffer, B. W.; Berger, R. J.; Makkee, M.; Kapteijin, F.; Moulijn, J. A. *Applied Catalysis A: General* 2003, **251**, 1.
- 7 Robert L. Augustine, *Heterogeneous Catalysis for the Synthetic Chemist*, Marcel Dekker, Inc, ISBN 0-8247-9021-9
- 8 G.C. Bond, *Heterogeneous Catalysis – Principles and Applications*, Second Edition, Oxford Scientific Productions, ISBN 0-19-855525
- 9 Rajashekharam, M.; Jaganathan, R.; Chaudhari, R. V. *Chemical Engineering Science*, 1998, **53**, 787
- 10 Valerius, G.; Zhu, X.; Hofman, H.; Haus, A. T. *Chemical Engineering and Processing*, 1998, **35**, 11
- 11 Valerius, G.; Zhu, X.; Hofman, H.; Haus, A. T. *Chemical Engineering and Processing*, 1998, **35**, 1
- 12 Huang, Y.; Sachtler, W. M. H. *Applied Catalysis A: General* 1999, **182**, 365.
- 13 Huang, Y.; Sachtler, W. M. H. *Journal of Catalysis* 1999, **188**, 215.
- 14 Arai, M.; Kanno, M.; Nishiyama, Y.; Torii, K.; Shirai, M. *Journal of Catalysis* 1999, **182**, 507.
- 15 Bond, G. C. *Accounts of Chemical Research* 1993, **26**, 490.

- 16 Braos-Garcia, P.; Maireles-Torres, P.; Rodriguez-Castellon, E.; Jimenez-Lopez, A. *Journal of Molecular Catalysis A: Chemical* 2003, **193**, 185.
- 17 Hochard, F.; Jobic, H.; Massardier, J.; Renouprez, A. J. *Journal of Molecular Catalysis A: Chemical* 1995, **95**, 165.
- 18 Huang, Y.; Adeeva, V.; Sachtler, W. M. H. *Applied Catalysis A: General* 2000, **196**, 73.
- 19 Huang, Y.; Adeeva, V.; Sachtler, W. M. H. *Applied Catalysis A: General* 2000, **196**, 73.
- 20 Li, H.; Wang, M.; Xu, Y. *Chemistry Letters* 2000, 1048.
- 21 Rode, C. V.; Arai, M.; Shirai, M.; Nishiyama, Y. *Applied Catalysis A: General* 1997, **148**, 405.
- 22 David R. Lide, *CRC Handbook of Chemistry and Physics*, 83<sup>rd</sup> Edition, (2002) ISBN 0849304830.

# *Chapter 4*

# CHARACTERISATION

---

## 4. CHARACTERISATION

---

Catalyst characterisation allows us to determine certain aspects of the physical and chemical structure of the catalyst. This data can then be used to explain the catalyst behaviour. In this chapter the main characterisation methods used are X-Ray Diffraction (XRD), Surface Area Determination by the Brunauer-Emmett-Teller (BET) [1] method and Temperature Programmed Reduction. The intention of gaining structural information on these catalysts is in order to relate structure to activity for the adiponitrile hydrogenation reaction. This data will be referred back to when discussing the activity data in chapter 5.

### 4.1. Powder X-Ray Diffraction

Powder X-ray diffraction can be used to identify crystalline phases present in a catalyst. In this section it has been used mainly to look for the presence of oxide or large clusters of metal species. The supports used in this project have been mainly non-crystalline and so do not diffract X-rays or diffract very poorly, in the case of SiO<sub>2</sub>.

4.1.1. *Pricat Catalysts*

Figure 4.1 shows the diffraction pattern obtained from two catalysts provided by Johnson Matthey; Pricat NI62/15P and Pricat NI55/5P. Both of these catalysts are high loading nickel catalysts containing Ni and NiO phases on powdered mixed supports. Pricat NI55/5P contains Ni/NiO on aluminium oxide, zinc oxide and diatomaceous earth which has a chemical composition of typically 86% silica, 5% sodium, 3% magnesium and 2% iron. Pricat NI62/15P contains Ni/NiO supported on silica, magnesia and graphite.

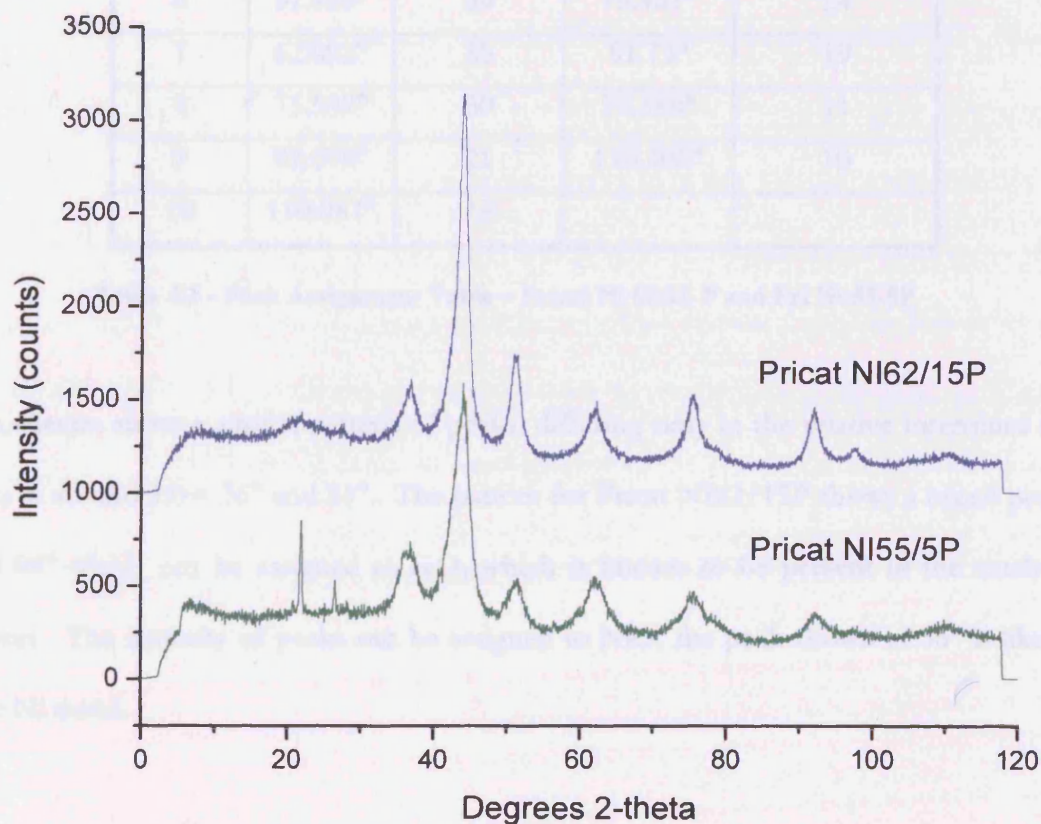


Figure 4.1 - XRD pattern for Pricat Catalysts

Table 4.1 shows the peak assignment table for Pricat NI62/15P and Pricat NI55/5P. By comparing this with the JCPDS database files for Ni and NiO we can assign peaks.

Peak Number	Pricat NI62/15 P		Pricat NI55/5P	
	Angle 2 $\theta$	Intensity	Angle 2 $\theta$	Intensity
1	21.84°	53	21.463°	19
2	26.48°	33	36.717°	26
3	36.659°	44	43.996°	100
4	40.806°	36	51.043°	34
5	43.967°	100	62.208°	21
6	51.449°	34	75.461°	24
7	62.092°	35	91.73°	19
8	75.548°	30	97.588°	11
9	92.078°	21	110.406°	10
10	110.087°	18		

**Table 4.1 - Peak Assignment Table – Pricat Ni 62/15 P and Pri Ni 55/5P**

Both spectra show a similar pattern of peaks, differing only in the relative intensities of peaks at around  $2\theta = 36^\circ$  and  $51^\circ$ . The pattern for Pricat NI62/15P shows a broad peak at  $21.84^\circ$  which can be assigned to  $\text{SiO}_2$  which is known to be present in the catalyst support. The majority of peaks can be assigned to NiO; the peak shown at  $36^\circ$  is likely to be Ni metal.

4.1.2. Nickel on Magnesia Catalysts

The Nickel on magnesia catalysts were prepared by a method described by Serra et al.[2] in which nickel nitrate hexahydrate is ground with MgO in a ratio of 4:1 Ni:MgO. This is then calcined in a tube furnace at 400°C for 4 hours. The substance produced at this stage is named M1c. This is then reduced in flowing H<sub>2</sub>/Argon (5%). The substance produced following reduction is then referred to as M1r.

XRD powder patterns were taken of both materials. The reduced material was analysed immediately after reduction but will have become re-oxidised upon sample transfer to the TPR machine, and therefore does not show its fully reduced state in the XRD pattern. This may be why the two patterns are very similar, although there are subtle differences in the relative peak intensities. Also the pattern from M1c has sharper peaks and higher counts therefore showing it to be more crystalline and have larger crystallites than M1r which has slightly broader peaks showing it to have either smaller crystallite sizes or lower crystallinity. Using JCPDS files it has been possible to match these substances to known materials, this is tabulated in table 4.3 and table 4.4. It can be seen that the above catalysts appear to match certain peaks of Nickel Oxide, Magnesium Nickel Oxide, Nickel and Magnesium Oxide.

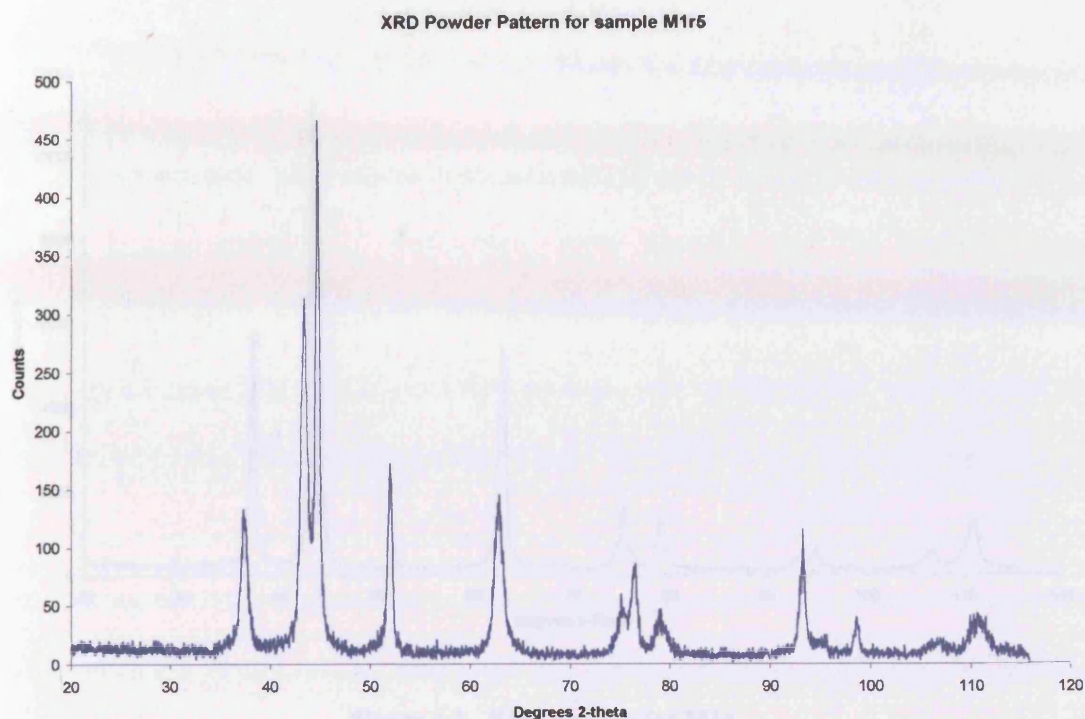


Figure 4.2 – XRD Pattern for M1r5

Pattern M1r		Matching Lines in Standard Patterns									
		A		B		C		D		E	
Angle	I	Angle	I	Angle	I	Angle	I	Angle	I	Angle	I
37.33	27	2.412	60	2.42	40	2.421	45			2.431	10
43.48	67	2.088	100	2.095	100	2.097	100				
44.78	100							2.034	100	2.106	100
52.18	34							1.762	42		
62.96	31	1.476	35	1.482	35	1.483	50			1.489	52
75.35	10	1.26	18	1.264	9	1.264	14			1.270	4
76.59	18							1.246	21		
79.17	10	1.206	16	1.210	8	1.210	15			1.216	12
93.27	25							1.062	20	1.053	5
95.50	3	1.044	8								
98.78	6							1.017	7		
106.4	4	0.958	6	0.961	2	0.962	5			0.966	2
110.9	8	0.934	10	0.937	5	0.937	15				

Table 4.3 – Peak assignment table for XRD of M1r5

- A. NiO – Nickel Oxide – JCPDS No 22-1189
- B. MgO.4NiO.6O – Magnesium Nickel Oxide – JCPDS No 34-0410
- C. MgNiO<sub>2</sub> – Magnesium Nickel Oxide – JCPDS No 24-0712
- D. Ni – Nickel – JCPDS No 4-0850
- E. Magnesium Oxide/Periclase syn = MgO - JCPDS No 4-0829  
(Periclase – mineral form of MgO)

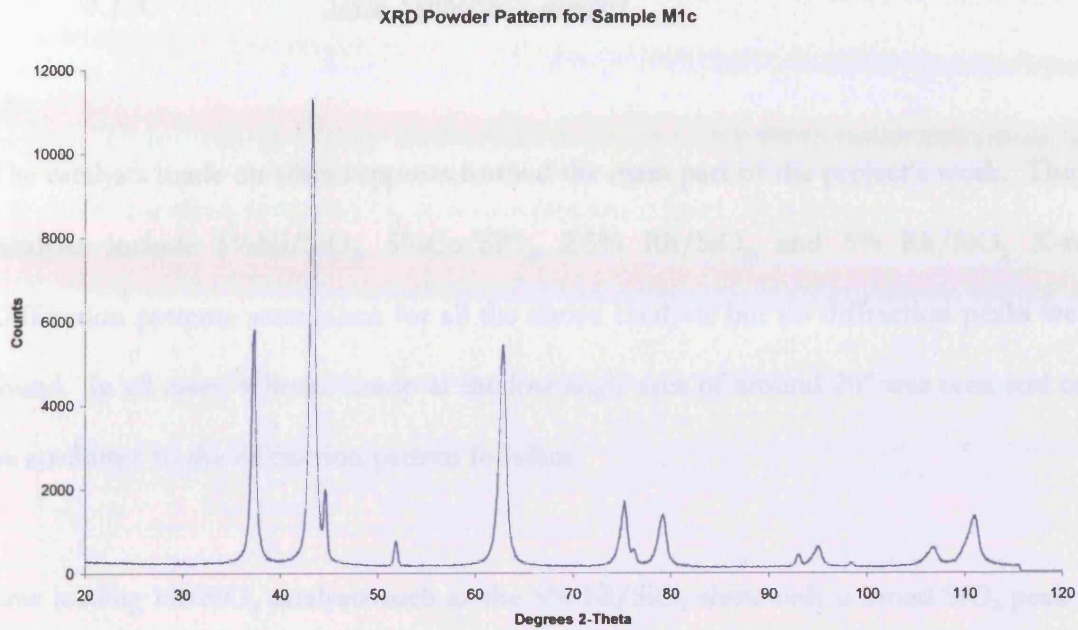


Figure 4.3 - XRD pattern for M1c

Pattern M1c		Matching Lines in Standard Patterns									
Angle	Rel. I	A		B		C		D		E	
37.47	51	2.412	60	2.42	40	2.421	45			2.431	10
43.42	100	2.088	100	2.095	100	2.097	100			2.106	100
44.67	18							2.034	100		
51.94	7							1.762	42		
62.93	48	1.477	35	1.482	35	1.483	50			1.489	52
75.32	15	1.26	18	1.264	9	1.264	14			1.270	4
76.36	5	1.586	12					1.246	21		
79.23	12	1.206	16	1.210	8	1.210	15			1.216	12
93.12	4							1.062	20		
95.18	5	1.044	6	1.474	2	1.048	6				
106.8	5	0.959	6	0.961	2	0.962	5			0.966	2
111.1	12	0.934	10	0.937	5	0.937	15			0.942	17

Table 4.4 – Peak assignment table for XRD of M1c

- A. NiO – Nickel Oxide – JCPDS No 22-1189
- B. MgO.4NiO.6O – Magnesium Nickel Oxide – JCPDS No 34-0410
- C. MgNiO<sub>2</sub> – Magnesium Nickel Oxide – JCPDS No 24-0712
- D. Ni – Nickel – JCPDS No 4-0850
- E. Magnesium Oxide/Periclase syn = MgO - JCPDS No 4-0829  
(Periclase – mineral form of MgO)

### 4.1.3. Silica Supported Catalysts

The catalysts made on silica supports formed the main part of the project's work. These catalysts include 5%Ni/SiO<sub>2</sub>, 5%Co/SiO<sub>2</sub>, 2.5% Rh/SiO<sub>2</sub>, and 5% Rh/SiO<sub>2</sub>. X-ray Diffraction patterns were taken for all the above catalysts but no diffraction peaks were found. In all cases, a broad hump at the low angle area of around 20° was seen and can be attributed to the diffraction pattern for silica.

Low loading Ni/SiO<sub>2</sub> catalysts such as the 5% Ni/SiO<sub>2</sub> show only a broad SiO<sub>2</sub> peak in XRD and so the phases present after reduction cannot be determined using this method. XRD patterns of the 20% loading catalyst have been taken both before and after reduction at 600°C. This can be seen in figure 4.4.

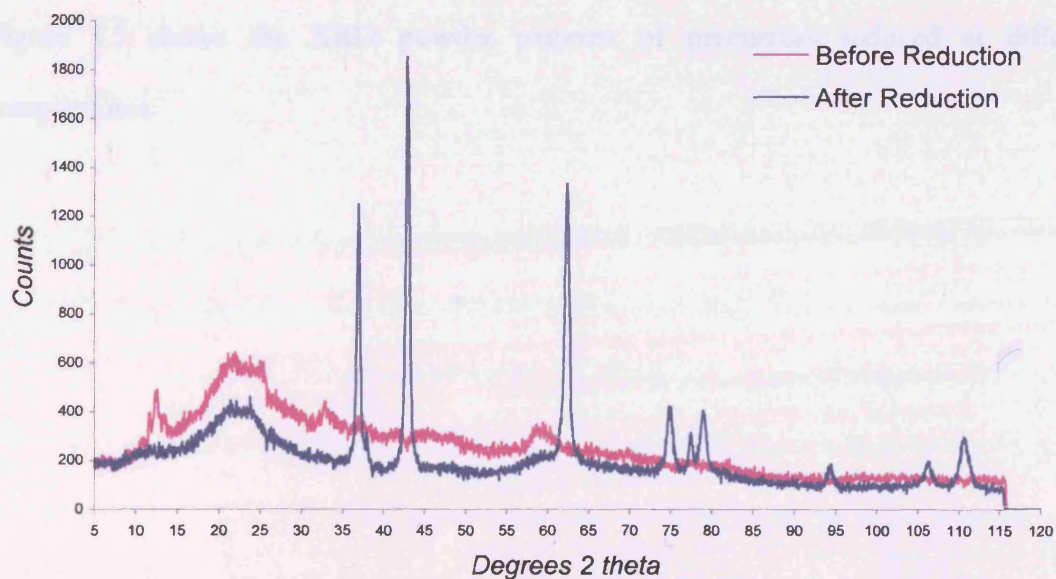


Figure 4.4 - XRD pattern for 20% Loading Ni/SiO<sub>2</sub>

The table below shows how the peaks present in the XRD pattern relate to the expected peaks for NiO, the peaks show a good correlation. SiO<sub>2</sub> has a characteristic broad peak around 21° and this is present in the pattern above. The other peaks present in the unreduced sample correspond to nickel nitrate phases from the precursor.

*Ni/SiO<sub>2</sub> reduced catalyst – XRD peak assignment table*

Pattern of Red. Catalyst			Matching lines in NiO (4-835)		
2 theta	Intensity	D spacing	2 theta	Intensity	hkl
21.535	25	4.126	SiO <sub>2</sub> – broad peak		
37.253	64	2.414	37.281	91	111
43.314	100	2.089	43.298	100	200
62.802	49	1.48	62.917	57	220
75.504	20	1.259	75.445	16	311
79.419	17	1.207	79.393	13	222
95.05	8	1.045	95.083	8	400
106.824	9	0.96	107.009	7	331
111.029	15	0.935	111.159	21	420
			129.208	17	422
			146.705	7	511

**Table 4.5 - Peak Assignment Table for 20% Ni/SiO<sub>2</sub>**

Figure 4.5 shows the XRD powder patterns of precursors reduced at different temperatures.

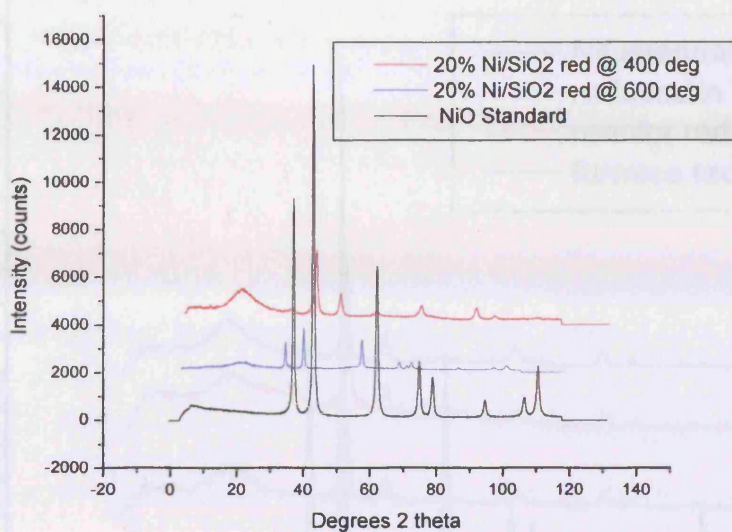
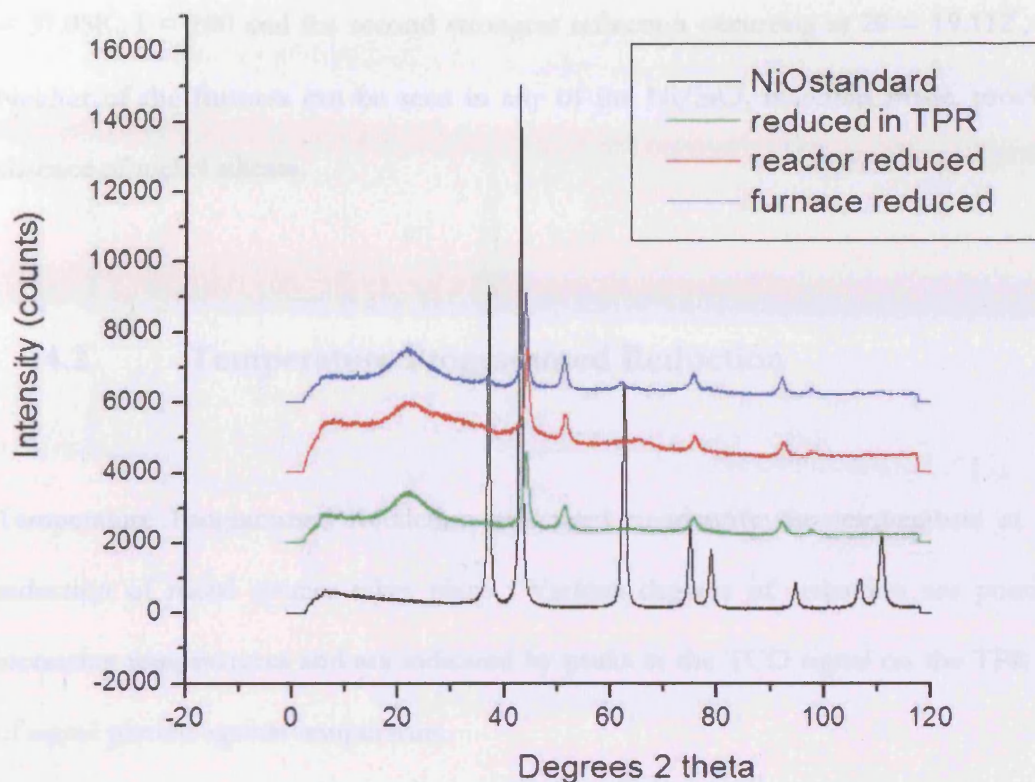


Figure 4.5 – XRD pattern for Ni/SiO<sub>2</sub> at different reduction temperatures

Although the XRD pattern appears shifted, due possibly to an artefact of the machine, the sample reduced at 600°C shows mainly NiO phase. On reduction at the lower temperature of 400°C more of the Ni metal phase is present and NiO peaks are smaller or disappeared.

Also investigated was the method of reduction. Reduction was undertaken in three different environments. The first method effected reduction in a tube furnace under flowing H<sub>2</sub>/Argon 5%. The second method performed *in situ* reduction in the reaction tube using helium as the diluents. The third method involved reduction in the TPR tube during analysis. The TPR tube and reactor tube are effectively the same method as the gasses flow through the catalyst precursor. In the tube furnace the precursor sits in a quartz boat and gasses are passed over it. Figure 4.6 shows the XRD powder patterns of catalysts prepared by these methods.



**Figure 4.6 – 20% Ni/SiO<sub>2</sub> XRD showing different reduction conditions**

It can be seen that both of the methods involving gas flow through the precursor result in a sample with less of the NiO peaks present and more Ni metallic phase for which the predominant peak is at  $2\theta=44^\circ$  and the second most predominant peak being  $2\theta=52.18^\circ$ . The following three peaks in the Ni pattern also match up where  $2\theta=76^\circ$  and  $2\theta=93^\circ$ , having equal intensities and the final peak at  $2\theta=98^\circ$  which has lowest intensity.

A common problem incurred with using nickel on silica is the formation of nickel silicates. From the XRD patterns above it is clear at the level required to be observed by XRD that nickel silicate has not been formed. The JCPDS file for nickel silicate can be found on the JCPDS database. It can be compared with the Ni/SiO<sub>2</sub> catalyst XRD patterns. The main feature of the nickel silicate pattern is that its major line occurs at  $2\theta$

= 37.058°, I = 100 and the second strongest reflection occurring at  $2\theta = 19.112^\circ$ , I=40. Neither of the features can be seen in any of the Ni/SiO<sub>2</sub> materials made, proving an absence of nickel silicate.

## 4.2. Temperature Programmed Reduction

Temperature Programmed Reduction was used to identify the temperature at which reduction of metal species takes place. Various degrees of reduction are possible at increasing temperatures and are indicated by peaks in the TCD signal on the TPR graph of signal plotted against temperature.

### 4.2.1. 20% Ni/SiO<sub>2</sub>

When investigating the preparation of Nickel on silica, a TPR was run over a broad temperature range of 0 - 600°C. This TPR can be seen in figure 4.7.

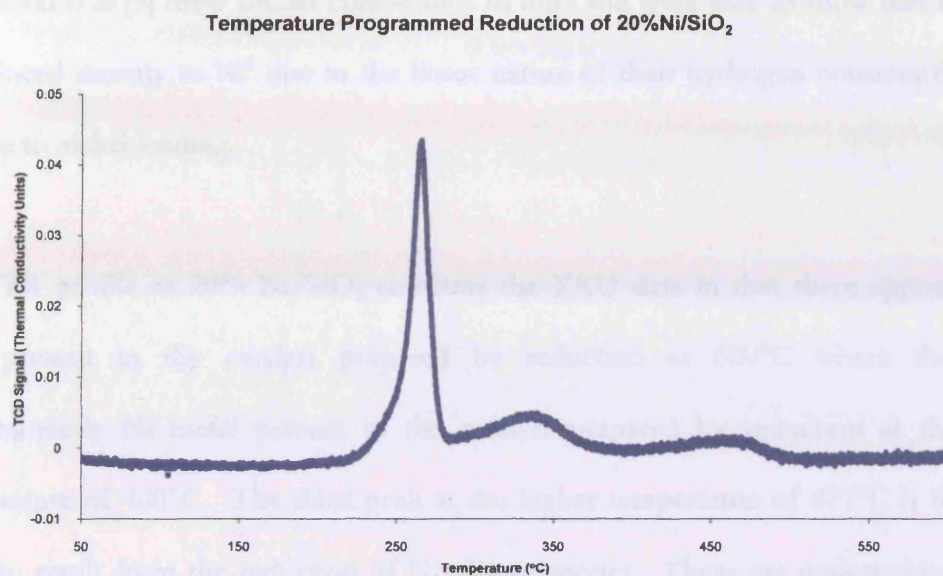


**Figure 4.7 - TPR of 20%Ni/SiO<sub>2</sub>**

The major peak in this TPR trace is shown at 266°C it is sharp and well defined. It is followed by a peak at 340°C which is shallower and then another very shallow peak at 471°C. This may indicate three stages of reduction. As is seen in literature [3, 4, and 5] three TPR events are commonly expected. Mile *et al* also looked at silica supported Ni and found there to be peaks at ~200°C, ~300°C and ~500°C. They attributed the lower temperature peak to Ni<sup>3+</sup>, the 300°C peak to Ni<sup>2+</sup> from NiO having little or no interaction with the support and the highest temperature peak to the NiO small crystallites strongly attached to the surface. “Free” NiO could be present due to the method of catalyst preparation. A point of caution raised by Augustine [6] proposes that rapid drying of the impregnated catalyst precursor can lead to precipitation of unadsorbed salts which then can then be reduced in to unsupported metal black along with the support metal. This precipitation of the nickel salt could lead to presence of Ni<sup>3+</sup> in the absence of a calcination step. The preparation method of catalysts in this project involved a calcination step which would convert all remaining precursor salts to NiO, which prevented any Ni<sup>3+</sup> formation, hence the absence of a signal at 200°C.

Kirumakki *et al* [3] drew similar conclusions to ours and were able to show that  $\text{Ni}^{2+}$  can be reduced directly to  $\text{Ni}^0$  due to the linear nature of their hydrogen consumption data relative to nickel loading.

The TPR profile of 20% Ni/SiO<sub>2</sub> confirms the XRD data in that there appears to be NiO present in the catalyst prepared by reduction at 600°C where there was predominantly Ni metal present in the catalyst prepared by reduction at the lower temperature of 400°C. The third peak at the higher temperature of 471°C is therefore likely to result from the reduction of Ni silicate species. These are undesirable for this reaction and thus it was concluded that 400°C was the optimum temperature for reduction of this catalyst.

#### 4.2.2. 5% Ni/Al<sub>2</sub>O<sub>3</sub>

The Ni/Al<sub>2</sub>O<sub>3</sub> catalyst (MO4443) was analysed by TPR from 0 to 800°C and the resulting trace is shown in figure 4.8. Two peaks can be seen. The first peak at 275°C is a sharp peak and this is accompanied by a broad peak at 520°C. This appears to suggest that the majority of Ni present is easily available for reduction.

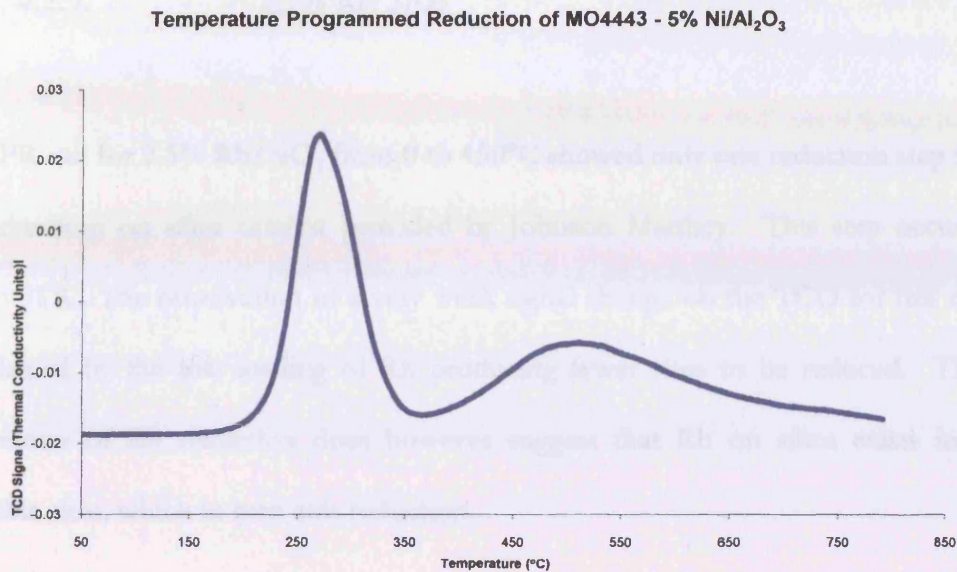


**Figure 4.8 – TPR of MO4443 – 5%Ni/Al<sub>2</sub>O<sub>3</sub>**

The TPR trace obtained for 5% Ni/Al<sub>2</sub>O<sub>3</sub> (MO4443) is typical of Ni/Al<sub>2</sub>O<sub>3</sub> [3]. Nickel on alumina has been seen in literature to have lower reduction temperatures [3] than Ni/SiO<sub>2</sub>, proving that nickel interacts more strongly with silica than with alumina. The two peaks here also correspond to reduction of NiO, some of which is strongly interacting with the surface and the remainder interacting very weakly.

The two peaks observed in MO4443 were in agreement with the findings of Kirumakki et al. They found that only at higher loadings of nickel were three TPR peaks found. They attributed this to an absence of nickel silicate in the lower Ni loading catalysts. XRD data for the higher loading catalyst 20%Ni/SiO<sub>2</sub> did not find any nickel silicate although it cannot be disregarded as it may be amorphous and thus visible in TPR and not XRD.

4.2.3. 2.5% Rh/SiO<sub>2</sub>

The TPR run for 2.5% Rh/SiO<sub>2</sub> from 0 to 450°C showed only one reduction step for the 2.5% rhodium on silica catalyst provided by Johnson Matthey. This step occurred at around 91°C. The observation of a very weak signal change on the TCD for this catalyst is explained by the low loading of Rh producing fewer sites to be reduced. The low temperature of Rh reduction does however suggest that Rh on silica exists in easily accessible sites, which in turn aids reduction.

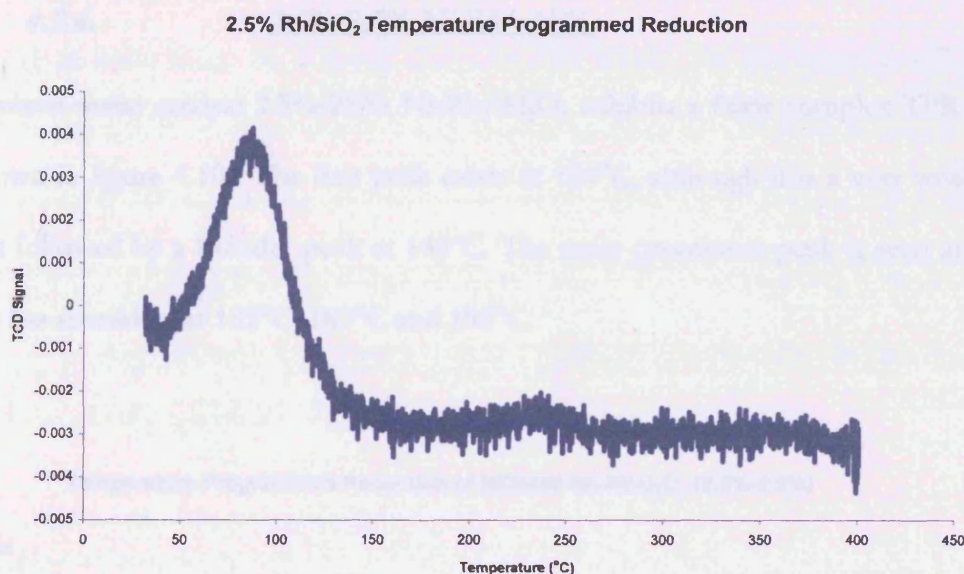


**Figure 4.9 - TPR of 2.5% Rh/SiO<sub>2</sub> (note – scale is factor of 10 smaller than earlier TPRs)**

Literature surrounding Rh/SiO<sub>2</sub> [7] catalysts shows there to be 2 overlapping peaks of reduction at low temperatures between 80-180°C. These different reduction temperatures are attributed, in the literature, to the different Rh oxide species present on the surface. Rh can exist as I+, II+ and III+ oxidation states leading to oxides of Rh<sub>2</sub>O, RhO and Rh<sub>2</sub>O<sub>3</sub>. Given the stable oxide Rh<sub>2</sub>O<sub>3</sub> is said to be easier to reduce it was



identified as the low temperature reduction peak. The second peak observed was assigned to the other Rh oxides.

The TPR of our 2.5%Rh/SiO<sub>2</sub> catalyst showed a strong peak at 91°C, which could be assigned to reduction of Rh<sup>3+</sup> to Rh<sup>2+</sup> in Rh<sub>2</sub>O<sub>3</sub>. The further shallow peak can be assigned to other oxidation states of Rhodium being reduced although it is very small and could also be due to reduction of support or support interacted Rh.

#### 4.2.4. 2.5%-2.5% Ni-Rh/Al<sub>2</sub>O<sub>3</sub>

The mixed-metal catalyst 2.5%-2.5% Ni-Rh/Al<sub>2</sub>O<sub>3</sub> exhibits a fairly complex TPR profile as shown in figure 4.10. The first peak exists at 121°C, although it is a very weak peak, and is followed by a broader peak at 143°C. The most prominent peak is seen at 171°C and it has shoulders at 182°C, 187°C and 193°C.

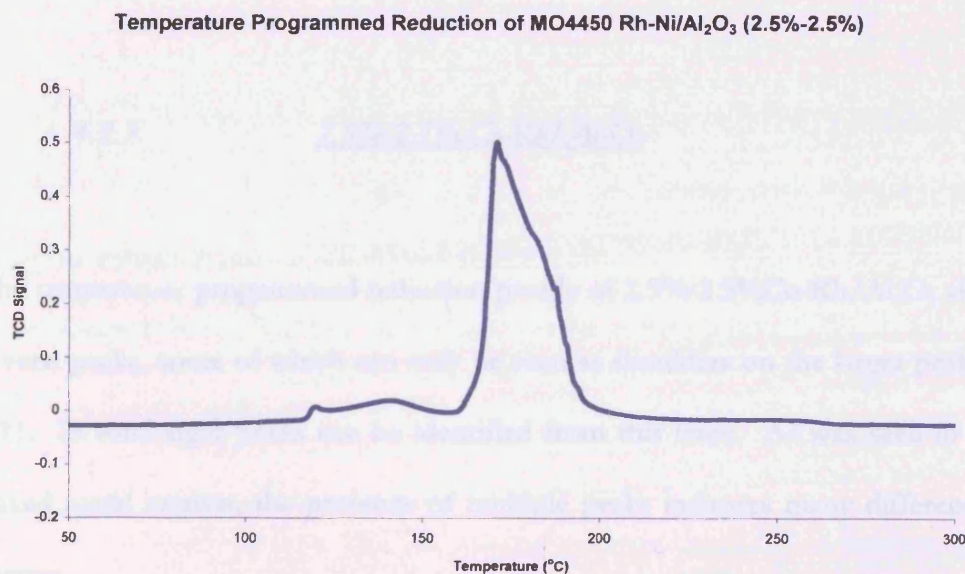


**Figure 4.10 - TPR of MO4450 2.5% Rh-2.5% Ni/Al<sub>2</sub>O<sub>3</sub>**

It has already been shown from our 5%Ni/Al<sub>2</sub>O<sub>3</sub> TPR data concluded the predominant species for nickel on alumina is loosely interacting NiO, with a signal at 273°C. Also in the literature Hou et al [8] show the TPR of Rh/Al<sub>2</sub>O<sub>3</sub> to contain a single peak below 200°C for Rh at a loading of 5% while Hwang *et al* [9] shows that Rh/Al<sub>2</sub>O<sub>3</sub> reduction can occur around 100°C in multiple stages for a range of loadings from 0.9% -23%Rh. These stages are attributed to reduction of RhO<sub>x</sub> species and RhO<sub>y</sub>Cl<sub>z</sub> on the calcined samples. However complete reduction removes the chloride ions as HCl with re-oxidation resulting in only RhO<sub>x</sub> species on the surface and thus a single peak in the TPR.

With this in mind it can be deduced from the data shown for this mixed metal catalyst that the presence of rhodium acts to lower the temperature of reduction to nearer that of the pure metal. This is shown with reduction of the mixed metal catalyst being complete by 220°C whereas for pure Ni/Al<sub>2</sub>O<sub>3</sub> a TPR peak above 500°C was seen. The complexity of the TPR does suggest the presence of a variety of mixed metal oxides and metal support interactions, with all of these species appearing easily reduced.

#### 4.2.5. 2.5%-2.5% Co-Rh/Al<sub>2</sub>O<sub>3</sub>

The temperature programmed reduction profile of 2.5%-2.5%Co-Rh/Al<sub>2</sub>O<sub>3</sub> also exhibits several peaks, some of which can only be seen as shoulders on the larger peaks in figure 4.11. In total eight peaks can be identified from this trace. As was seen in the Ni-Rh mixed metal catalyst, the presence of multiple peaks indicates many different reducible species.

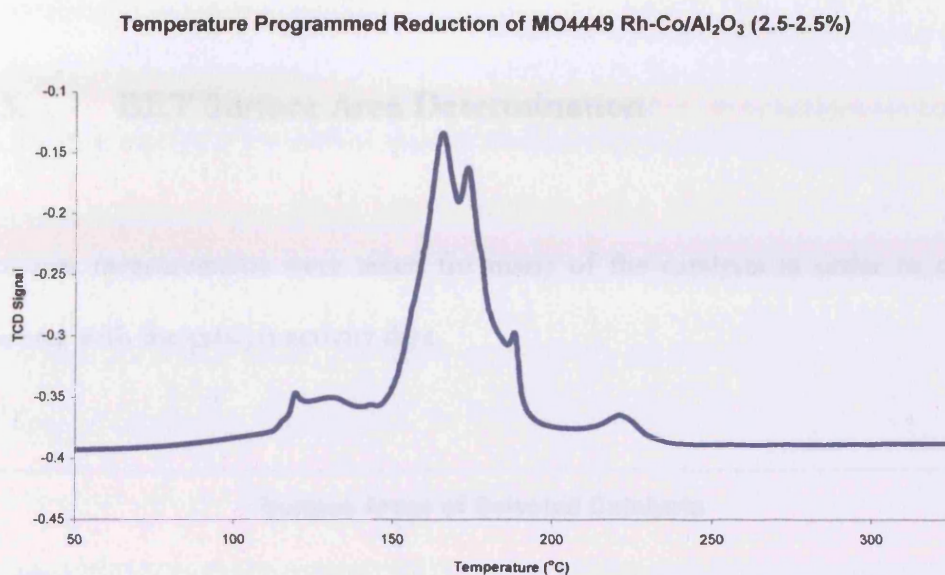


**Figure 4.11 – MO4449 - 2.5%-2.5%Co-Rh/Al<sub>2</sub>O<sub>3</sub>**

Literature of this catalyst shows the major reduction to be observed in Co/Al<sub>2</sub>O<sub>3</sub> is that of Co<sub>3</sub>O<sub>4</sub> which occurs in two stages, these being Co<sup>3+</sup> → Co<sup>2+</sup> → Co<sup>0</sup>[10]. This reduction is observed as occurring at between 260-400°C in the literature. In the case of MO4449 2.5%Co-2.5%Rh/Al<sub>2</sub>O<sub>3</sub> the same reduction occurs at far lower temperatures.

Rh/Al<sub>2</sub>O<sub>3</sub> TPR data discussed previously in this chapter indicates a rhodium on alumina reduction temperature of less than 200°C. In combination with the lower temperature signal of cobalt, it can be concluded that the presence of rhodium in this catalyst once again increases the reducibility of the base metals in the catalyst, this indicated by a lower reduction temperature.

Unfortunately XRD traces of the low loading catalysts showed no diffraction peaks other than the amorphous support peak. A lack of XRD data for these low loading catalysts means we cannot confirm the final species present.

### 4.3. BET Surface Area Determination

Surface area measurements were taken for many of the catalysts in order to compare surface area with the catalyst activity data.

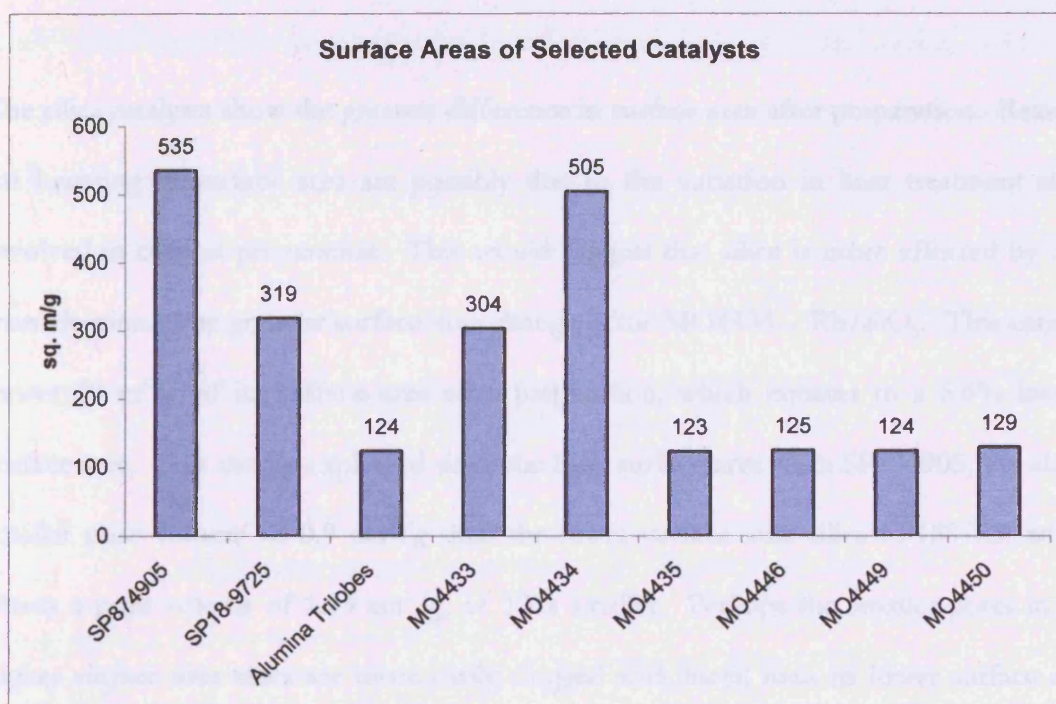


Figure 4.12 - BET Surface Areas, (each surface area is the average of 3 measurements, catalyst codes are defined in table 4.5).

Catalyst	Metal Present (%)	Support Used
MO4433	5% Rh	SP189725
MO4434	5% Rh	SP87905
MO4435	5% Rh	Alumina Trilobes
MO4446	5%Ni	Alumina Trilobes
MO4449	2.5%Co-2.5%Rh	Alumina Trilobes
MO4450	2.5%Ni-2.5%Rh	Alumina Trilobes

Table 4.6 – BET Surface Area Chart Key

From the bar chart in figure 4.12 it is clear to see that in the majority of cases the surface areas of the catalysts are just below that of their un-impregnated supports. The highest surface area support is granulated silica SP874905. This support was used to produce catalyst MO4434 - 5%Rh/SiO<sub>2</sub>. The granulated silica support SP189725 was used to make MO4433 – 5%Rh/SiO<sub>2</sub>. The catalysts MO4435, MO4446, MO4449 and MO4450 were prepared on alumina trilobes.

The silica catalysts show the greatest difference in surface area after preparation. Reasons for lowering in surface area are possibly due to the variation in heat treatment steps involved in catalyst preparation. This would suggest that silica is more affected by heat than alumina. The greatest surface area change is for MO4434 – Rh/SiO<sub>2</sub>. This catalyst loses 30 m<sup>2</sup>/g of its surface area after preparation, which equates to a 5.6% loss in surface area. This can be explained since the high surface area silica SP874905, has also a smaller pore volume of 0.9 cm<sup>3</sup>/g than the lower surface area silica SP189725, which shows a pore volume of 1.03 cm<sup>3</sup>/g, *i.e.* 13% smaller. Perhaps the smaller pores in the higher surface area silica are more easily clogged with metal than its lower surface area counterpart, which only loses 4.7% of its surface area upon catalyst loading. This would have the affect of making some pores inaccessible. It should not be ruled out however that experimental error may be enough to present the observed differences upon impregnation.

The alumina supported catalysts MO4435, MO4446 and MO4449 show very little change in surface area upon catalyst preparation, with only a (+/-) 1% change. The 2.5%Ni-2.5%Rh/Al<sub>2</sub>O<sub>3</sub> (MO4450) catalyst shows an increase in surface area (+4%), relative to alumina trilobes although once again this is possibly due to the experimental anomaly.

Surface areas were also taken of the Ni/MgO catalyst prepared at the beginning of the project. These catalysts were made by incipient wetness technique using either nickel acetate or nickel nitrate solutions made up such that the nickel to magnesium ratio was 4:1 or 1:1. These catalysts were produced on powdered supports and were eventually found to be unsuitable for use in the flow system reactors because the fine powders clogged the system and did not allow flow through the trickle bed. In the gas phase reactor the fine powder stuck together with condensed reactants and ceased flow. For this reason, no activity data was recorded for these. Figure 4.13 shows the surface areas of these catalysts.

The surface area of the calcined precursor is lower than the original un-doped support.

The surface area is further reduced by the reduction process.

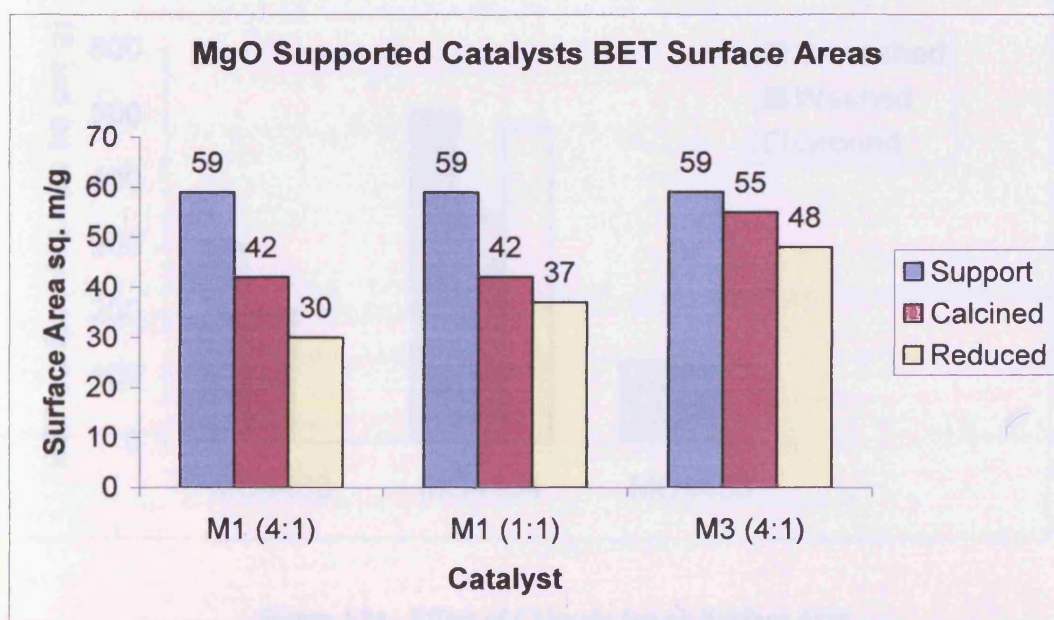


Figure 4.13 – MgO catalyst BET surface areas

Both the catalysts produced from nickel nitrate (M1) and nickel acetate (M3) showed the same trend and there was very little difference in the behaviour of the lower loading nickel nitrate catalyst. M3 was prepared using nickel acetate and it appears to lose less surface area during the calcination process, but still loses a significant proportion of its surface area to the reduction step.

The effect of chloride ions on the activity of the catalysts was investigated using the autoclave. Chloride ions were removed by stirring in warm ammonia. Figure 4.14 shows the change in surface area of these catalysts during the washing process. A ground catalyst was also included in order to ascertain if the vigorous stirring results in catalyst break up and so may have been the reason for the surface area change.

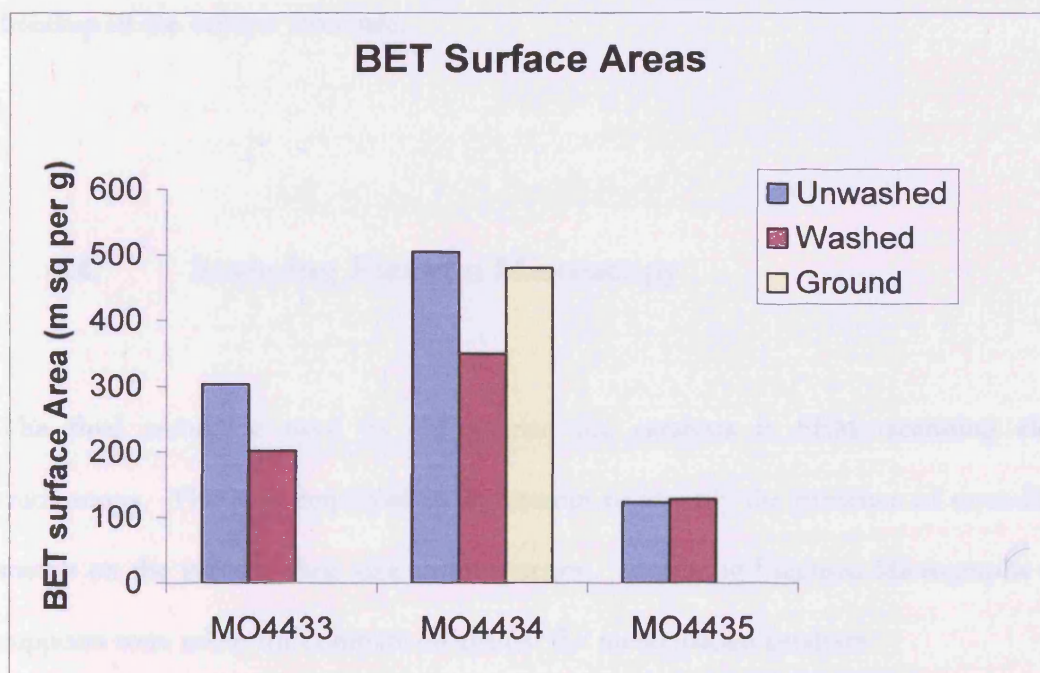


Figure 4.14 - Effect of Chloride Ion on Surface Area

	Unwashed	Washed
MO4433	304m <sup>2</sup> /g	202 m <sup>2</sup> /g
MO4434	505 m <sup>2</sup> /g	349 m <sup>2</sup> /g
MO4435	123 m <sup>2</sup> /g	128 m <sup>2</sup> /g

**Table 4.7 - Effect of washing on surface area**

It can be seen that surface area decreases in the two silica supported catalysts on washing (Table 4.7). The alumina supported catalyst MO4435 is unaffected by the ammonia treatment. It can also be seen that the ground sample of catalyst MO4434 proves that the surface area change is certainly due to the ammonia treatment and not to the physical breakup of the catalyst structure.

#### 4.4. Scanning Electron Microscopy

The final technique used to characterise the catalysts is SEM, scanning electron microscopy. This was employed in an attempt to identify the presence of crystallites of metals on the surface, their size and dispersion. Scanning Electron Micrographs of the supports were taken for comparison against the metal loaded catalysts.

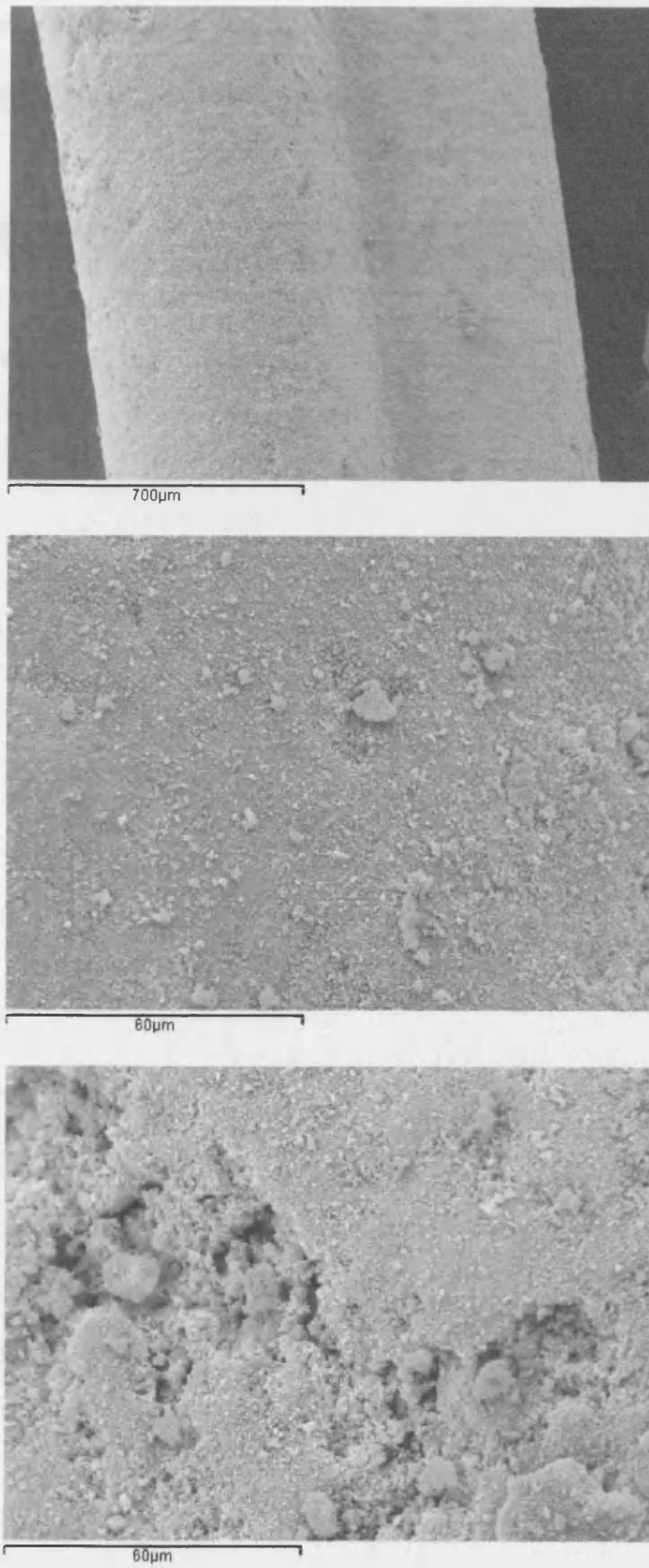


Figure 4.15 - SEM images of alumina trilobes

Figure 4.15 shows SEM images of alumina trilobes at different magnifications and shows the rough surface of the support before addition of any metal.

The two types of silica, SP18-9725 (Figure 4.16) and SP874905 (Figure 4.17) are shown below. Both appear to have similar surfaces showing both rough and smooth areas with steps and grains visible on the surface.

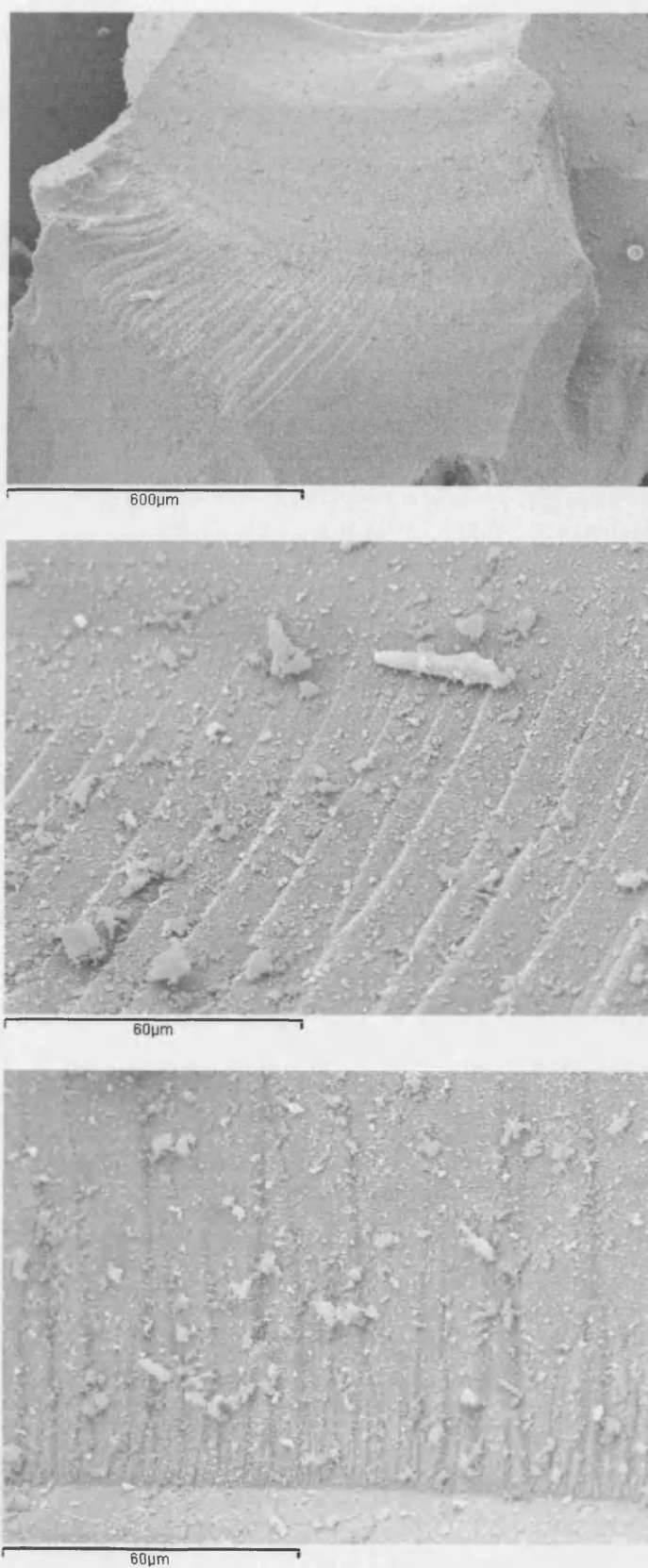


Figure 4.16 – SEM images of silica support SP189725

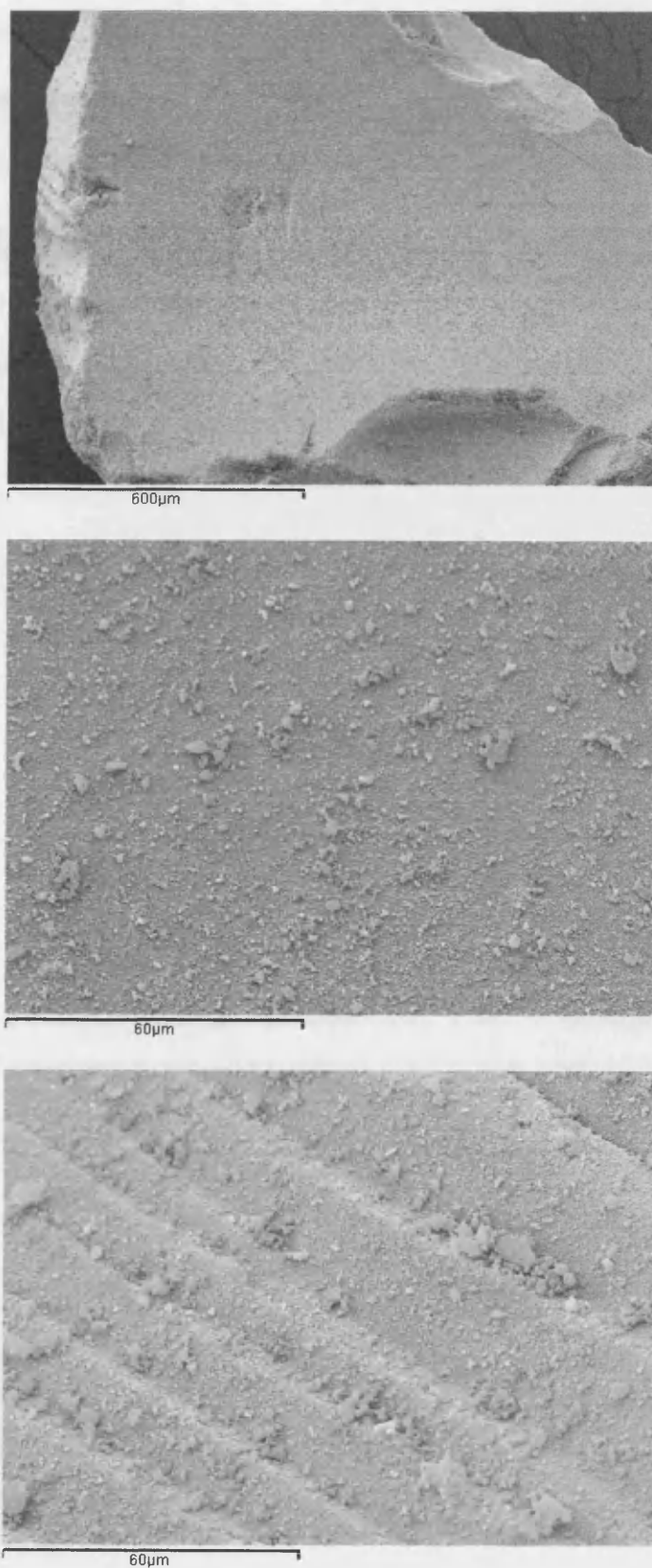
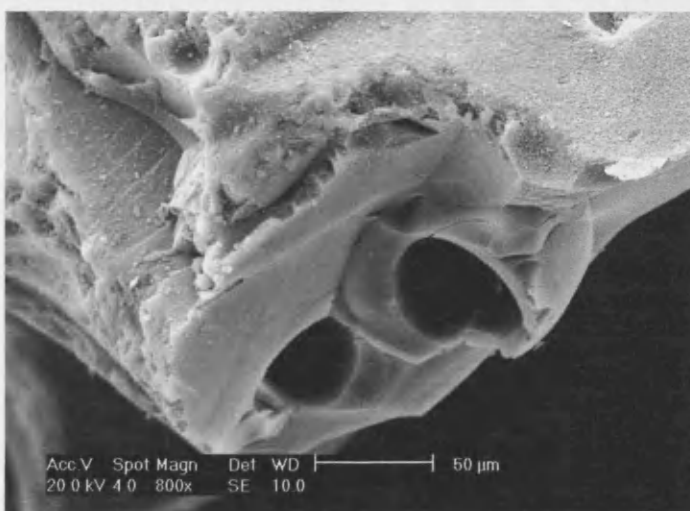
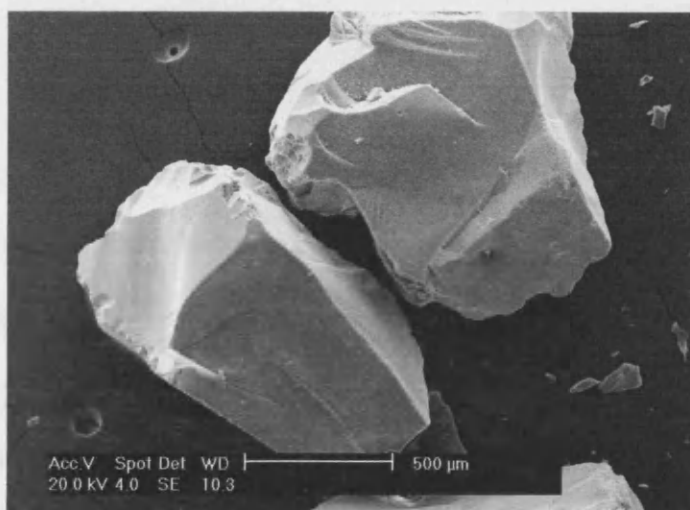


Figure 4.17 - SEM images of silica support SP874905

SEM appears to show no discernable differences in the surface of the silica supports. After catalyst preparation, one might expect to see a change in morphology of the support due to heat treatment. Indeed this might be the case; the surface areas of the catalyst are known to be lower than that of the un-impregnated support and changes seen in SEM may also account for this. As the supports are non-crystalline their structures are dependant on the shapes they were produced to be. The alumina trilobes were formed by extrudates in to the trilobes shape.



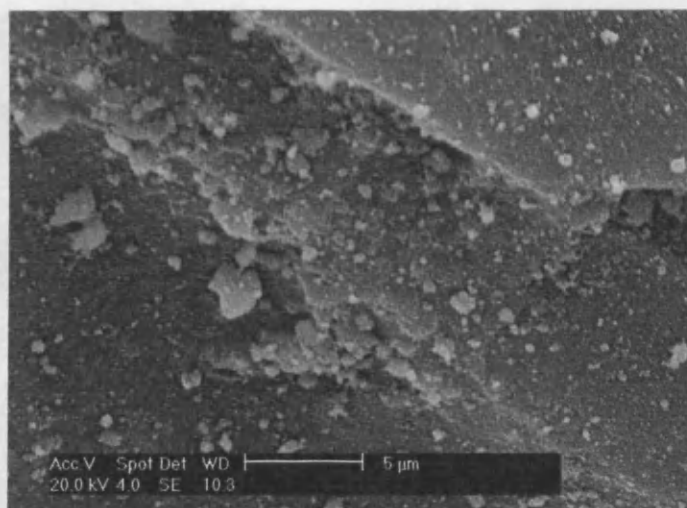
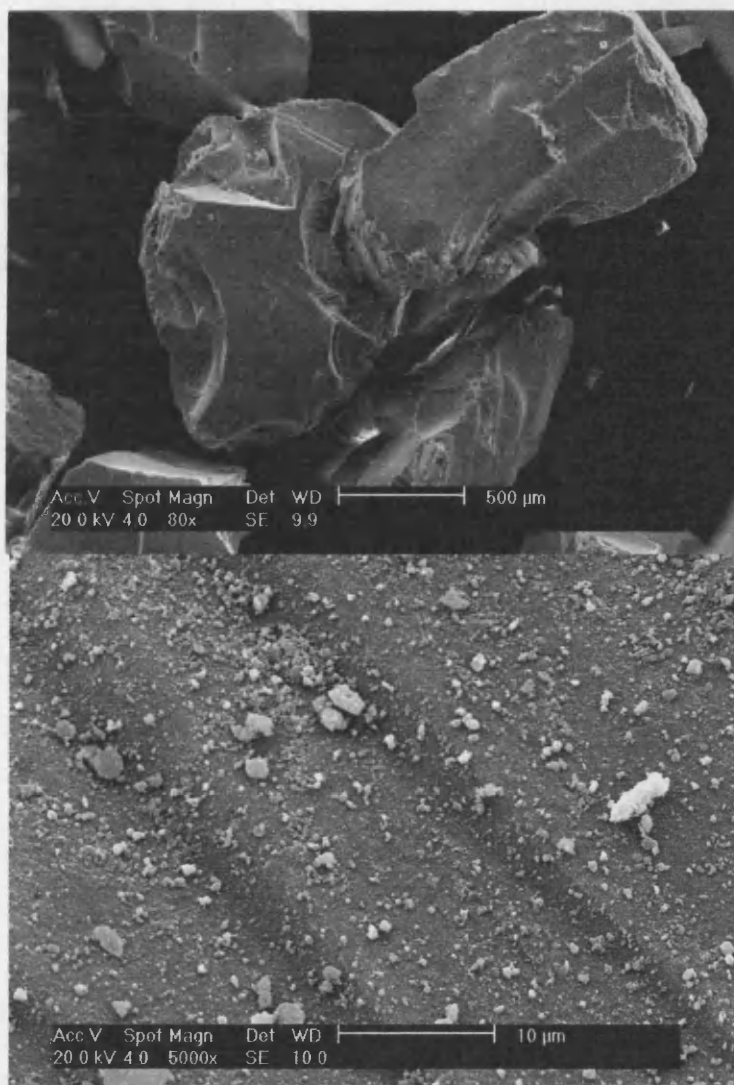


Figure 4.18 – SEM images of MO4433

The SEM image of 5% Rh/SiO<sub>2</sub> (SP189725) catalyst MO4433 (Figure 4.18) shows that there is no distinct difference between the morphology of the loaded catalyst and that of the support on its own.

It was also possible to analyse the elemental make up at specific points on the surface using the X-ray spectroscopy within the SEM. From this it was possible to confirm that the clusters seen on the surface are of the same composition as the flat areas. It was ascertained that there is an even distribution of metal on the catalysts' surface in what seems to be a film as opposed to larger crystallites at this low loading. The rhodium concentration is consistent throughout.



**Figure 4.19 – SEM images of MO4434 before washing**

MO4434, 5% Rh/SiO<sub>2</sub> (SP874905), shows a similar effect of rhodium being equally dispersed across the surface (Figure 4.19). The surface of the catalyst after washing in ammonia was also examined by SEM and can be seen in figure 4.20.

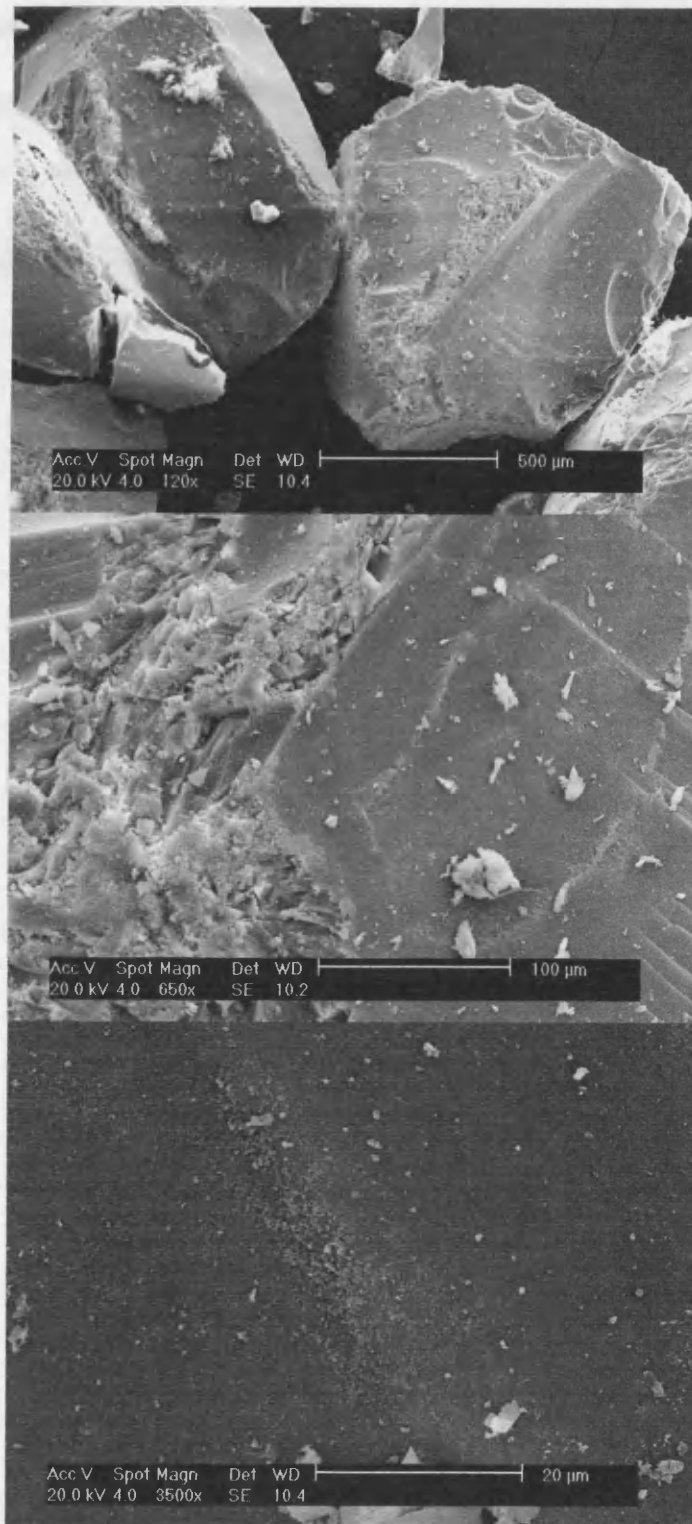


Figure 4.20 – SEM images of MO4434 after washing in NH<sub>3</sub>

It can be seen that the surface is more cracked and may have been altered from the effect of the ammonia washing, which had to be performed in order to eliminate chloride ions from the catalyst in order to prevent poisoning.

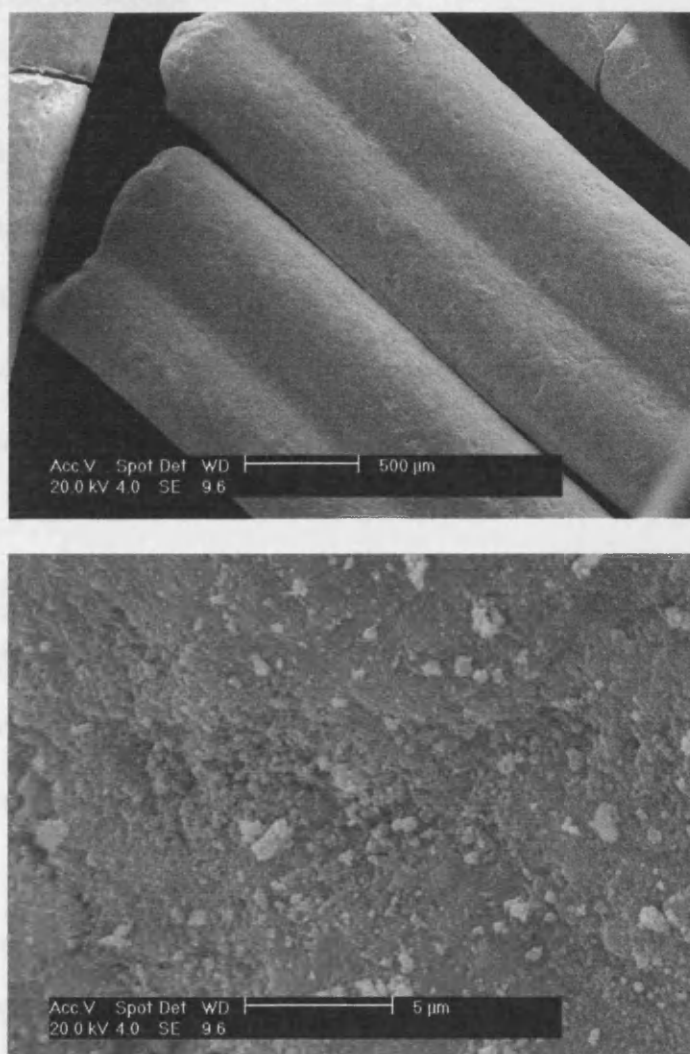


Figure 4.21 – SEM image of MO4445

The surface of 5% Co/Al<sub>2</sub>O<sub>3</sub> (MO4445) also shows that the process of catalyst production did not affect the morphology of the support (Figure 4.21). The rough surface is the same after calcination and reduction, as it was before and there were also

no cobalt dense regions to be found on the surface, which suggested even metal distribution.

## **4.5. Conclusions**

The characterisation of these catalysts was performed in order to gain an insight in to the structure and chemical composition of each catalyst and the effect of the support and catalyst preparation method on its final structure. The data from these catalysts can then be correlated with the activity data for the adiponitrile hydrogenation in the three different reactors, in Chapter 5.

XRD data was taken for all the catalysts but unfortunately the low metal loading catalysts showed no identifiable diffraction data for the metal species. The Pricat catalysts were identified to have NiO and Ni phases present along with diffraction peaks relating to their individual support combinations.

The Ni/MgO catalysts illustrated the reduction process as it was clear to see, by XRD, the depletion of the peaks relating to NiO and the increase of peaks for Ni when comparing the reduced and calcined samples. BET surface areas for these catalysts also showed standard changes to occur during the catalyst preparation heat treating stages of calcination and reduction. The surface area for the three different Ni/MgO catalysts diminished at each stage.

It was possible to get a clear XRD of 20% Ni/SiO<sub>2</sub> with the powder pattern for its precursor showing only weakly diffracting precursor peaks until after reduction, when Ni and NiO then became apparent. This catalyst was used to investigate a suitable reduction temperature and method. It was found that at higher temperatures peaks began to appear which could correspond to nickel silicate formation. A temperature of 400°C was optimal. Three methods of reducing the catalyst were tested. The methods in which the reducing gas was passed through a suspended sample of the catalyst proved to be most efficient. This highlights the possibility of reducing the catalyst *in situ* within the gas phase reactor in order to have more Ni metal present.

TPR proved to be a useful technique. For the 20% loading Ni/SiO<sub>2</sub> catalyst it was found that the reduction of nickel when on a silica support occurs at around 266°C, this being in agreement with the literature. Two main forms of Ni are expected to participate in the reduction events, both “free” NiO and “bound” NiO depending on how strongly the Ni is interacting with the surface. The alumina supported nickel was found to display a weaker interaction with the surface than that of nickel on silica.

Ni catalysts on alumina have been shown to have two reduction stages at ~250 and 500°C, and literature shows that cobalt has a series of reduction steps between 200 and 700°C [12]. Rh alone on alumina is known to have a reduction temperature of around 200°C [8]. The addition of a precious metal, such as rhodium, to a base metal, either cobalt or nickel as in MO4449 and MO4450 respectively, allowed for the overall reduction temperature to be lowered, with both showing signals below 200°C. Complex reduction profiles indicate the presence of many reducible species, possibly an indication of alloying between the base metal and precious metal.

A brief investigation into the effect of washing to remove chloride ions from the metal chloride prepared catalysts was undertaken. It was found that the surface area of the washed catalysts had decreased. In order to eliminate physical stirring as being the cause of the surface area decrease, a ground sample was successfully shown to not affect the overall surface area. This led to the conclusion that washing both Rh/Al<sub>2</sub>O<sub>3</sub> and Rh/SiO<sub>2</sub> with ammonia causes a significant decrease in surface area. This decrease is most pronounced in the silica catalysts but negligible in the alumina supported catalyst.

Finally, SEM was used in an attempt to gain a view of the catalyst surface. It was found that the metals were evenly distributed across the catalyst surface and not, as had been feared, clustered up as a result of sintering at high temperatures or from the formation of large crystallites. This may be due to the low loadings.

The significance of the structural and chemical differences in the prepared catalysts will be revealed when considered alongside the activity data in Chapter 5.

#### 4.6. References

- 12 S. Brunauer, P. H. Emmett, and E. Teller, *Journal of the American Chemical Society*, 1938, **60**, 309.
- 13 Serra M, Salagre P, Cesteros Y, Medina F, Sueiras J.E, *Journal of Catalysis*, 2002, **209**, 202
- 14 S. R. Kirumakkia, B. G. Shpeizera, G. V. Sagarb, K. V. R. Charyb, and A. Clearfield, *Journal of Catalysis*, 2006, **242**, 319.
- 15 S. Xu and X. Wang, *Fuel*, 2005, **84**, 563.
- 16 B. Mille, D. Stirling, M. A. Zammitt, A. Lovell and M. Webb, *Journal of Molecular Catalysis*, 1990, **62**, 179.
- 17 R. L. Augustine, *Heterogeneous Catalysis for the Synthetic Chemist*, Marcel Dekker Inc, 1996.
- 18 T. Wu, Q. Yanb, F. Maoa, Z. Niua, Q. Zhanga, Z. Lia and H. Wan, *Catalysis Today*, 2004, **93-95**, 121.
- 19 Z. Hou and T. Yashima, *Catalysis Letters*, 2003, **89**, 193.
- 20 C.-P. Hwang, C.-T. Yeha and Q. Zhu, *Catalysis Today*, 1999, **51**, 93.
- 21 H. Xiong, Y. Zhang, S. Wang, and J. Li, *Catalysis Communications*, 2005, **8**, 512.
- 22 R. Bechara, D. Balloy, J.-Y. Dauphin, and J. Grimblot, *Chemistry of Materials*, 1999, **11**, 1703.

*Chapter 5*

**ACTIVITY TESTING**

---

## 5. ACTIVITY TESTING

---

### 5.1. Introduction

Catalytic activity has been tested for the catalysts produced and obtained. Three different reactors were used to compare and contrast the efficiency and selectivity of the adiponitrile hydrogenation reaction in different phase systems and for comparing a batch process to flow systems. For liquid phase batch reaction a Parr autoclave was used. This was contrasted to a flow system in the Trickle-Bed reactor. The third reactor investigated was the Gas-Phase Fixed-Bed flow reactor. Products from all three reactors were collected and analysed mainly by gas chromatography and the reaction data is shown as percentage conversion and selectivity to certain products. Each experiment was run at least three times for each set of conditions in order to prove reproducibility therefore each point on each graph represents multiple experiments. Results are quoted from the first experimental time point of three hours, itself selected in view of the poor conversions seen at shorter reaction times during provisional screening.

### 5.2. Autoclave Reactor

#### 5.2.1. *Pricat Catalysts*

The Pricat catalysts obtained from Johnson Matthey has been tested in the autoclave reaction. Pricat Ni 62/15P consists of Ni/NiO supported on silica, magnesia and graphite. Pricat catalysts have between 30-40% Ni loading. Continuous sampling is not

possible using the equipment as it is currently set up. Each experiment is conducted individually for the time period indicated.

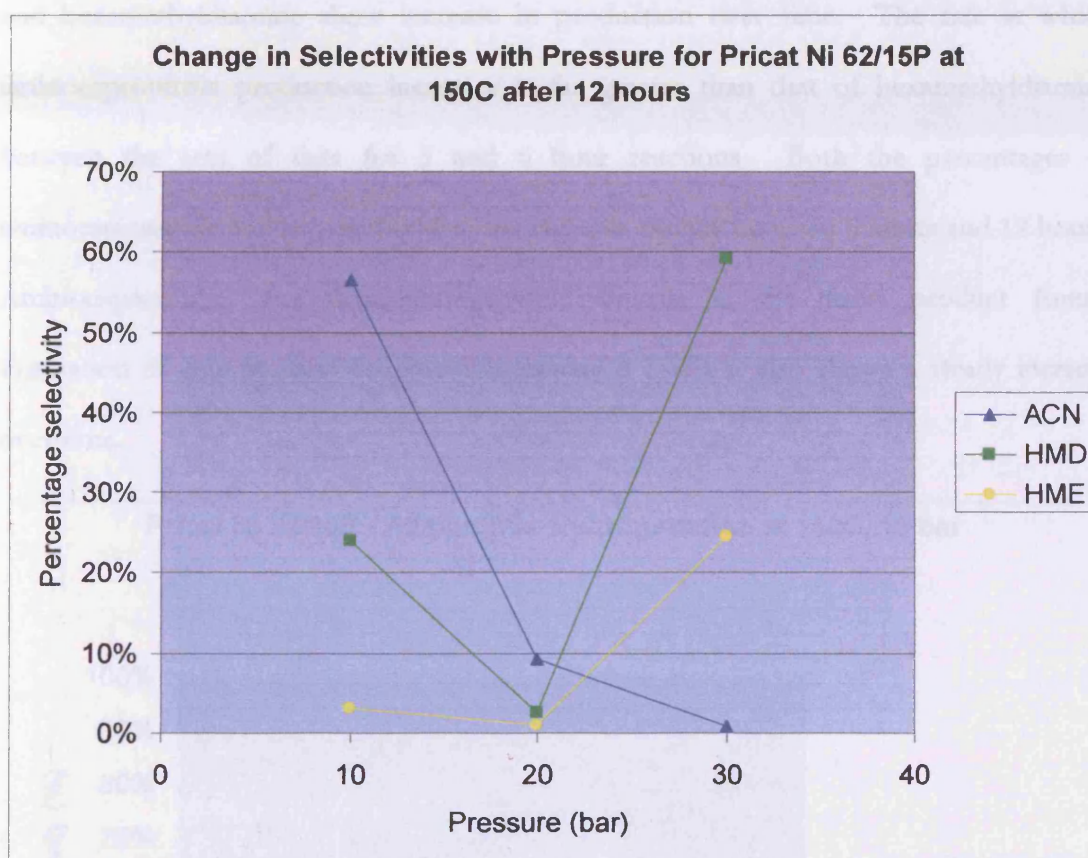


**Figure 5.1 – Graph of selectivity against pressure for Pricat Ni62/15P**

Figure 5.1 shows the data for reaction of adiponitrile hydrogenation in the autoclave at 150°C over a range of pressures from 10 to 30 bar. The data is taken for 12 hours reaction time. It can be seen that formation of aminocapronitrile (ACN) is favoured over hexamethyldiamine (HMD) formation at lower pressure with the reverse being true at higher pressures. The formation of the by product hexamethyleneimine (HME) appears to increase at higher pressures. The experiment conducted at 20 bar yielded unexpectedly low results. This data can be seen in more detail in the graph in figure 5.3, where further explanation will be given.

Results for the reaction at 10 bar can be seen in figure 5. 2. The conversion steadily increases with the time of reaction until reaching a value of 90%. Both aminocapronitrile and hexamethyldiamine show increase in production over time. The rate at which aminocapronitrile production increases is far greater than that of hexamethyldiamine between the sets of data for 3 and 6 hour reactions. Both the percentages of aminocapronitrile and hexamethyldiamine increase equally between 6 hours and 12 hours. Aminocapronitrile, the hemi-hydrogenated dinitrile is the main product found. Formation of side product hexamethyleneimine is low but also shows a steady increase over time.

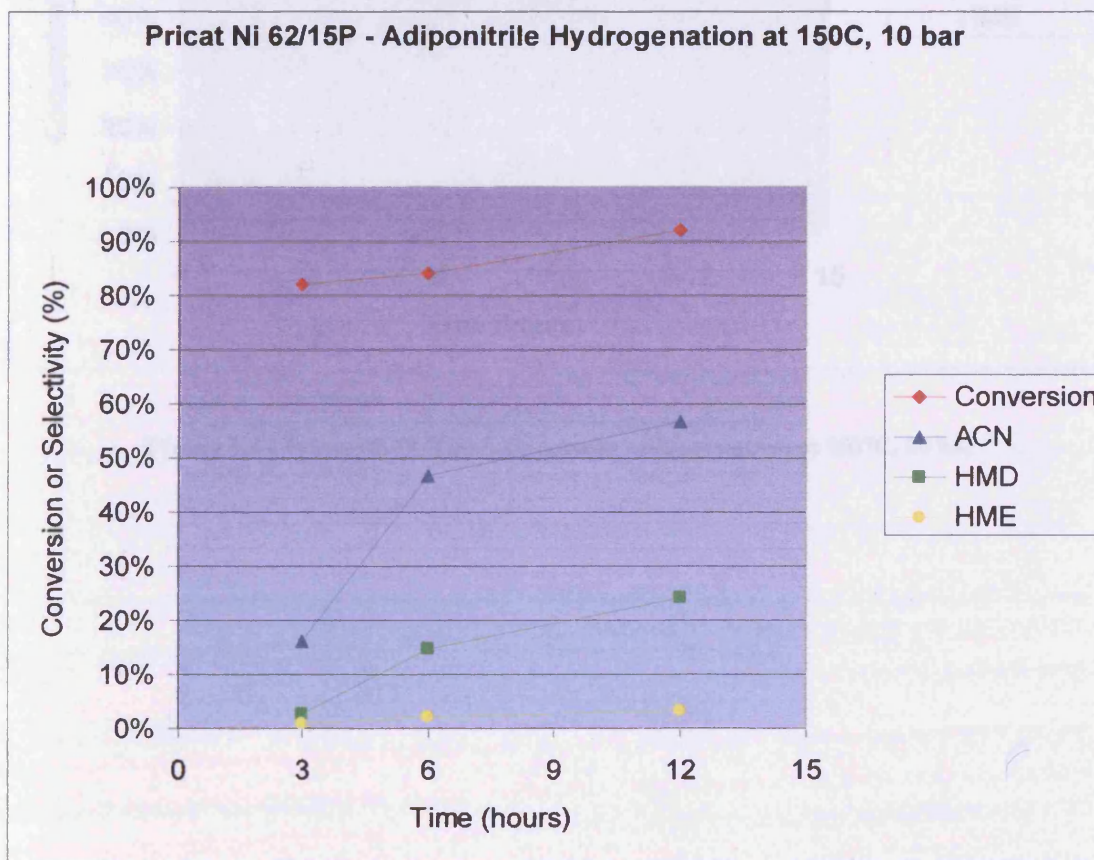


Figure 5. 2 – Pricat Ni 62/15P Adiponitrile hydrogenation at 150°C, 10 bar

The data from the 20 bar reactions show that although conversion is high, the reaction is not yielding any of the desired products in significant quantities as shown in figure 5.3.

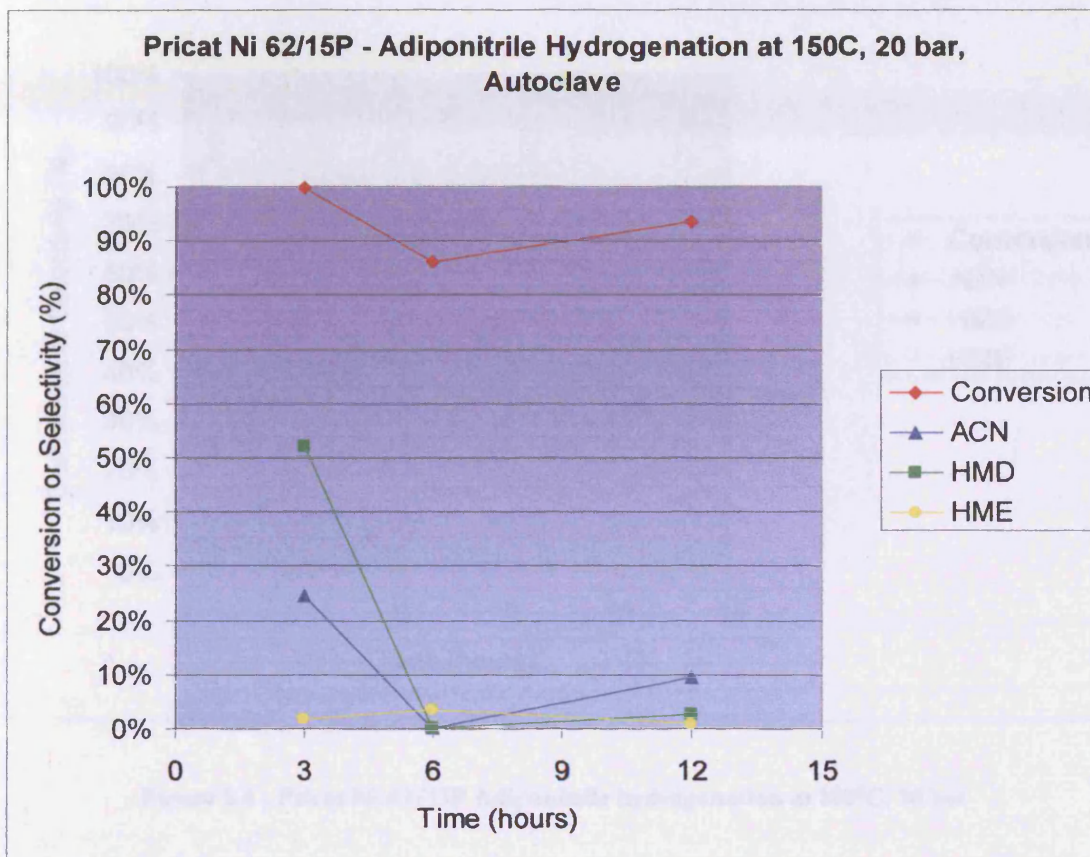
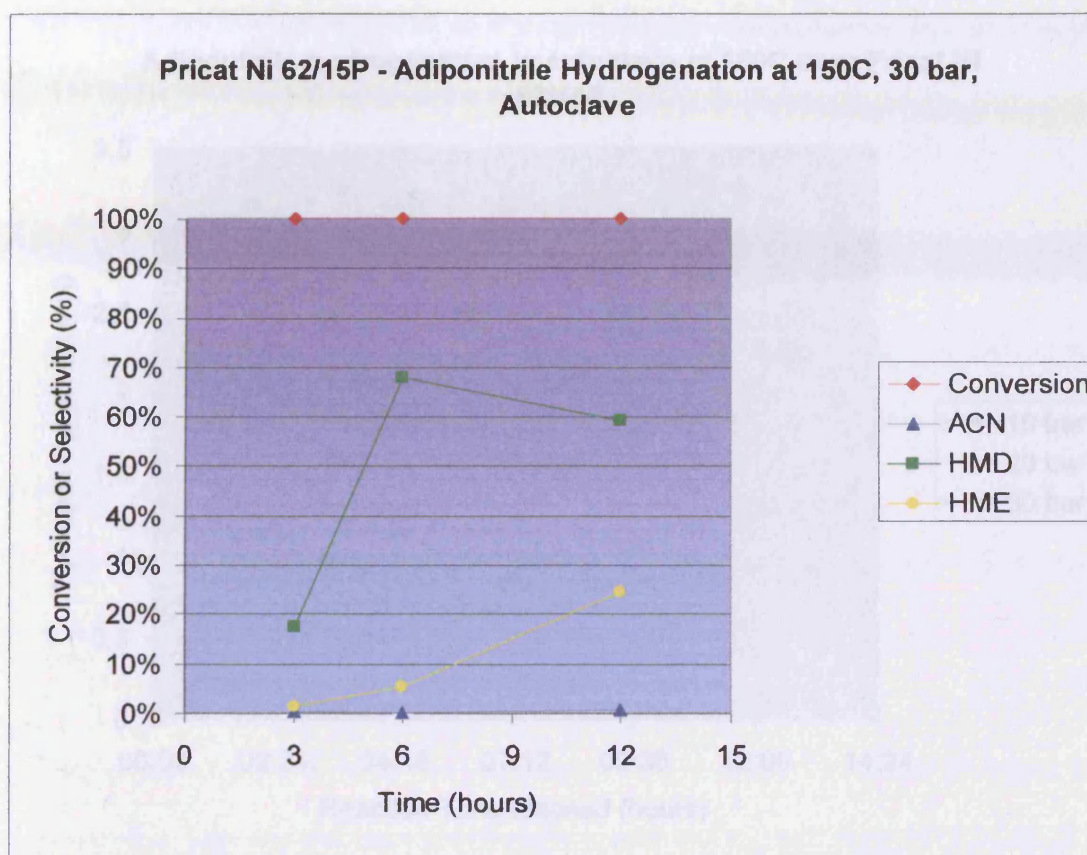
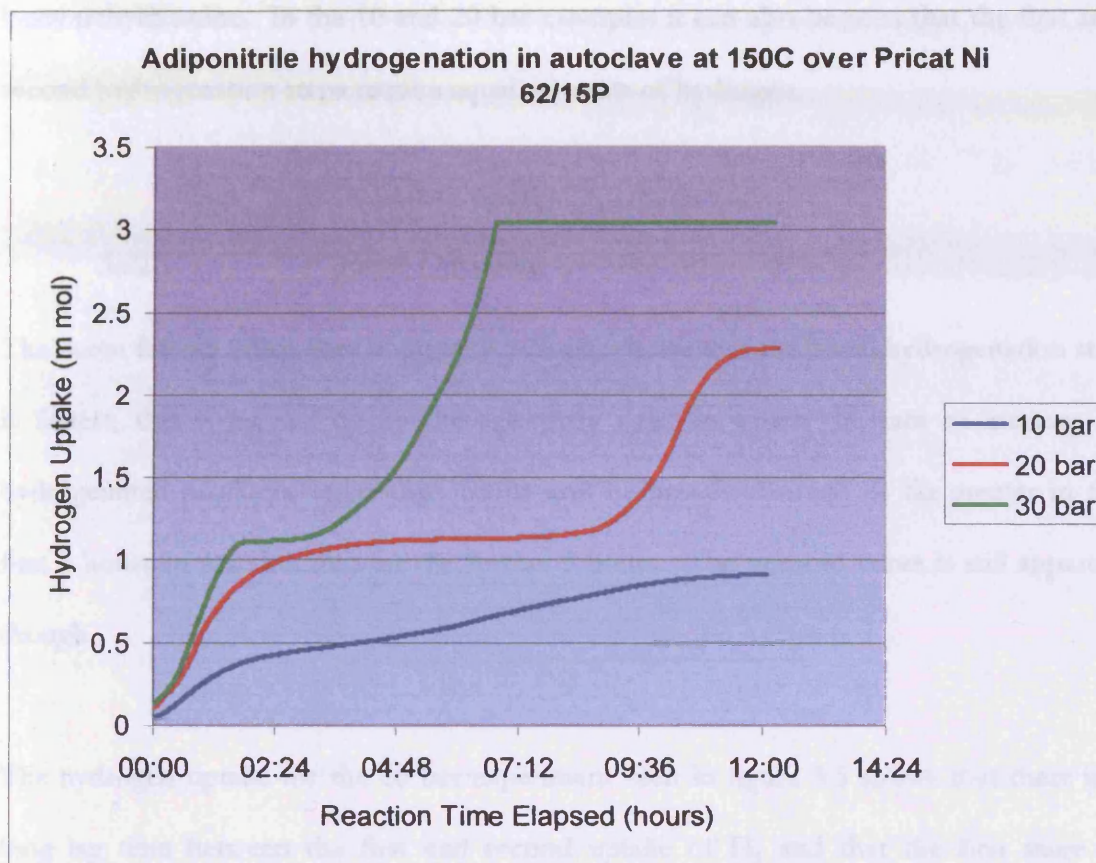


Figure 5.3 - Pricat Ni 62/15P Adiponitrile hydrogenation at 150°C, 20 bar



**Figure 5.4 - Pricat Ni 62/15P Adiponitrile hydrogenation at 150°C, 30 bar**

Full conversion is found for the reaction at 30 bar pressure running for a duration of 3 hours. The main product is hexamethyldiamine. The very low levels of aminocapronitrile indicate that it has all been converted into hexamethyldiamine. When the reaction is allowed to run for 12 hours it can be seen that the percentage of hexamethyldiamine is lower than after 6 hours. This could be due to hexamethyleneimine (HME) production or dimerisation of hexamethyldiamine.



**Figure 5-5 – Hydrogen uptake data for Pricat Ni 62/15P adiponitrile hydrogenation at 150°C**

Hydrogen uptake data were taken during these reactions by virtue of a computer monitoring the hydrogen delivery system. These data shows us in figure 5.5 a reaction profile. The reaction appears to occur in two steps. Initially the hydrogen uptake is fast and linear and this levels out for a period most distinctly in the case of the 20 bar reaction. After the period of levelling out the uptake again increases and finally the reaction comes to completion. This sigmoid shaped curve is very subtle in the slower 10 bar reaction. These two steps could correspond to firstly the initial formation of aminocapronitrile then the second stage of hydrogen up take represents the further hydrogenation step in which aminocapronitrile is hydrogenated further in to

hexamethyldiamine. In the 10 and 20 bar examples it can also be seen that the first and second hydrogenation steps require equal amounts of hydrogen.

### 5.2.2. Pricat Discussion

The curve for the 10bar data in figure 5.5 clearly shows that the initial hydrogenation step is fastest, this is backed up by the selectivity data, in which the rate of increase of hydrogenated products, aminocapronitrile and hexamethyldiamine, is far greater in the first 3 hours of reaction than for the further 9 hours. The sigmoid curve is still apparent though.

The hydrogen uptake for the 20 bar experiment seen in figure 5.5 shows that there is a long lag time between the first and second uptake of H<sub>2</sub> and that the first stage of hydrogenation is over by the three hour point. At this point selectivity data shows that the diamine product is twice as abundant as the monoamine. It could be suggested that during the lag time, there is formation of some intermediate which has not been identified. Possibly the pressure is not yet great enough to force the reaction through to diamine and during this lag in hydrogen uptake, the diamine already formed either dimerises or otherwise reacts without hydrogen forming other side products.

At 30 bar the lag time is very short and by 6 hours we can already see hexamethyldiamine as the dominant product this can be seen in figure 5.4. Trace amounts of aminocapronitrile are present and the side product is formed in significant quantities (23.5%). It can also be noted that the second hydrogen uptake even requires far more hydrogen than the first.

This shows that at higher pressures the reaction is forced through to the second hydrogenation step. All aminocapronitrile is converted to hexamethyldiamine. The side product formed is likely the result of a cyclisation of hexamethyldiamine. This reaction would be best stopped after 6 hours for maximum hexamethyldiamine yield.

The high conversions seen with these catalysts are most likely due to the high Ni content which was identified by atomic absorption to be 38.7% nickel by wt for the Pricat (15P). This catalyst was supported on a mixture of amorphous supports, on XRD as seen in figure 4.1 chapter 4, shows that the predominant species present is NiO. This shows NiO to be highly active to adiponitrile hydrogenation.

### 5.2.3. Nickel on Silica Catalysts

Nickel catalysts were prepared on granulated silica and fumed silica with various metal loadings. Base metal catalysts are usually used at higher loadings than precious metals both due to their lower cost and because they are generally found to be less active in low concentrations compared to precious metal catalysts.

#### 5.2.3.1. Catalyst S12 – Ni/SiO<sub>2</sub>

Catalyst S12 comprises 20%Ni supported on silica and it has been tested in the autoclave at 20 and 30 bar and 150°C for adiponitrile hydrogenation.

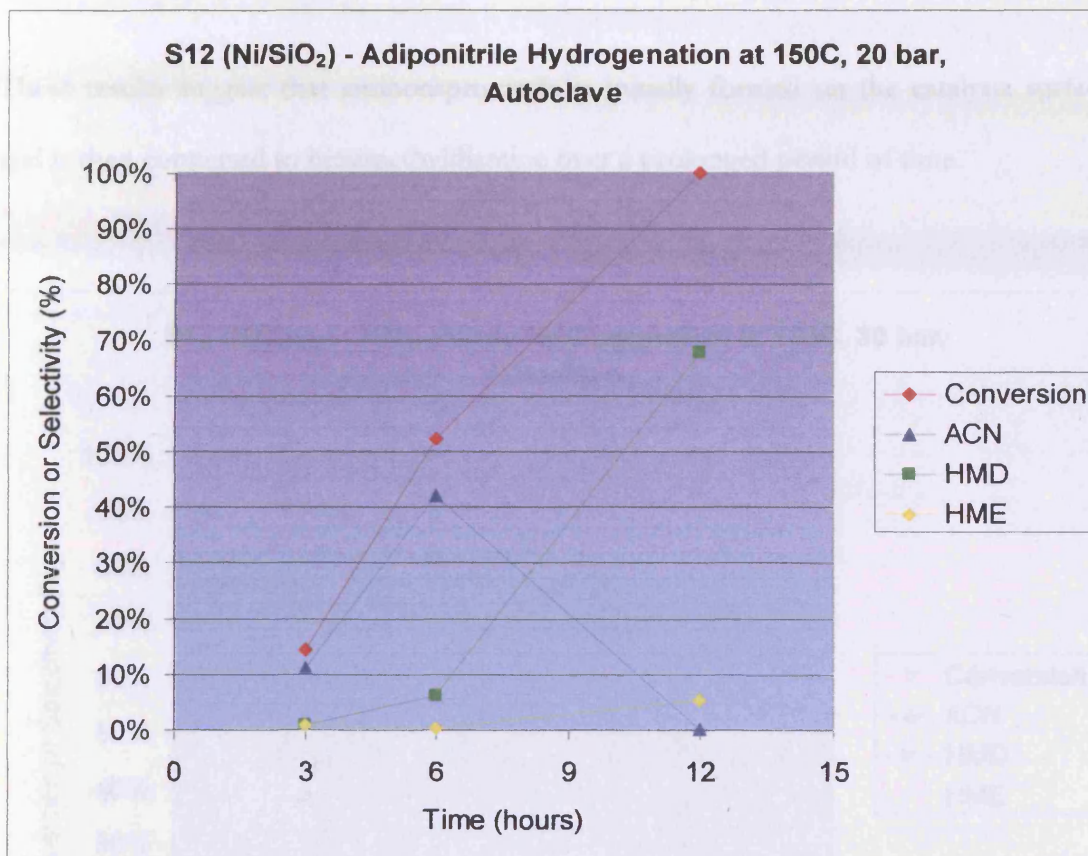


Figure 5.6– Activity data for 20% Ni/SiO<sub>2</sub> at 150°C, 20 bar

Figure 5.6 clearly shows conversion and selectivity for this reaction using this catalyst against time. Nickel on silica, 20% was found to have fairly low conversions so 10 bar experiments were avoided. At 20 bar it can be seen that the conversion increases rapidly with time. After 3 hours there is low conversion and the main product seen is aminocapronitrile. After 6 hours the reaction is coming to 50% conversion and this is mainly still aminocapronitrile. Small percentages of hexamethyldiamine can be seen, but negligible side product formation occurs. The reaction when allowed to run for 12 hours shows that hexamethyldiamine is now the favoured product and levels of aminocapronitrile are extremely low. All experiments yielded very low levels of side product, as the reaction time increased some of these side products became slightly more prevalent (8.2%).

These results suggest that aminocapronitrile is initially formed on the catalysts surface and is then converted to hexamethyldiamine over a prolonged period of time.

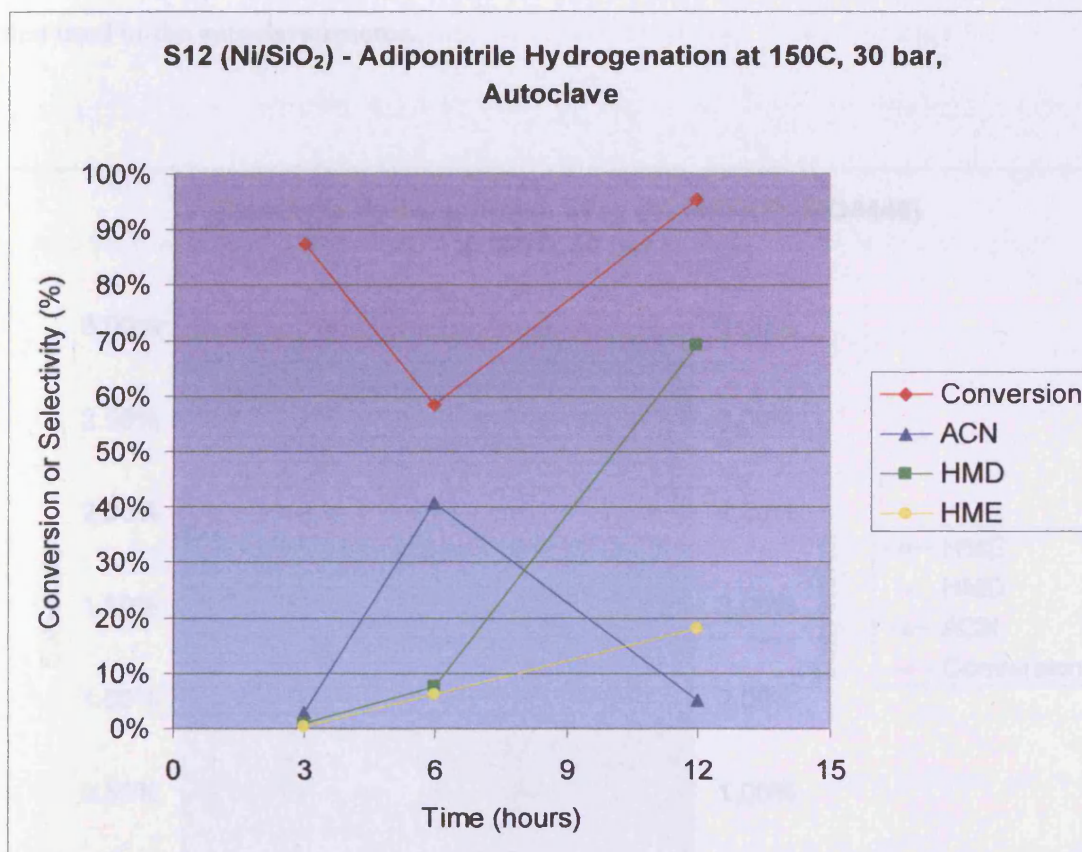


Figure 5.7 - Activity data for 20% Ni/SiO<sub>2</sub> at 150°C, 30 bar.

In general at 30 bar as seen in figure 5.7, conversion increases with time. The lower rate of conversion in the 6 hour reaction is an unusual anomaly. Otherwise it can be seen that the same trend as at 20 bar is observed; as HMD concentration increases, ACN concentration decreases and formation of side products increases slowly over time.

5.2.4. 5% Ni/SiO<sub>2</sub> - (MO4446)

In order to compare catalysts containing base metals with rhodium on the basis of the weight of the metal component, a sample of 5% Ni on silica was prepared. This was first used in the autoclave reactor.

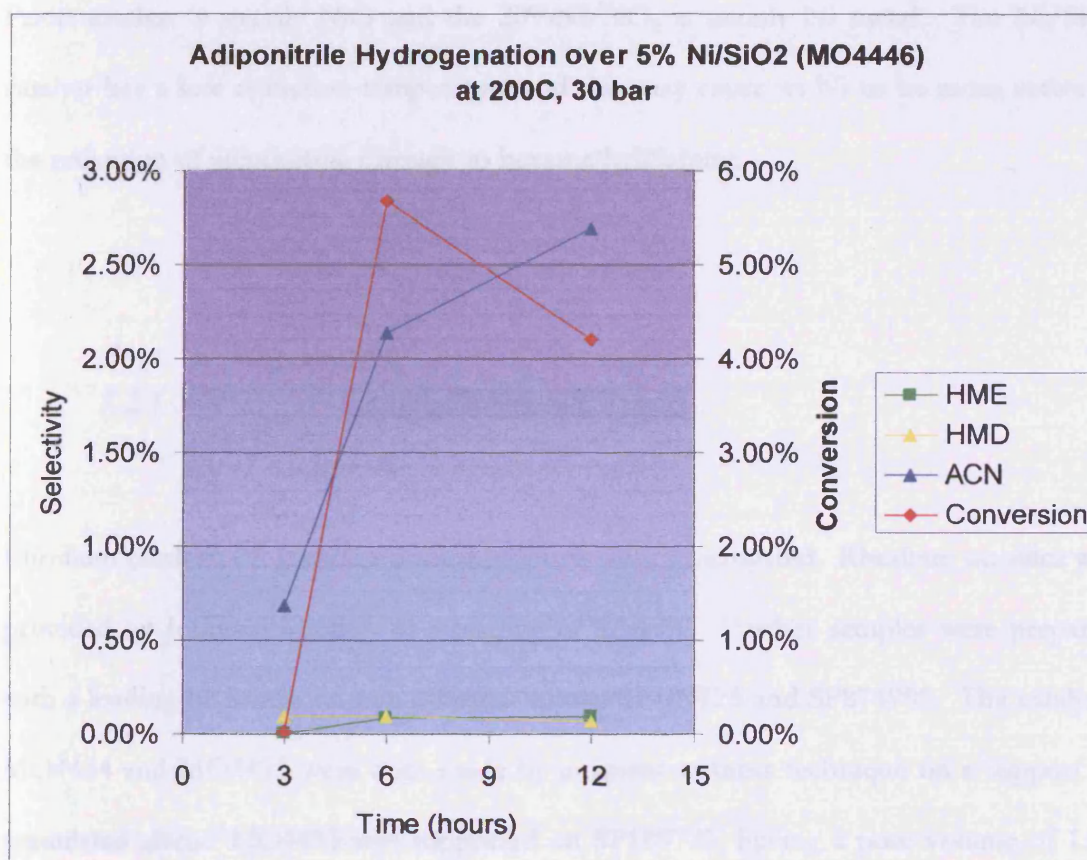


Figure 5.8 - Activity data for 5% Ni/SiO<sub>2</sub> at 200°C, 30 bar

The results are shown in figure 5.8. For reactions up to 12 hours the conversions are below 6% and therefore extremely low. It is however worth noting that the favoured product is, as would be expected, aminocapronitrile as this is the first hydrogenation step. This would be expected as the lower concentration of nickel would be less likely to allow full hydrogenation to hexamethyldiamine.

5.2.4.1. *Discussion – Ni catalysts*

Comparing the 20% Ni on silica to the Pricat catalyst it is interesting to note that although the percentage of Ni in Pricat catalyst was more than double that of 20%Ni/SiO<sub>2</sub>, the conversions and selectivities were similar. From characterisation data in chapter 4 it can be seen that the major difference in these two catalysts is that the Pricat catalyst is mainly NiO and the 20%Ni/SiO<sub>2</sub> is mainly Ni metal. The Ni/SiO<sub>2</sub> catalyst has a low reduction temperature and this may cause its Ni to be more active in the reduction of adiponitrile through to hexamethyldiamine.

5.2.5. *Supported Rhodium Catalysts*

Rhodium catalysts on granulated silica supports were investigated. Rhodium on silica was provided by Johnson Matthey at a loading of 2.5wt%. Further samples were prepared with a loading of 5 wt% on two different silicas, SP189725 and SP874905. The catalysts MO4434 and MO4433 were both made by incipient wetness technique on a support of granulated silica. MO4433 was supported on SP189725, having a pore volume of 1.03 cm<sup>3</sup>/g and surface area of 535 m<sup>2</sup>/g as discussed in chapter 4 and MO4434 was supported on SP874905, surface area 319 m<sup>2</sup>/g pore volume 0.9 cm<sup>3</sup>/g.

## 5.2.5.1.

2.5% Rh/SiO<sub>2</sub> (JM catalysts)

Rhodium catalysts showed very low conversions in autoclave reaction at both 150°C and 200°C, as shown in figure 5.9 and 5.10. At 150°C the main product is seen to be the hemi-hydrogenated product aminocapronitrile, although this is in low abundance (1.12%). This makes it difficult to draw any accurate conclusions in view of experimental error. On increasing the reaction temperature to 200°C as shown in figure 5.10 the results are still extremely low in terms of conversion and selectivity. The result is once again inconclusive as any variations in concentration of products may not be significant enough with respect to experimental error.

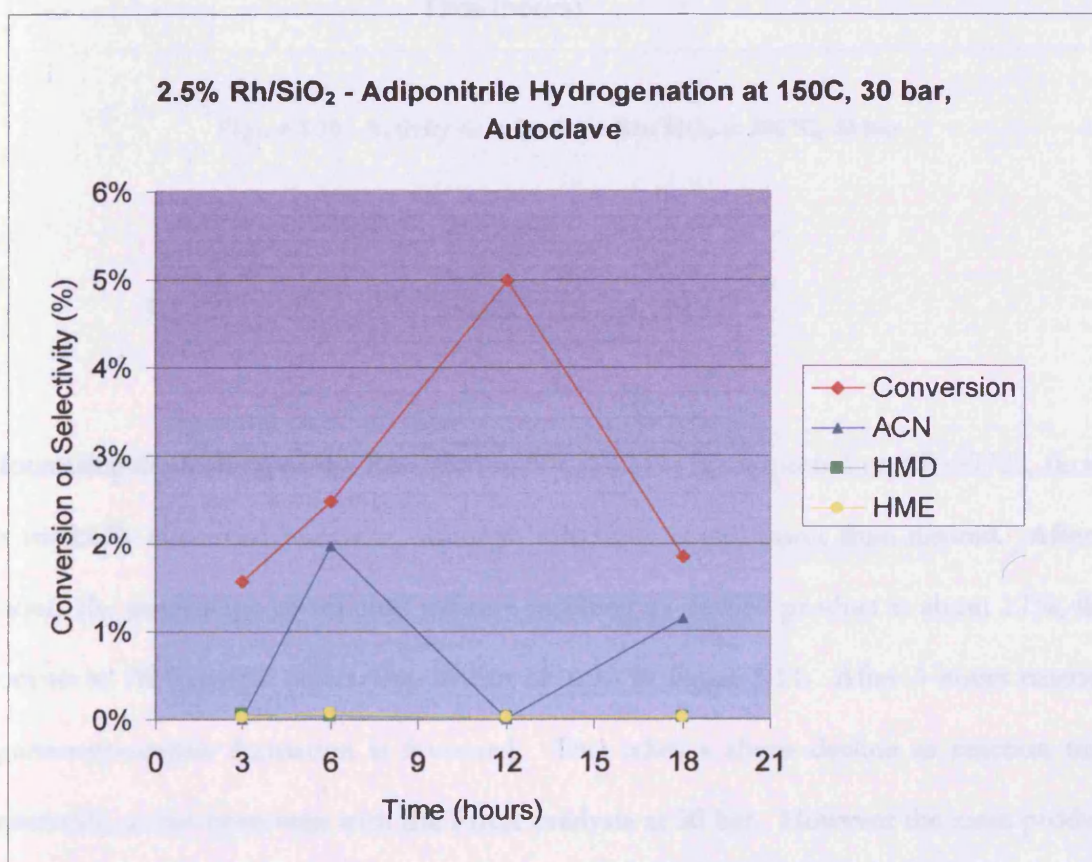


Figure 5.9 - Activity data for 2.5% Rh/SiO<sub>2</sub> at 150°C, 30 bar

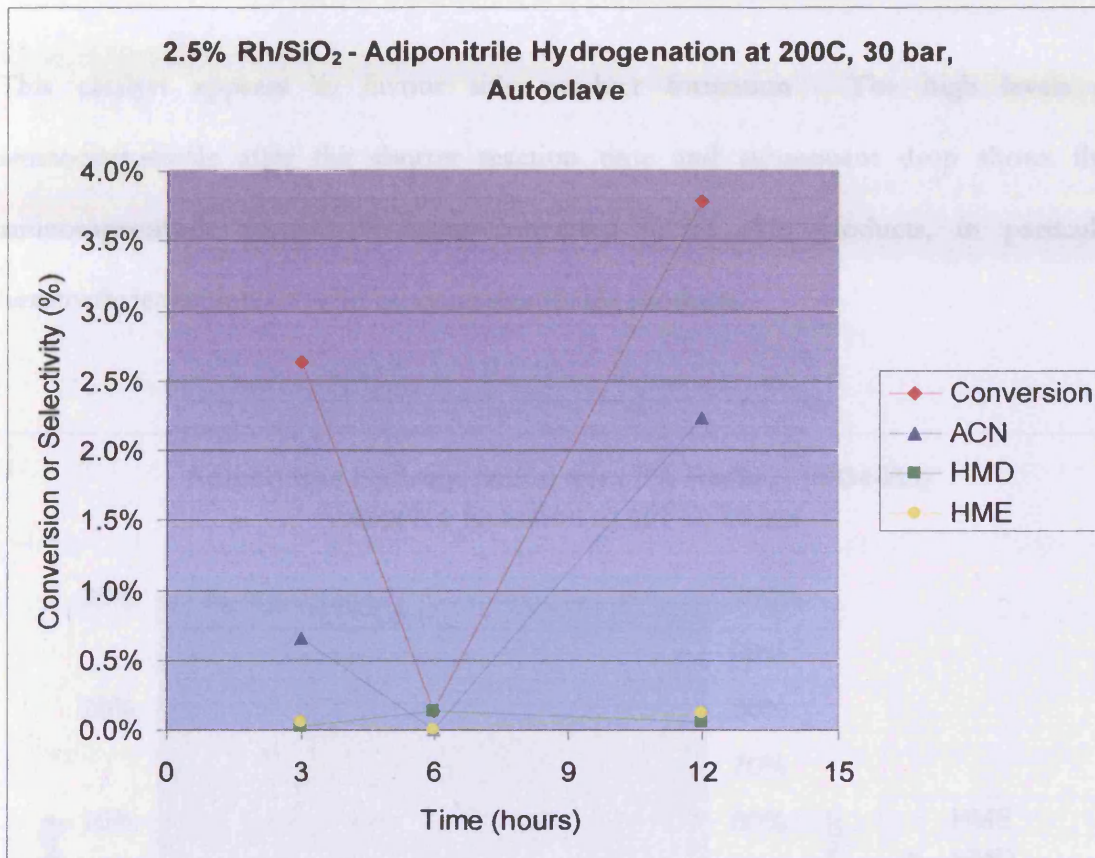


Figure 5.10 - Activity data for 2.5% Rh/SiO<sub>2</sub> at 200°C, 30 bar

#### 5.2.5.2. 5%Rh/SiO<sub>2</sub> (MO4433)

Increasing the loading of the Rhodium to 5% (MO4433), supported on SP189725, shows a markedly improved reactivity, although selectivity is still lower than desired. After 3 hours the percentage of reaction mixture resulting as desired product is about 17%, this occurs at 76% overall conversion as can be seen in figure 5.11. After 3 hours reaction aminocapronitrile formation is favoured. This takes a sharp decline as reaction time proceeds, as has been seen with the Pricat catalysts at 30 bar. However the main product is HME instead of HMD caused by an internal ring closure. Hexamethyldiamine formation slowly increases with time but is no higher than 10% of the product mixture.

This catalyst appears to favour side product formation. The high levels of aminocapronitrile after the shorter reaction time and subsequent drop shows that aminocapronitrile formed is being converted in to side products, in particular hexamethyleneimine, but also other unidentifiable products.

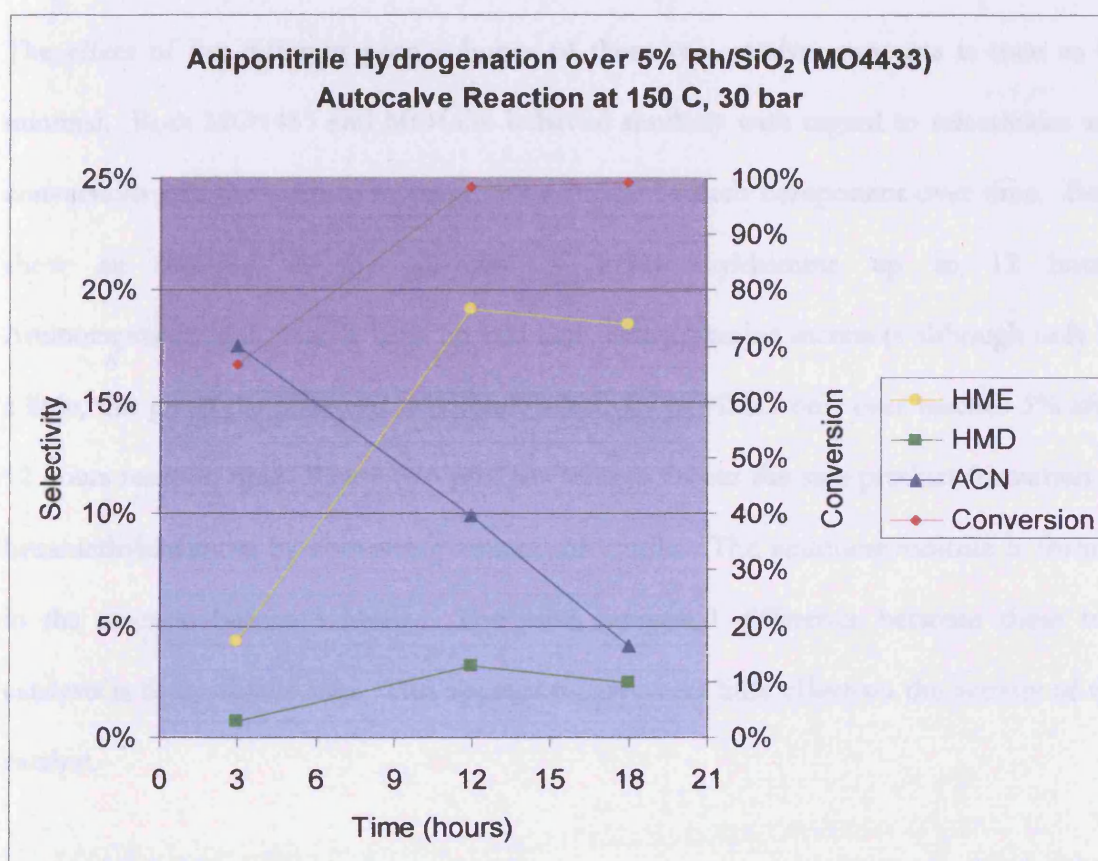


Figure 5.11 - Activity data for 5% Rh/SiO<sub>2</sub> at 150°C, 30 bar (MO4433)

5.2.5.3. *5%Rh/SiO<sub>2</sub> (MO4434)*

High conversion was also found over 5% Rh/SiO<sub>2</sub> (MO4434), supported on SP874905, shown in figure 5.12 although the percentage of desired products was found to be low once again. The most abundant side product is hexamethyleneimine.

The effect of the different pore volumes of these two catalyst supports is seen to be minimal. Both MO4433 and MO4434 behaved similarly with regard to selectivities and conversions and the rates of increase and decrease of each component over time. Both show an increase in the quantity of hexamethyldiamine up to 12 hours. Aminocapronitrile is steadily used up and hexamethyldiamine increases although only by a little, this given the observed maximum selectivity to HMD only ever reaches 3% after 12 hours reaction time. These two catalysts tend to favour the side product formation of hexamethyleneimine by converting aminocapronitrile. The aminocapronitrile is formed in the reaction before 3 hours. The main structural difference between these two catalysts is their surface area. This appears to have very little effect on the activity of the catalyst.

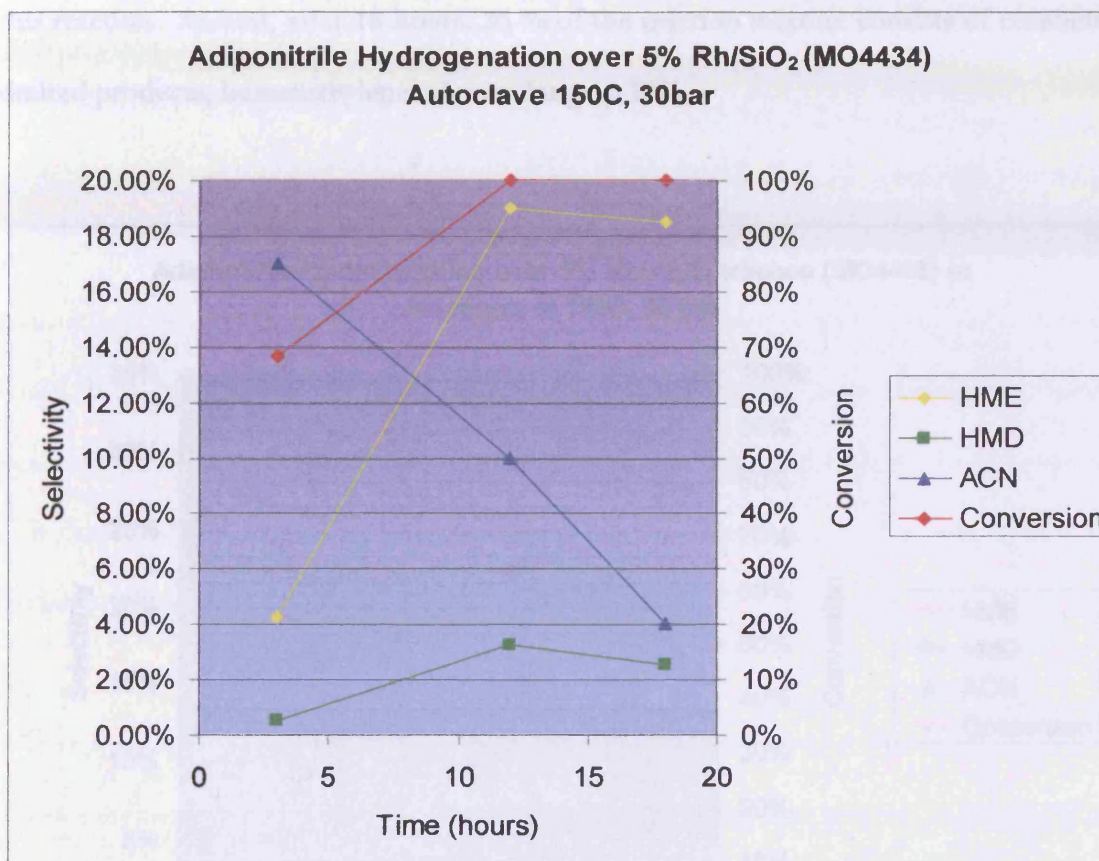


Figure 5.12 - Activity data for 5% Rh/SiO<sub>2</sub> at 150°C, 30 bar (MO4434)

#### 5.2.5.4. 5% Rh/Al<sub>2</sub>O<sub>3</sub> trilobes (MO4435)

5% Rhodium supported on alumina, catalyst was also used. Figure 5.13 shows the results of adiponitrile hydrogenation reaction at 150°C and 30 bar hydrogen pressure. The conversion (right hand axis) is found to reach 57% after 6 hours and 88% after 16 hours. This is much higher than that for 2.5% Rh/SiO<sub>2</sub> but lower than for 5% Rh/SiO<sub>2</sub>, although selectivity with the Rh/Al<sub>2</sub>O<sub>3</sub> was higher. The selectivity follows a similar trend with the preferred product being aminocapronitrile initially. After 16 hours the amount of HME increases, accompanied by a decrease in ACN as it is suspected that ACN is favouring side product formation. Hexamethyldiamine formation is low once again for

this reaction. At best, after 18 hours, 26 % of the reaction mixture consists of combined desired products, hexamethyleneimine making up 15%.

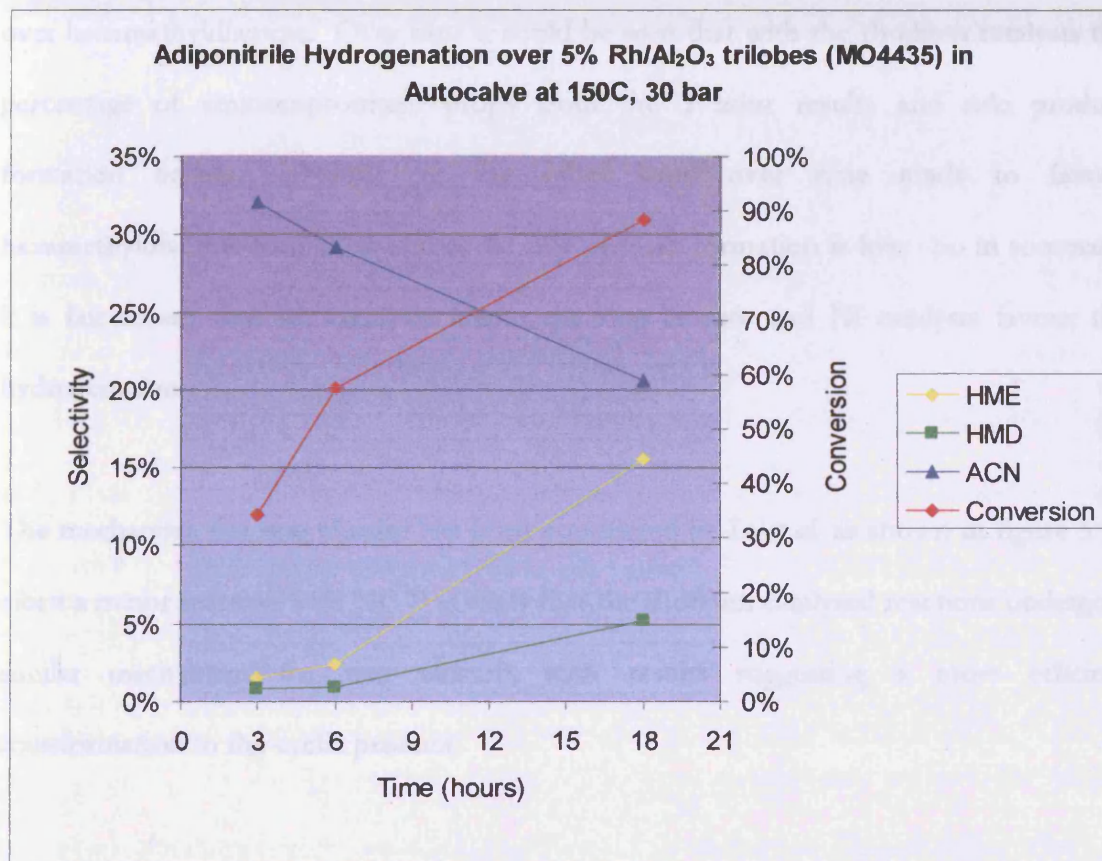


Figure 5.13 - Activity data for 5% Rh/Al<sub>2</sub>O<sub>3</sub> at 150°C, 30 bar

As a single metal in low loading, Rh is relatively poor. The best support found for this reaction is alumina as although it had the lowest surface area of all the supports tested, it produced the greatest amount of desired product, aminocapronitrile but did this at low conversions with many side products.

## 5.2.5.5.

## Discussion – Rh vs. Ni

Rhodium catalysts overall appeared to favour the production of hexamethyleneimine over hexamethyldiamine. Over time it could be seen that with the rhodium catalysts the percentage of aminocapronitrile drops from the 3 hour results and side product formation occurs. Nickel on the other hand over time tends to favour hexamethyldiamine formation and cyclic side product formation is low. So in summary, it is fair to say that Rh catalysts favour the ring closure and Ni catalysts favour the hydrogenation.

The mechanism for ring closure has been considered by Li *et al*, as shown in figure 5.14 albeit a minor reaction with Ni. It is likely that the rhodium catalysed reactions undergo a similar mechanism for ring closure, with results suggesting a more efficient transformation to the cyclic product.

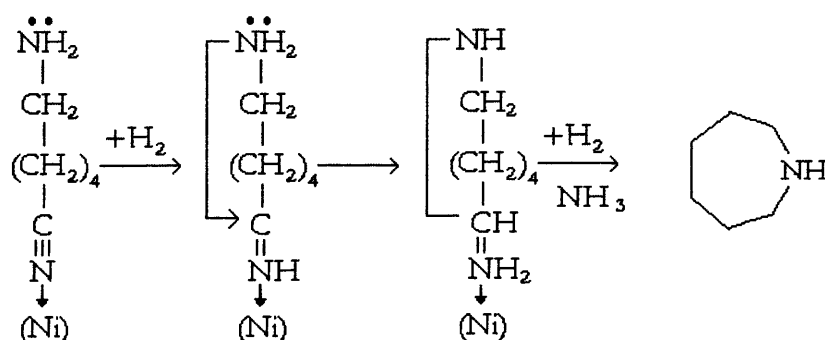


Figure 5.14 - Hexamethyleneimine formation

In the above example the metal attracts the nitrile end of the aminocapronitrile molecule as it is electron rich in the triple bond. This causes a polarisation of the cyano group resulting in the carbon which is attached to the nitrogen becoming more electropositive

and thus attracting the lone pair from the nitrogen at the other end to react forming a seven membered ring with the elimination of ammonia.

5.2.5.6. *Discussion - Rhodium Catalysts Compared*

The bar chart figure 5.15 shows the comparison between compositions of products using 5% Rh/SiO<sub>2</sub> (MO4433) and 5% Rh/Al<sub>2</sub>O<sub>3</sub> (MO4435). For comparison the results of reaction of adiponitrile in an autoclave over 5%Ni/SiO<sub>2</sub> (MO4446) under the same conditions has been shown. The MO4446 has low conversion but shows greater selectivity to aminocapronitrile (ACN). This is to be expected because at lower concentrations base metals are known to have lower activities therefore one would expect only the first hydrogenation to be affected at best. The 5% rhodium catalysts although more active than the previously shown 2.5% have a tendency to produce higher quantities of side product than desired products. In view of this it is worth noting that the alumina supported catalysts does appear to affect side product formation which occurs much more slowly than silica supported counterparts.

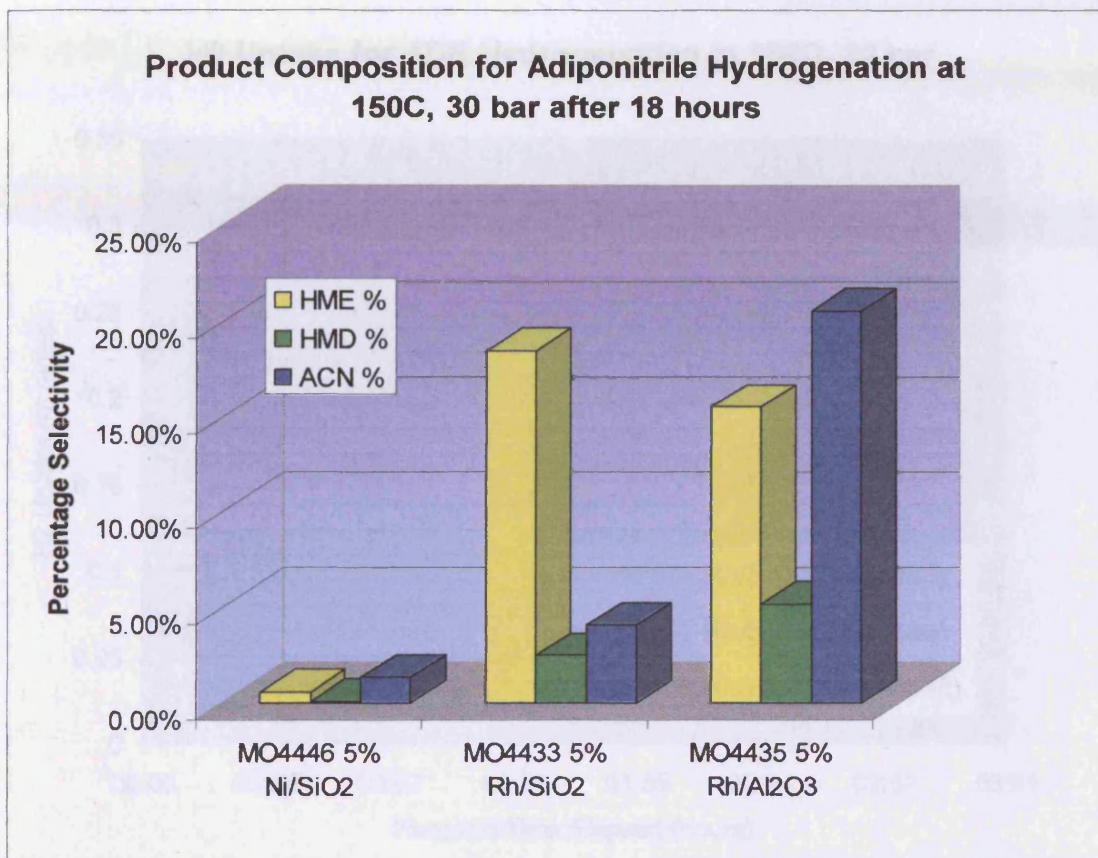


**Figure 5.15 – Product composition of ADN hydrogenation in autoclave at 150°C, 30 bars, and 18 hours by different catalysts**

This reduction in rate of side product formation can be explained by the hydrogen uptake data for these reactions figure 5.16 which show significant differences between catalysts supported on silica and those supported on alumina. Here it can be seen that the silica supported catalysts can reach a higher level of uptake than the catalysts supported on alumina. The silica supported catalyst also show vastly faster initial rates of uptake. This would suggest that silica catalysts either adsorb H<sub>2</sub> better or present the metal better than on the alumina. The hydrogen uptake rate is an indication of dispersion and shows silica to have a higher dispersion. The difference in polarity of the two supports is also a key factor.

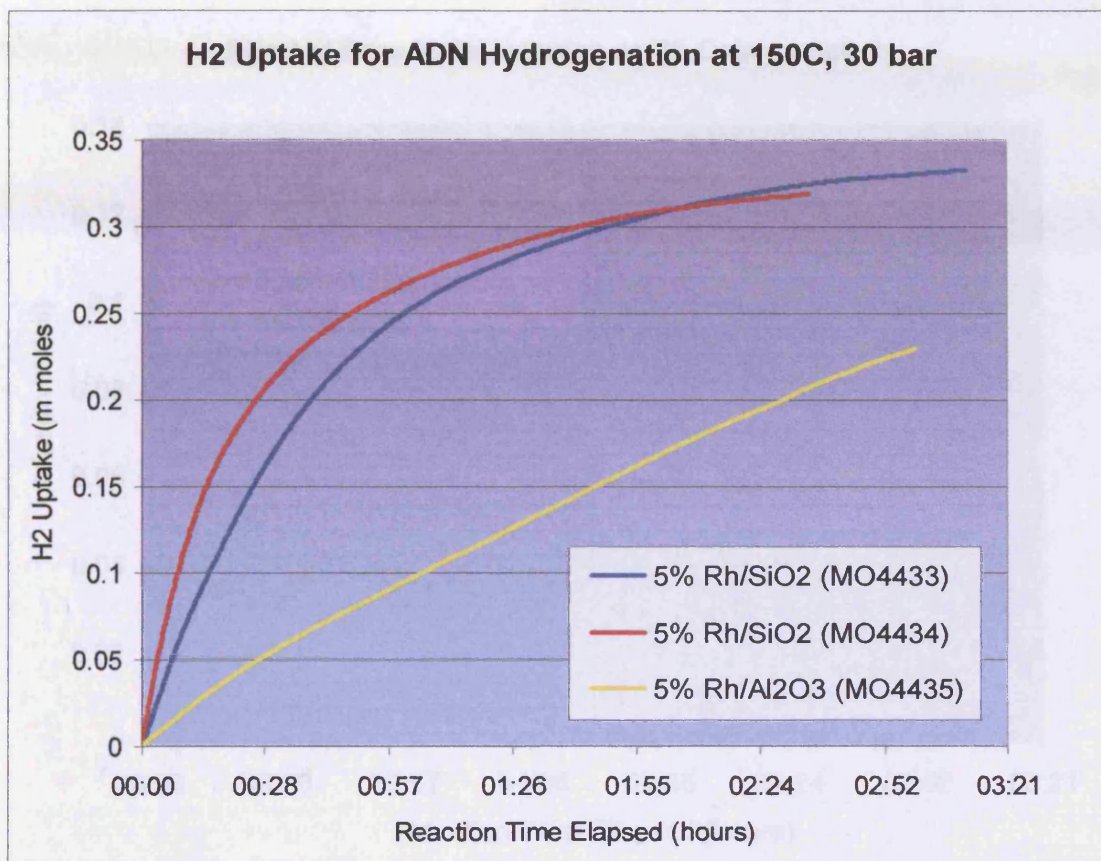


Figure 5.16 – Hydrogen uptake during ADN hydrogenation at 150°C, 30 bar for different catalysts

### 5.2.6. Mixed Metal Catalysts

#### 5.2.6.1. 2.5%-2.5% Ni-Rh/Al<sub>2</sub>O<sub>3</sub> and

#### 2.5%-2.5% Co-Rh/Al<sub>2</sub>O<sub>3</sub>

Catalysts were prepared by incipient wetness to contain both a base metal either Ni or Co and rhodium. They were tested in the autoclave and the hydrogen uptake monitored to indicate reaction rates.

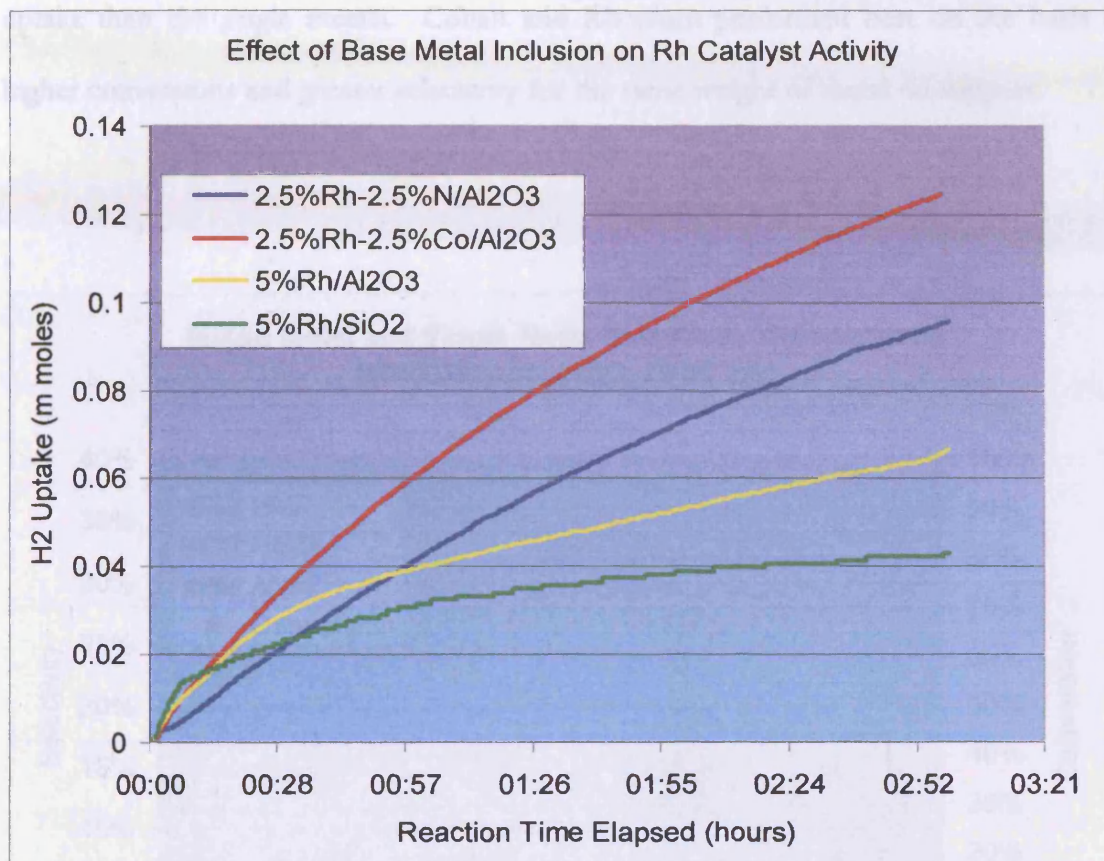


Figure 5.17 – Hydrogen up take data for mixed metal catalysts compared with single metal catalysts

Figure 5.17 shows the hydrogen uptake. It is clear to see that the two single metal rhodium catalysts have vastly different reaction rates than the mixed metals. Rhodium on silica shows a fast initial rate rapidly slowing down and resulting in lower hydrogen uptake indicating that the reaction has not gone as far to completion as the other three catalysts. Rhodium on alumina responds similarly to rhodium on silica but has not got quite as rapid an initial rate and achieves a higher final hydrogen uptake. This suggests greater conversion.

Interestingly, the graph shows that the catalysts consisting of 5% metal on silica where half of the metal by weight is nickel or cobalt but showed significantly higher hydrogen

uptake than the single metals. Cobalt and Rhodium performed best on the basis of higher conversions and greater selectivity for the same weight of metal on support.

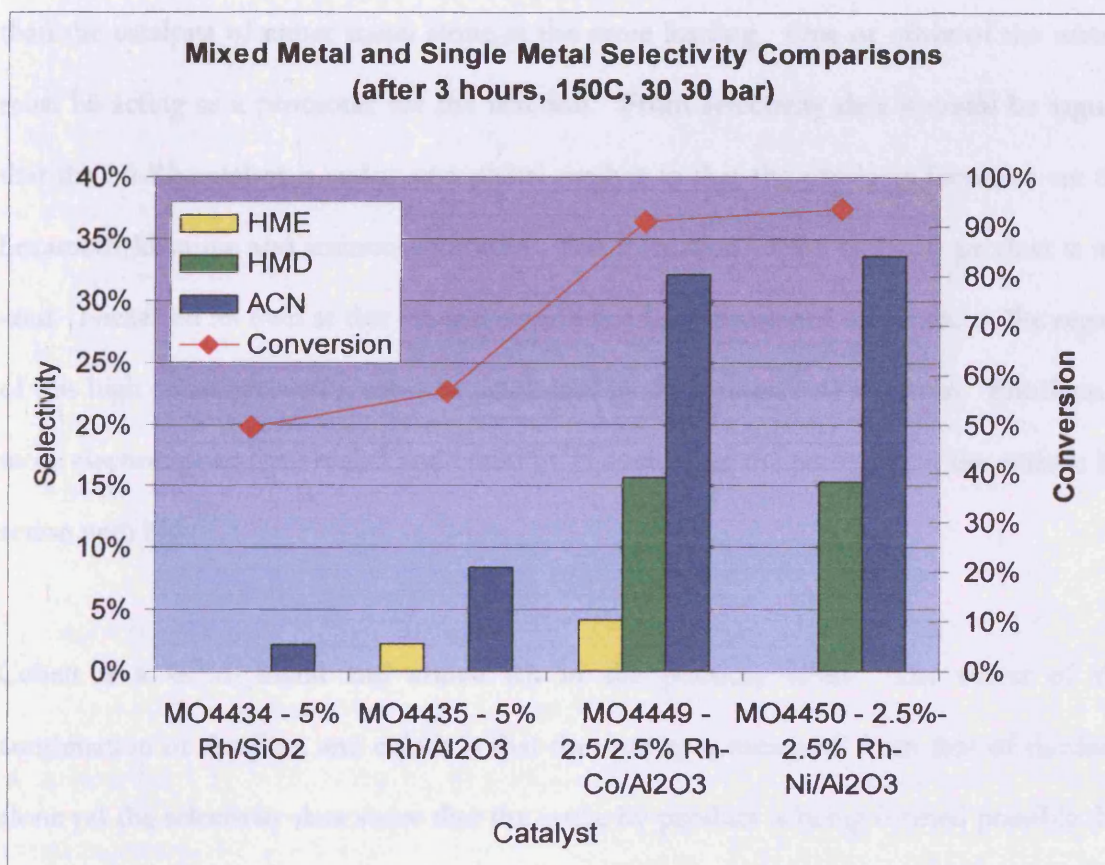


Figure 5.18 Mixed metal and single metal catalyst, selectivity comparisons after 3 hours.

Figure 5.18 shows the selectivity and conversion data for these reactions. It can be seen that conversion nearly doubles on inclusion of a base metal to the catalyst. The two catalyst with base metals also showed higher selectivity to desired products with the cobalt containing catalyst producing more side product than the nickel.

5.2.6.2.

*Discussion – Mixed Metals*

The mixed metal catalysts function better with respect to conversion of adiponitrile and production of two of the desired products hexamethyldiamine and aminocapronitrile than the catalysts of either metal alone at the same loading. One or other of the metals must be acting as a promoter for the reaction. From selectivity data it could be argued that the Ni-Rh catalyst is acting as a nickel catalyst in that the products favoured are the hexamethyldiamine and aminocapronitrile. The formation of the cyclic by product is not seen. Nickel on its own at this loading would not have produced anywhere in the region of this high conversion so it must be attributed to the presence of rhodium. Rhodium is more electron poor than nickel and could be coordinating the molecule to the surface for action with Ni.

Cobalt is a  $4s^23d^7$  metal and above Rh in the periodic table. The effect of the combination of rhodium and cobalt is that the activity is increased from that of rhodium alone yet the selectivity data show that the cyclic by-product is being formed possibly due to the increased pull of both metals being very electron poor thus encouraging ring closure as the reaction scheme figure 5.14 would suggest.

TPR data shows that the inclusion of precious metal rhodium with base metals either cobalt or nickel has the effect of lowering the reduction temperature. This lowering of reduction temperature could also indicate a higher ability to reduce adiponitrile as a catalyst. The TPR data also supports the idea that the metals are in fact mixed due to the radically different TPR profiles of the mixed metal catalysts to the individual metals. If no mixing had occurred, the TPR profiles would show characteristic peaks for each metal. What is observed is a set of quite different peaks resulting from strong

interactions between the metals. Indeed here it is seen that the activity of the mixed metal catalysts is higher.

5.2.7. Discussion - Autoclave

The Pricat catalyst is most active for the hydrogenation of adiponitrile to aminocapronitrile and hexamethyldiamine under the reaction conditions investigated. The product composition is mainly hexamethyldiamine and aminocapronitrile. The only significant side product is hexamethyleneimine. At lower pressures there are less side products and at higher pressures and temperature the fully hydrogenated product is prevalent.

In the 20%Ni/SiO<sub>2</sub> catalyst the relationship between hexamethyldiamine and aminocapronitrile concentrations can be clearly seen showing the aminocapronitrile to be an intermediate in hexamethyldiamine formation. Side product formation is low and overall conversion is fairly high.

Of the rhodium catalysts it can be concluded that 2.5% loading is too low for reaction under these conditions. At 5% loading conversion is much better but selectivity has been found to be very poor yielding many side products identifiable by GC but not yet determined.

Inclusion of base metal in the rhodium catalyst is shown to improve both the conversion and selectivity to hydrogenation products. This is remarkable because the mixed metal

catalysts perform better than single metal catalysts despite the loading of each metal being halved. Each metal must perform a promoting function to the other.

### 5.3. Fixed bed gas phase

#### 5.3.1. Pricat Catalysts

The pricat catalysts were only available as fine powders, which came with the added complication that they fall through the glass wool in the fixed bed reactor. Attempts were made to overcome this by using a high-pressure press to form pellets of this catalyst however this did not solve the problem as the pellets appeared to crumble and rendered the catalysts unusable in this system.

#### 5.3.2. Nickel catalysts

Temp	Conditions	Ni Loading	Conversion
150°C	25ml/min He, 25ml/min H <sub>2</sub> , 0.5g catalyst	1%	0.0%
200°C	25ml/min He, 25ml/min H <sub>2</sub> , 0.5g catalyst	1%	14%
300°C	25ml/min He, 25ml/min H <sub>2</sub> , 0.5g catalyst	1%	3%
300°C	50ml/min He, 0.5g catalyst	1%	1%
200°C	25ml/min He, 25ml/min H <sub>2</sub> , 0.5g catalyst	20%	3%
300°C	25ml/min He, 25ml/min H <sub>2</sub> , 0.5g catalyst	20%	1%

**Table 5.1 - Gas Phase Activity Data**

When using the nickel catalysts the problems observed with the pricat catalysts were no longer an issue as they were supported on granulated supports. However at 150°C the adiponitrile in the fixed-bed flow reactor does not function in the gas phase and so performs very poorly and in essence more in a three phase trickle bed fashion and has

0% conversion as can be seen in table 5.1. The highest conversions were seen at 200°C, closer to adiponitriles boiling point, however this may be misleading because many of the products formed in the reaction at 300°C were likely to be gaseous and were unable to be sufficiently condensed. Another observation from the 20% nickel on silica catalyst is that it produced significantly lower conversion than the 1% loading catalyst. This may be due to large crystallites being formed as the reduction is at such a high temperature.

### 5.3.3. Rhodium Catalysts

5% Rh/SiO<sub>2</sub> catalyst MO4433 has been tested in the gas phase fixed bed reactor. These samples were denoted with a prefix P and a number for each run. Fixed-bed reactions were undertaken at 150°C and 200°C. Autoclave reactions have also been done at these temperatures. Product numbers and reaction conditions are summarised in table 5.2.

GC analysis of products has not shown any conversion. It was felt at first that any products may be hidden under the large adiponitrile peak, as it is broad and so poor separation may be the reason for no identifiable products.

Product number	Catalyst used	Reactor type	Temperature
P105	5% Rh/SiO <sub>2</sub> (MO4433)	Fixed-Bed	200°C
P108	5% Rh/SiO <sub>2</sub> (MO4433)	Fixed-Bed	150°C

Table 5.2 - Gas-phase reaction conditions.

The physical properties of these samples were noticeably different from the starting material adiponitrile, being that all the samples took the form of a thick syrup. Given that GC analysis of the samples of these reactions showed no end products an alternative identification procedure was sought.

### 5.3.3.1. *Infrared Spectroscopy*

Infrared spectroscopy is a very sensitive tool for the identification of key functional groups in organic compounds such as amines and nitriles.

Infrared spectra have been taken of the products P105 and P108 as well as starting materials in order to determine if any conversion has taken place. Samples were prepared either as liquid film between NaCl plates or as a nujol mull in case of solid samples. In this case by using infrared it is possible to determine if there has been a change in the key structural feature i.e. a nitrile to an amine. Therefore the vibrations of most interested in were the C≡N stretch ( $2260\text{--}2240\text{ cm}^{-1}$ ), N-H stretch ( $3500\text{--}3100\text{ cm}^{-1}$ ) and the N-H bend ( $1640\text{--}1550\text{ cm}^{-1}$ ). The peak for N-H stretch can often be confused with the O-H in water and an air of caution needs to be taken with this peak.

The IR spectrum of product P105 is shown in figure 5.20, it can be seen that there is an increase in a peak at  $\sim 1627\text{ cm}^{-1}$ , relative to the starting material, figure 5.19; this may be attributed to a gain of NH bending vibrations. Indeed in P105 the C≡N signal can be seen to decline and the N-H stretch signal shift to a slightly higher wave number. This would suggest the possibility of some hydrogenation. This could be to either the

aminocapronitrile or hexamethyldiamine. To support this evidence given the possible confusion of water with the NH stretch, a third analytical technique was utilised.

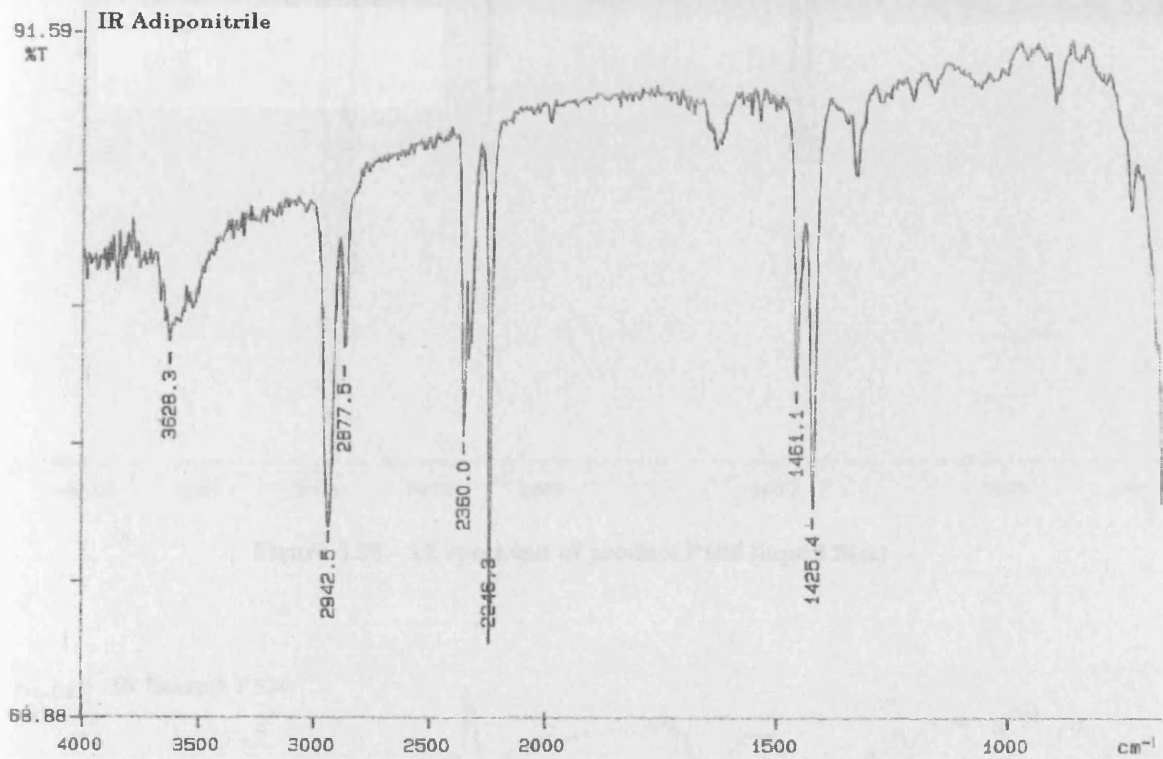


Figure 5.19 – IR spectrum of adiponitrile (liquid film)

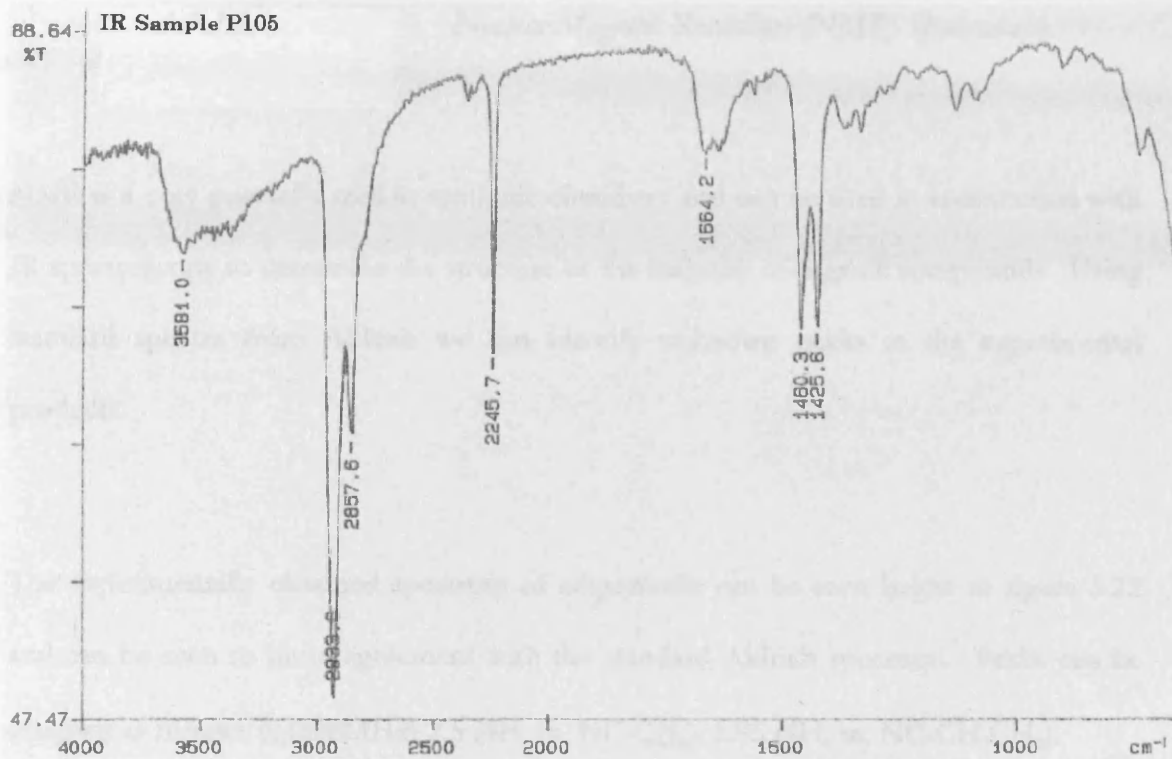


Figure 5.20 – IR spectrum of product P105 (liquid film)

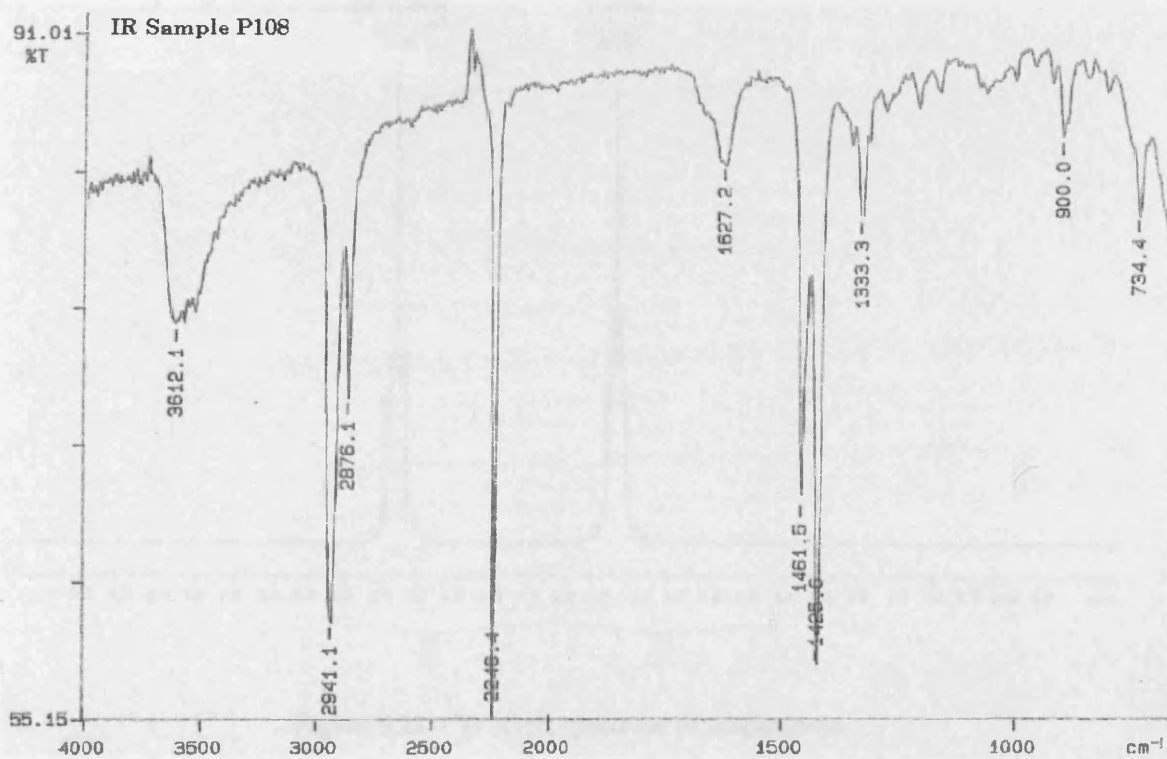


Figure 5.21 – IR spectrum of product P108 (liquid film)

## 5.3.3.2. Nuclear Magnetic Resonance (NMR) Spectroscopy

NMR is a very powerful tool in synthetic chemistry and can be used in conjunction with IR spectroscopy to determine the structure of the majority of organic compounds. Using standard spectra from Aldrich we can identify unknown peaks in the experimental products.

The experimentally obtained spectrum of adiponitrile can be seen below in figure 5.22 and can be seen to be in agreement with the standard Aldrich spectrum. Peaks can be assigned as follows  $\delta_{\text{H}}(500\text{MHz})$  2.5 (4H, m, NC-CH<sub>2</sub>), 1.95 (4H, m, NC-CH<sub>2</sub>CH<sub>2</sub>).

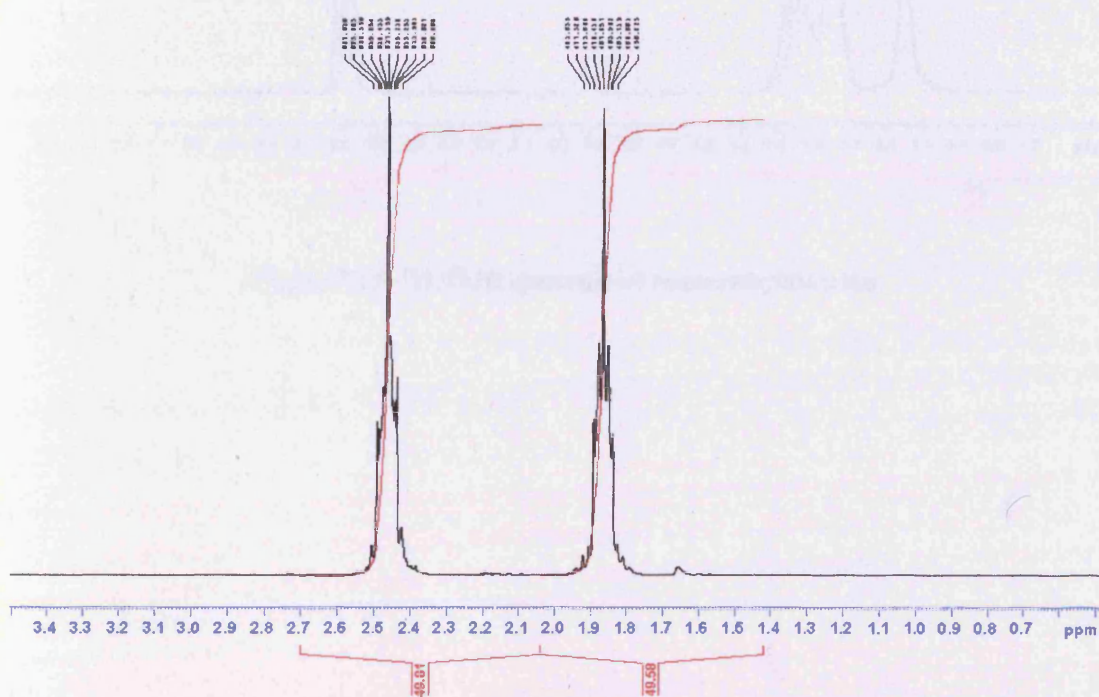


Figure 5.22 – <sup>1</sup>H NMR spectrum of adiponitrile.

The experimentally obtained spectrum for hexamethyldiamine can be seen below in figure 5.23 and can also be seen to be in agreement with its standard spectrum from Aldrich, peaks can be assigned as follows;  $\delta_{\text{H}}$ (250MHz) 2.55 (4H, t, J 6.8,  $\text{H}_2\text{NCH}_2$ ), 1.4 (4H, m,  $\text{H}_2\text{NCH}_2\text{CH}_2$ ), 1.3 (4H, m,  $\text{H}_2\text{NCH}_2\text{CH}_2\text{CH}_2$ ), 1 (4H, bs,  $\text{NH}_2$ ).

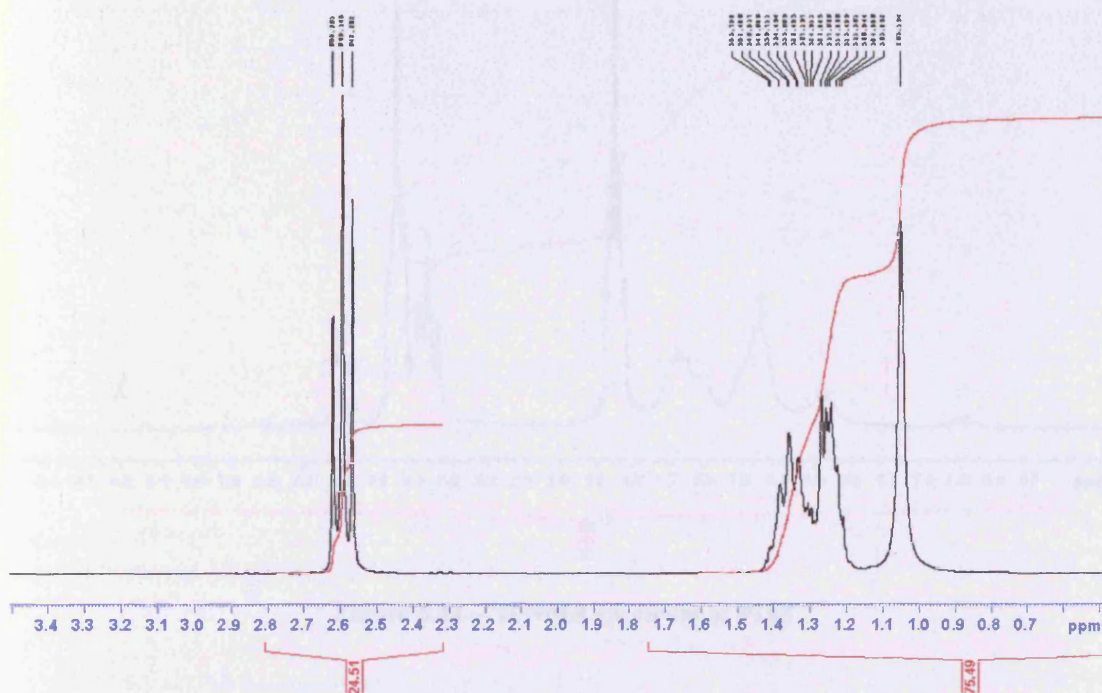


Figure 5.23–  $^1\text{H}$  NMR spectrum of hexamethyldiamine

$^1\text{H}$  NMR spectra were obtained for products P105 and P108. Figure 5.24 shows the  $^1\text{H}$  NMR spectrum of sample P105.

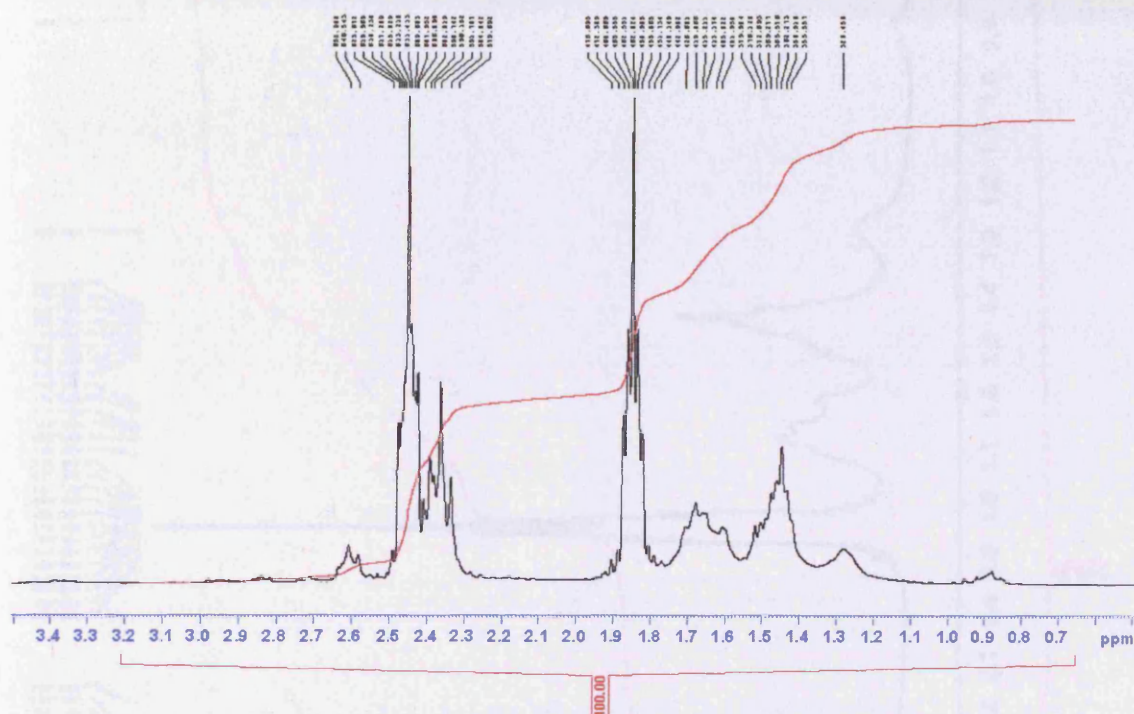
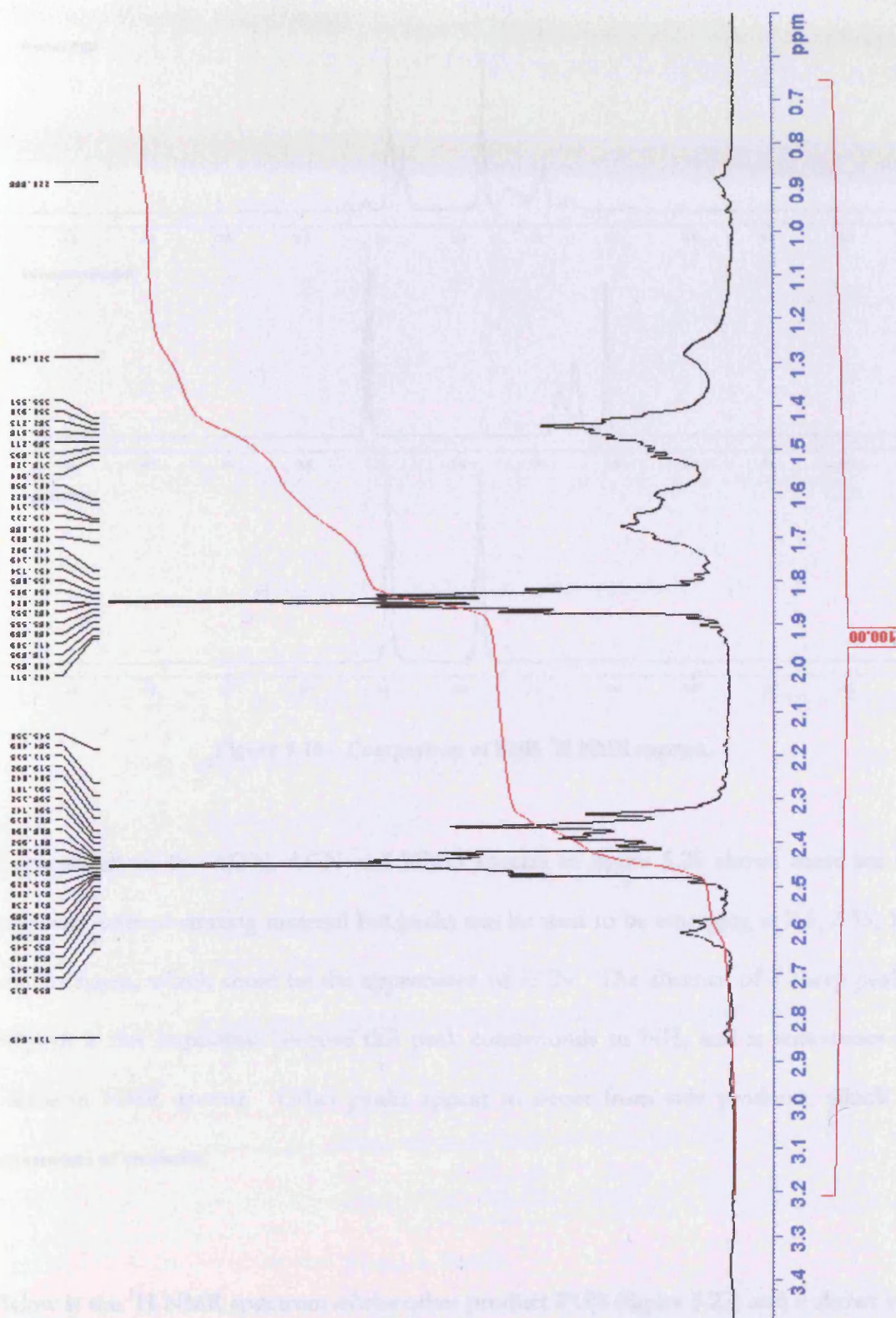
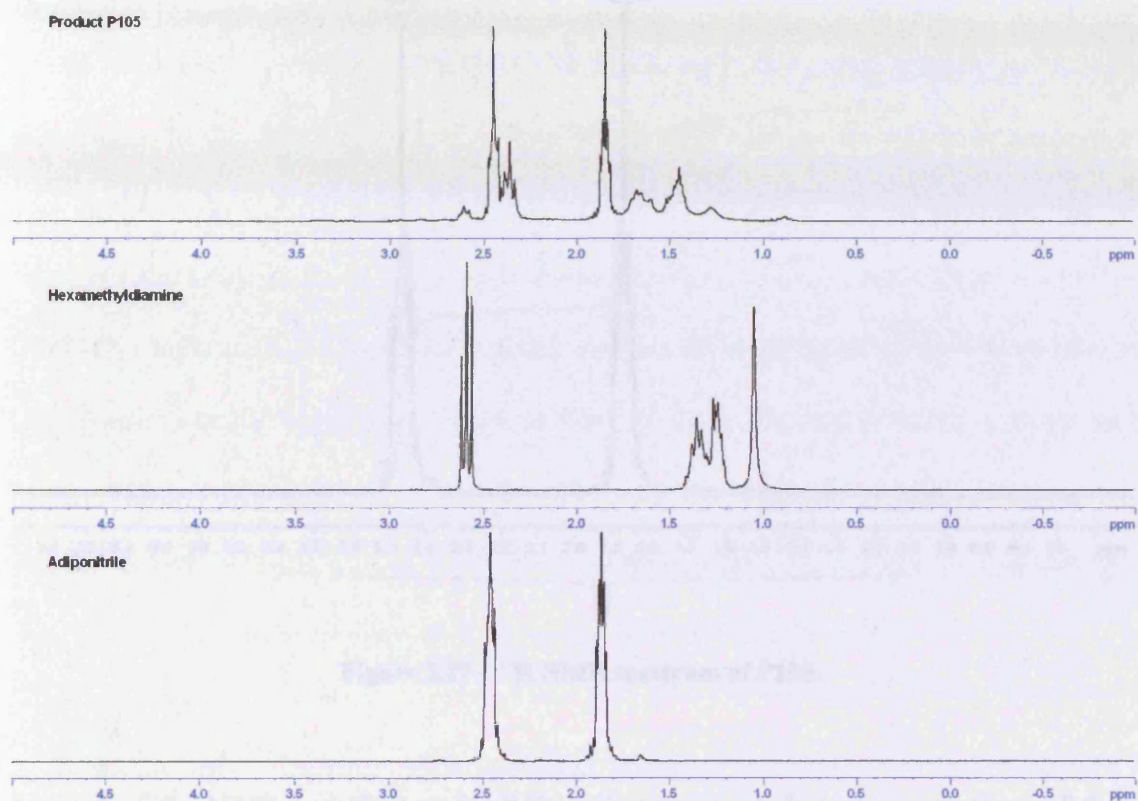


Figure 5.24 –  $^1\text{H}$  NMR spectrum of P105

The spectra show the starting material, ADN and the desired product aminocapronitrile along with the product P105. It can be seen that, in agreement with IR spectroscopy, a conversion has taken place, which appears to be due to formation of aminocapronitrile and some side products.





**Figure 5.26 – Comparison of P105  $^1\text{H}$  NMR spectra.**

Comparison to the ADN, ACN and HMD spectra in figure 5.26 shows there are still large amounts of starting material but peaks can be seen to be emerging at 2.6, 2.35, 1.65 and 1.45ppm, which could be the appearance of ACN. The absence of a sharp peak at 4.7ppm is not important because this peak corresponds to  $\text{NH}_2$  and is sometimes not visible in NMR spectra. Other peaks appear to occur from side products, which are unknown at present.

Below is the  $^1\text{H}$  NMR spectrum of the other product P108 (figure 5.27) and it shows very little difference from the spectrum of the starting material (figure 5.22).

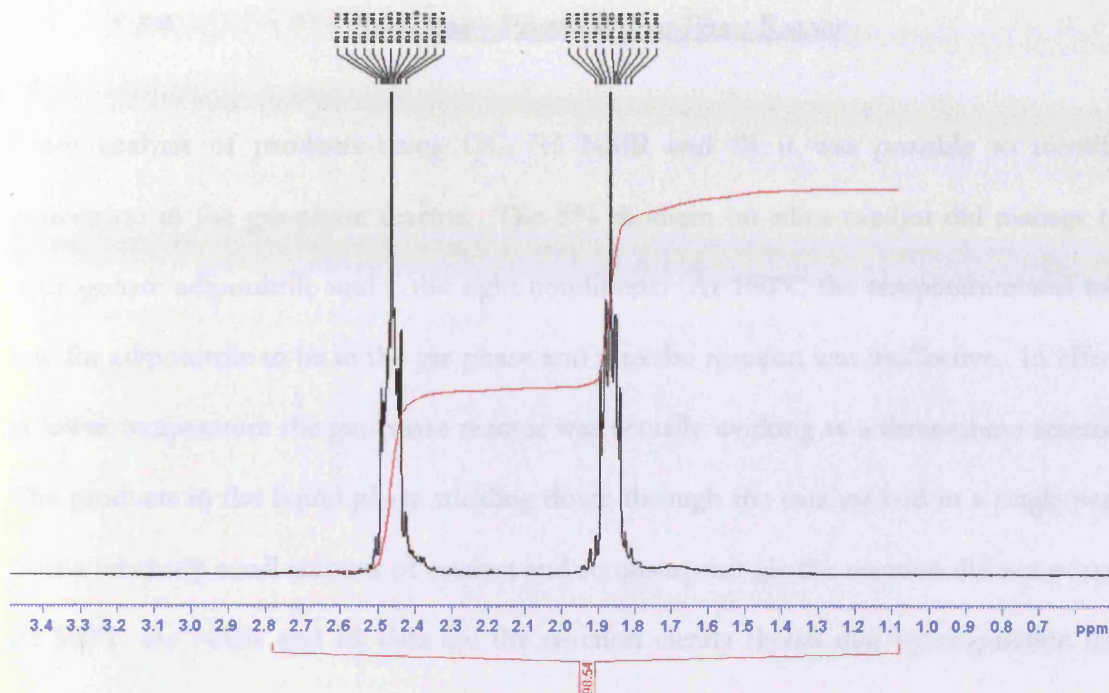


Figure 5.27 –  $^1\text{H}$  NMR spectrum of P108.

In view of the NMR and IR data for P105 efforts were made to separate some of these products. Using column chromatography it is possible to separate organic compounds according to their polarity, mass and size.

For this separation a silica column was used with a solvent system of ethyl acetate and petroleum ether. An elution gradient was used which ranged from 0% ethyl acetate through to 100%. This separation was not resolved sufficiently. Amines are inherently difficult to separate by column chromatography and any intermediate imines are not very stable and run the risk of being hydrolysed by the silica of the column. This makes it very hard to isolate the individual components cleanly.

5.3.4. Discussion - Fixed-bed Gas-Phase Reactor

From analysis of products using GC,  $^1\text{H}$  NMR and IR it was possible to identify conversion in the gas-phase reactor. The 5% rhodium on silica catalyst did manage to hydrogenate adiponitrile under the right conditions. At 150°C the temperature was too low for adiponitrile to be in the gas phase and thus the reaction was ineffective. In effect at lower temperature the gas-phase reactor was actually working as a three-phase reactor. The products in the liquid phase trickling down through the catalyst bed in a single pass over a relatively small amount of catalyst and so unsurprisingly the reaction did not occur. At 300°C the NMR and IR data for the reaction clearly shows that hydrogenation has taken place. Peaks can be seen which correspond to aminocapronitrile.

## 5.4. Trickle-Bed Reactor

5.4.1. Trickle-Bed Reactor vs Autoclave 20% Ni/SiO<sub>2</sub>

Reactor	Time	Vol ADN	Wt Catalyst	Conversion
TBR*	2 hours	30ml	2g	0.00%
TBR*	12 hours (Recycled)	30ml	2g	8.43%
AC*	2.5 hours	30ml	2g	8.56%
AC*	18 hours	30ml	0.5g	3.75%

Table 5.3 - Trickle-Bed vs Autoclave 20%Ni/SiO<sub>2</sub>

\* TBR = Trickle-bed reactor, AC = Autoclave

The trickle-bed reactor has been used at 150°C and shows that upon recycling the feed a 8.43% conversion can be achieved. The contact time has been calculated and so the reaction was repeated in the autoclave. The autoclave showed only slightly higher conversions but there was a noticeable amine smell from the vessel when it was opened so products may have been lost to gas.

#### 5.4.2. Trickle-bed reactor - Rhodium Catalysts

The use of a trickle-bed reactor with these catalysts caused some problems. During the reaction, the volume of liquid in the product reservoir decreased significantly over time. On closer inspection the liquid was found to have backed-up in the reactor tube. Figure 5.28 shows a schematic representation of what was observed. It was believed that this phenomenon may have been caused by insufficient pressure in the system or by a blockage within the glass frit. To test this the tube was cleaned with MeOH thoroughly to remove any solid organic matter and with aqua regia to remove any inorganic. The pressure was then increased in an attempt to circumvent any build up of product however this was unsuccessful. We also investigated using a solvent to assist the flow. At the reaction temperature a low boiling solvent would reflux building up pressure within the delicate reaction tube. Inert commercially available higher boiling point solvents would have made analysis by GC impossible and may have risked causing side reactions.

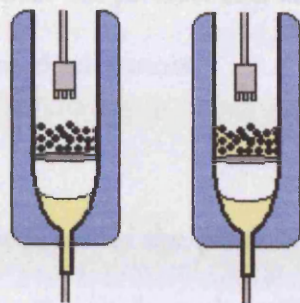


**Figure 5.28 – Blockage in the TPR tube showing liquid build up on catalyst bed.**

This problem was eventually solved by the removal of the lower needle valve, situated at the end of the reactor tube. This had originally been in place to maintain pressure within the reactor but was found to be unnecessary.

Upon solving this problem, it was possible to test three different catalysts. The catalysts 5% Rh/SiO<sub>2</sub> (MO4433), 5%Rh/Al<sub>2</sub>O<sub>3</sub> (MO4435) and 2.5%Ni-2.5%Rh/Al<sub>2</sub>O<sub>3</sub> (MO4450) were tested. All were tested at 150°C at a constant flow rate of adiponitrile (1mL/min) using 2g of catalyst for each experiment.

#### 5.4.2.1. *5% Rh/SiO<sub>2</sub> (MO4433)*

Adiponitrile was passed through the system for 6 hours by continuously recycling 15ml of adiponitrile. The product of this reaction was called TB203. GC analysis of the products showed similar results to the gas phase data although clearly a change had taken

place as the physical appearance of the product had altered. With the successful use of IR and NMR previously it was used once more.

Comparison of the infrared spectrum of the product TB203, figure 5.29, with that of adiponitrile showed a decline in the nitrile peak at  $2246\text{cm}^{-1}$  and new signals between  $1000\text{-}1400\text{cm}^{-1}$ . This suggested possible hydrogenation to some degree. To assess the nature of this hydrogenation more clearly  $^1\text{H}$  NMR spectroscopy was used.

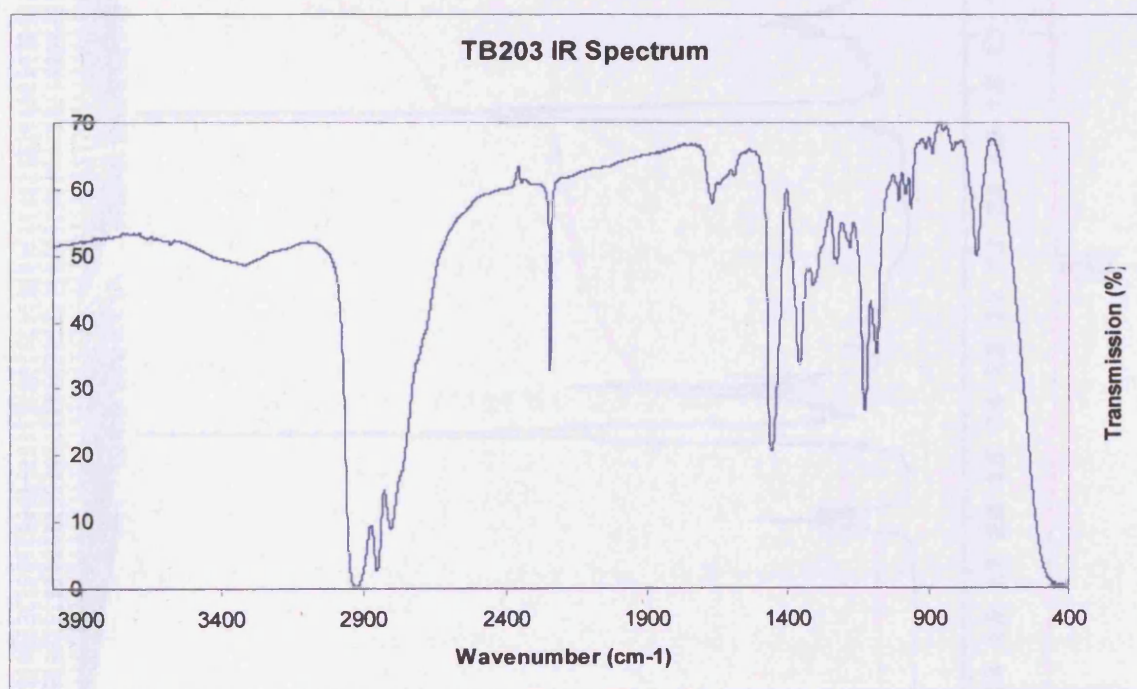


Figure 5.29 – IR spectrum of TB203 (liquid film).

The  $^1\text{H}$  NMR spectrum of TB203, shown in figure 5.30, appeared to show the presence of several compounds. Comparison of the  $^1\text{H}$  NMR spectra of product TB203, hexamethyldiamine and adiponitrile can be seen in figure 5.31.

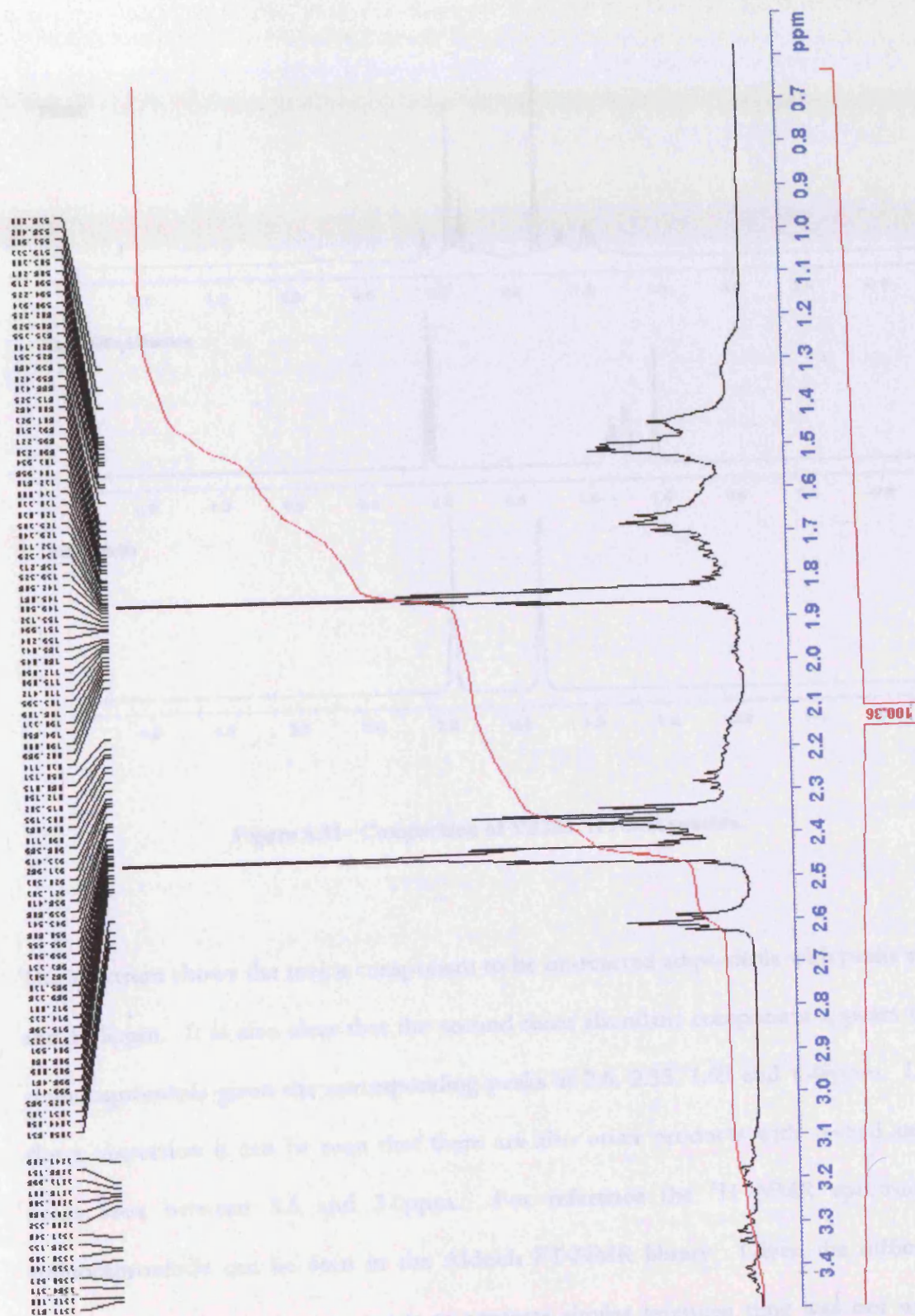
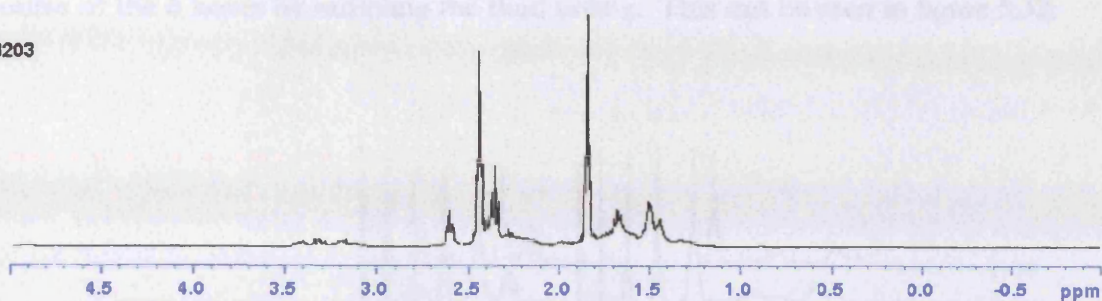
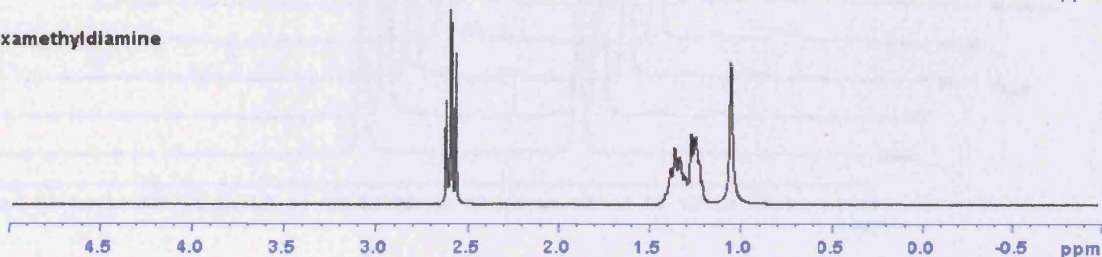


Figure 5.30 –  $^1\text{H}$  NMR spectrum of TB203.

TB203



Hexamethyldiamine



Adiponitrile

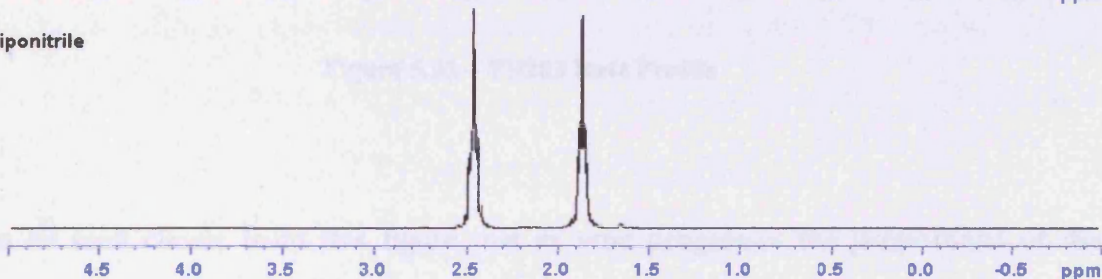
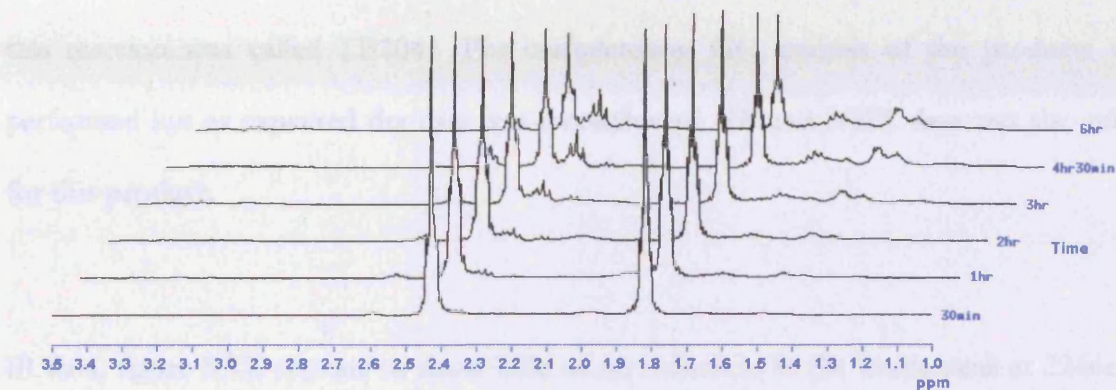


Figure 5.31– Comparison of TB203  $^1\text{H}$  NMR spectra.

The spectrum shows the major component to be un-reacted adiponitrile with peaks at 2.5 and 1.95ppm. It is also clear that the second most abundant component appears to be aminocapronitrile given the corresponding peaks at 2.6, 2.35, 1.65 and 1.45ppm. Upon closer inspection it can be seen that there are also other products with several smaller peaks seen between 3.5 and 3.0ppm. For reference the  $^1\text{H}$  NMR spectrum of aminocapronitrile can be seen in the Aldrich FT-NMR library. Given the difficulties encountered with previous attempts to separate similar mixtures time was not wasted trying to isolate these.

It was however possible to show the progression of the reaction at regular intervals over the course of the 6 hours by sampling the fluid online. This can be seen in figure 5.32.



**Figure 5.32 – TB203 Rate Profile**

It can be seen clearly from this figure that as time progresses the proportions of the various peaks can be seen to change. <sup>1</sup>H NMR uses peak areas, referred to as integrations, to determine relative quantities of each component present. After 6 hours the data showed there to be an approximate ratio of 1:4 aminocapronitrile to adiponitrile. This generates much confusion as to why the GC peak was not seen, unfortunately reasons for this are not known.

5.4.2.2.

5%Rb/ Al<sub>2</sub>O<sub>3</sub> (MO4435)

Catalyst MO4435 was also tested under the same conditions as MO4433. The product of this reaction was called TB204. For completeness GC analysis of the products was performed but as expected the data was inconclusive. IR and NMR data was also taken for this product.

IR data, figure 5.33, appears to show little or no reduction in the nitrile peak at 2246cm<sup>-1</sup> relative to the adiponitrile standard, which can be seen in figure 5.19. Indeed the <sup>1</sup>H NMR spectrum did show only very small quantities of aminocapronitrile with a ratio of 1:16 relative to the adiponitrile. This can be seen in figure 5.34.

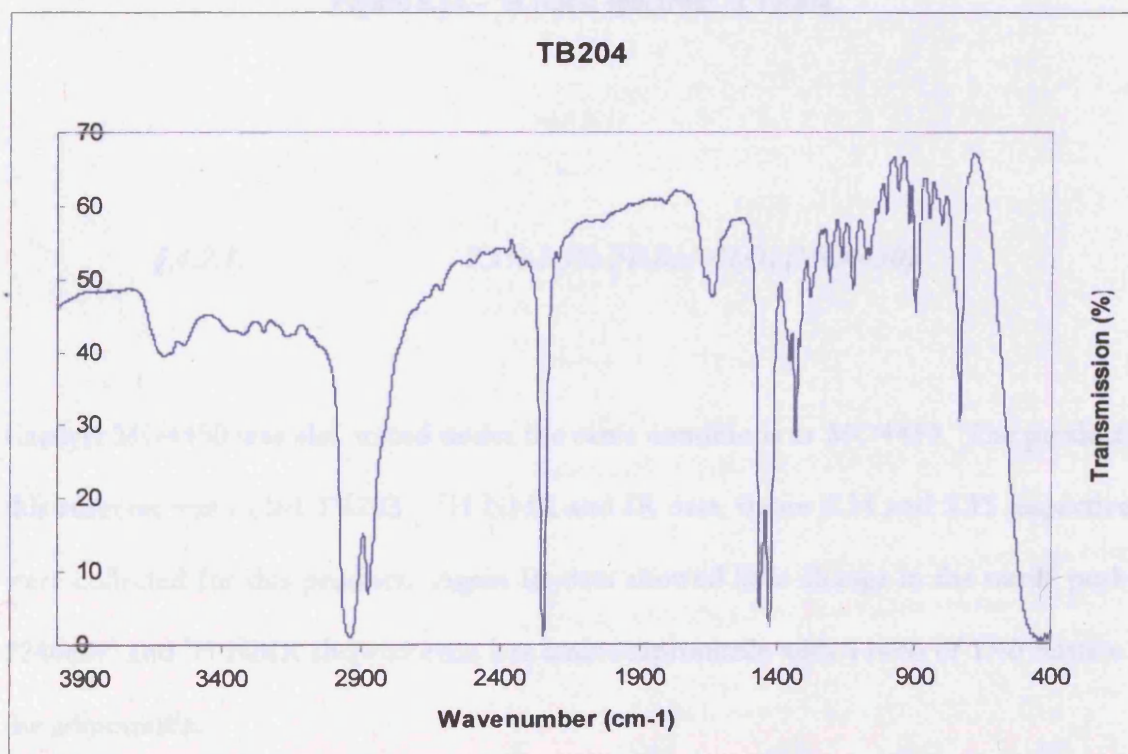


Figure 5.33 - IR spectrum of TB204 (liquid film).

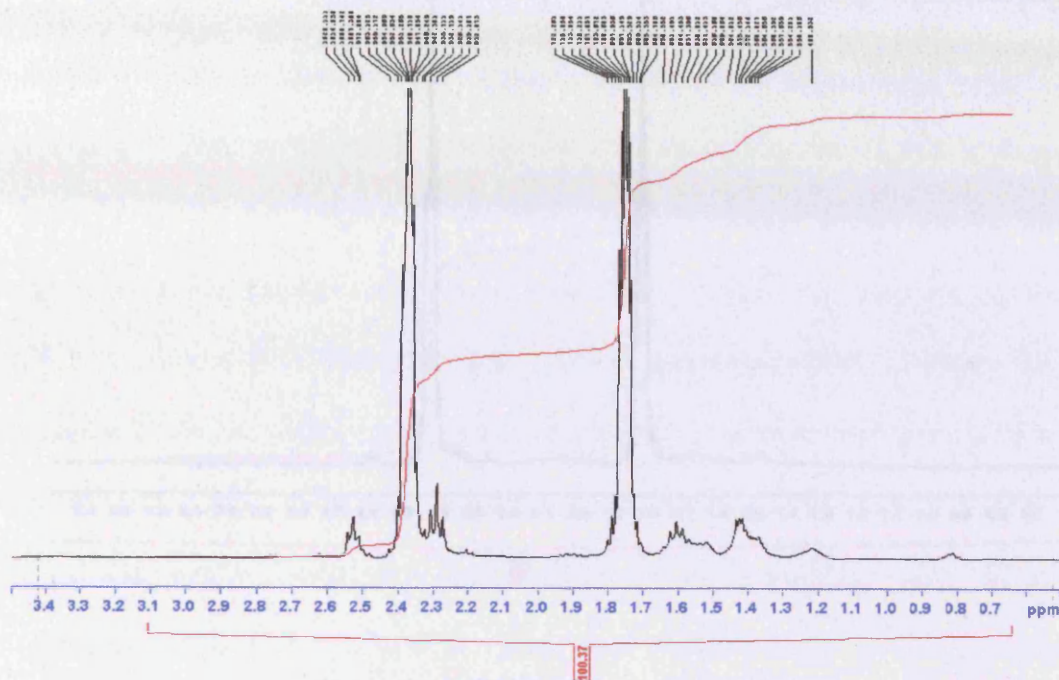


Figure 5.34 –  $^1\text{H}$  NMR spectrum of TB204.

#### 5.4.2.3. 2.5%-2.5% Ni-Rb/ $\text{Al}_2\text{O}_3$ (MO4450)

Catalyst MO4450 was also tested under the same conditions as MO4433. The product of this reaction was called TB205.  $^1\text{H}$  NMR and IR data, figure 5.34 and 5.35 respectively, were collected for this product. Again IR data showed little change in the nitrile peak at  $2246\text{cm}^{-1}$  and  $^1\text{H}$  NMR showed even less aminocapronitrile with a ratio of 1:40 relative to the adiponitrile.

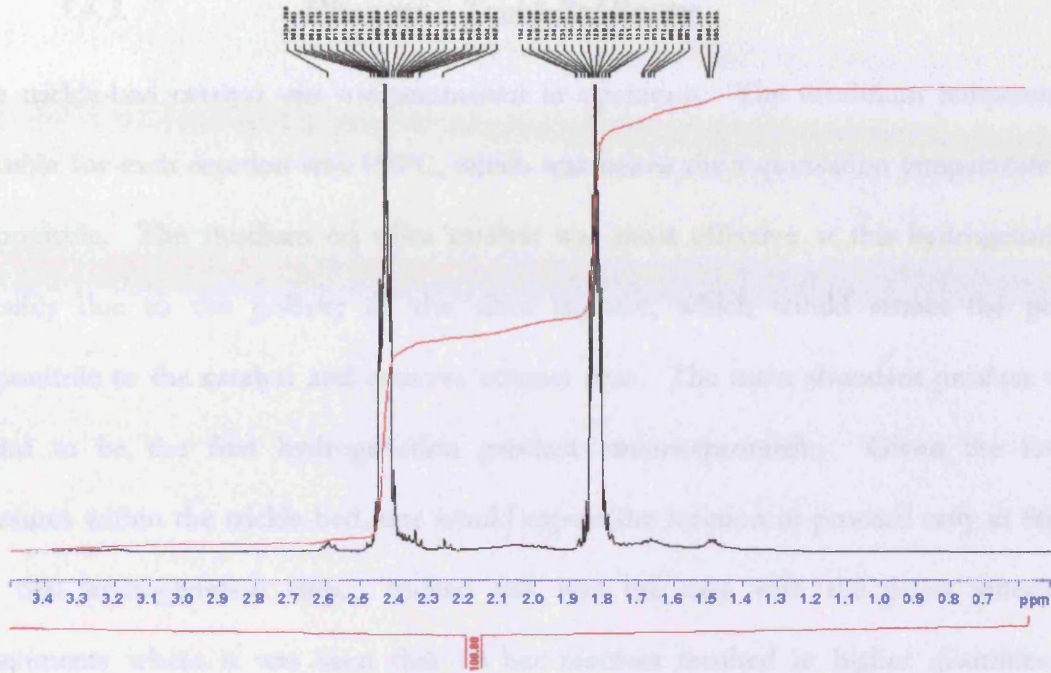


Figure 5.35 –  $^1\text{H}$  NMR spectrum of TB205.

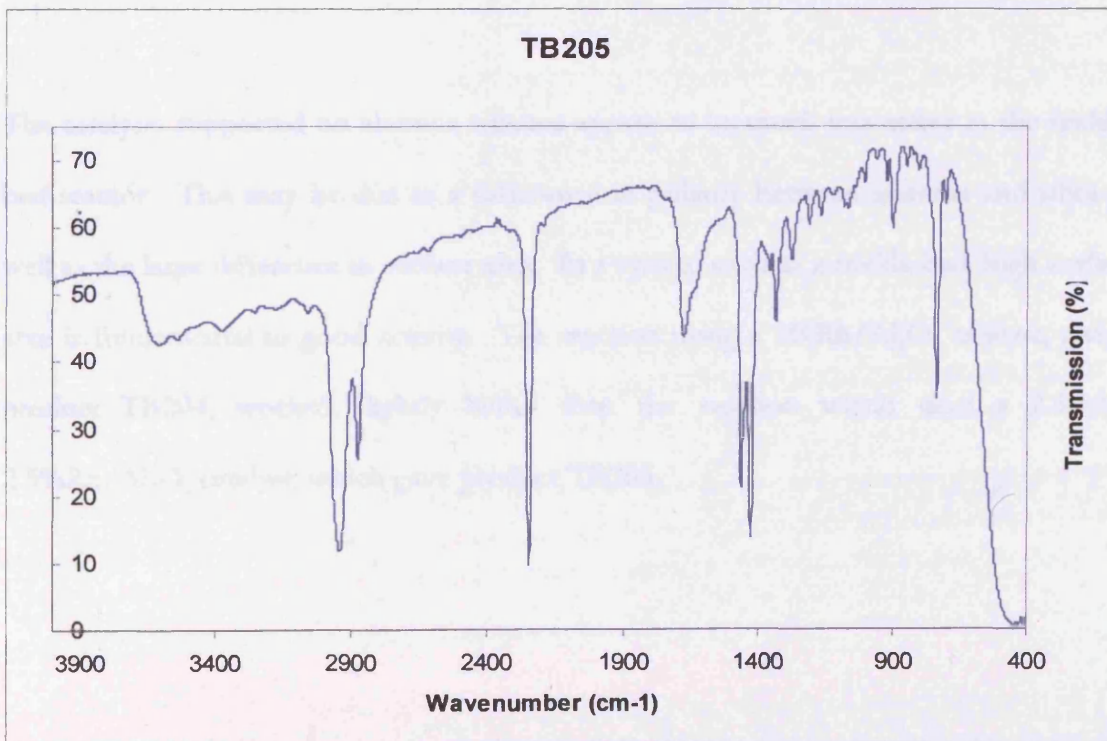


Figure 5.36 - IR spectrum of TB205 (liquid film).

5.4.3. Discussion – Trickle-Bed Reactor

The trickle-bed catalyst was temperamental in operation. The maximum temperature possible for each reaction was 150°C, which was below the vaporisation temperature of adiponitrile. The rhodium on silica catalyst was most effective at this hydrogenation possibly due to the polarity of the silica support, which would attract the polar adiponitrile to the catalyst and increase contact time. The most abundant product was found to be the first hydrogenation product aminocapronitrile. Given the lower pressures within the trickle-bed, one would expect the reaction to proceed only as far as the first hydrogenation step. Indeed this was the case with the pricat autoclave experiments where it was seen that 10 bar reaction resulted in higher quantities of aminocapronitrile. If the trickle-bed reactor were modified to cope with higher pressures perhaps it would be possible to force through the reaction to the fully hydrogenated hexamethyldiamine.

The catalysts supported on alumina trilobes appear to be much less active in the trickle-bed reactor. This may be due to a difference in polarity between alumina and silica as well as the large difference in surface area. In a system such as a trickle-bed, high surface area is fundamental to good activity. The reaction using a 5%Rh/Al<sub>2</sub>O<sub>3</sub> catalyst, giving product TB204, worked slightly better than the reaction which used a 2.5%Ni-2.5%Rh/Al<sub>2</sub>O<sub>3</sub> catalyst, which gave product TB205.

# *Chapter 6*

# CONCLUSIONS

---

## 6. CONCLUSIONS

---

In summary, three reactors have been constructed with the aim being to hydrogenate adiponitrile to aminocapronitrile and hexamethyldiamine. It was found that adiponitrile is very problematic to maintain in the gas phase under micro reactor conditions. Liquid-phase trickle-bed work was achieved but proved to also be problematic due to physical factors such as the high viscosity of the adiponitrile liquid. The autoclave was found to be the most efficient reactor as it was possible to achieve high pressures and temperatures necessary to push forward the reaction and avoid side product formation.

Industrially supplied “pricat” catalysts were used to test the system and gave an insight in to the nature of the hydrogenation reaction. Characterisation using XRD showed these to be mainly NiO catalysts with atomic absorption showing a high loading of nickel, in the region of 40%. The hydrogenation reaction was found to be temperature and pressure dependant. At lower pressures the first hydrogenation step dominated and at higher pressures more hexamethyldiamine was produced.

In our attempts to find a supported precious metal alternative catalyst for Raney nickel we looked at rhodium and compared it with supported nickel. The 20%Ni/SiO<sub>2</sub> catalyst was found to have very similar behaviour to the pricat catalysts in our test system producing high quantities of hexamethyldiamine and low levels of side product formation. The rhodium catalysts at 5% loading proved that silica supported Rh regardless of surface area was less efficient than alumina supported Rh. Whilst all the rhodium catalysts had low conversions and selectivities, the alumina supported catalysts major product was aminocapronitrile where the silica supported counterparts were producing mainly side products.

Perhaps one of the most interesting observations on this work is on the effect of combining base metal and precious metal on the support. It was found that both 2.5%-2.5%Ni-Rh/Al<sub>2</sub>O<sub>3</sub> and 2.5%-2.5% Co-Rh/Al<sub>2</sub>O<sub>3</sub> performed far better than their single metal counterparts. The reduction temperatures of the combined metal catalysts were shown to be far lower than that of their single metal counterparts. This is thought to be the main driving force behind the increase in activity.

Having observed blockages in the trickle-bed and gas phase systems, we questioned the causes given it was possible to partially unblock the system with an organic solvent. With GC having shown the presence of only adiponitrile, a liquid, it appeared that perhaps there may be another substance present. <sup>1</sup>H-NMR was successfully used to identify the presence of other moieties. The data was further backed up by secondary observations within the IR spectra. With this in mind, it was possible to use <sup>1</sup>H-NMR to show the effect of the catalyst over time in the trickle-bed system. This showed significant conversions to a range of products over the course of 6 hours. However, the difficulties attributed to purification meant that this technique also had its limits.

